2013

Studies of core-shell nanoGUMBOS and liposomal ionogels

Ashleigh Renee' Wright
Louisiana State University and Agricultural and Mechanical College, awrig14@tigers.lsu.edu

STUDIES OF CORE-SHELL NANOGUMBOS AND LIPOSOMAL IONOGELS

A Dissertation

Submitted to the Graduate Faculty of the
Louisiana State University and
Agricultural and Mechanical College
in partial fulfillment of the
requirements for the degree of
Doctor of Philosophy

in

The Department of Chemistry

by
Ashleigh Reneé Wright
B.S., Wofford College, 2004
M.S., North Carolina Agricultural and Technical State University, 2007
May 2013

DEDICATION

This dissertation is dedicated to my dearest Avery. Although you were only in my arms for a moment, you will be in my heart forever! I love you!!

-Mommy

ACKNOWLEDGEMENTS

It is with much gratitude that I recognize those who have been an integral part in the completion of this degree. First and foremost I must thank God for the many blessings that have been bestowed upon me. I know that who I am and where I am is because of the opportunities and experiences you have placed in my path. Thank God for FAVOR!! Sometimes I think about how I have gotten to places I have been and there is no explanation, but GOD! Thank you, Lord for giving me the wisdom to take advantage of my blessings, the strength to not give up, and guiding me as I have traversed along this journey.

Dr. Isiah M. Warner, thank you the opportunity to pursue doctoral research under your mentorship. Thank you for being scientifically and financially supportive as I have grown over the years. I am grateful for the work experiences I have had. They have served as training grounds toward becoming a confident, well-rounded chemist, speaker, and writer. You have definitely established a culture of excellence within the Warner research group that I am proud to have been a part. Your great expectations of me have always been a motivator to go above and beyond in order to do well. As you have told me several times before, you believed in me at times when I doubted myself. Thank you for believing in me! I appreciate your passion for research and will channel that enthusiasm as I move forward. There are so many dimensions to you and your career from which I have learned. I admire your desire to challenge, motivate, and mold young minds. I would also like to thank Mrs. Warner for her hospitality. She has been able to put a smile on my face when I did not feel like smiling. The both of you have helped to make Baton Rouge a home away from home.

To my committee members, Dr. S.D. Gilman, Dr. Kermit Murray, Dr. Jayne Garno, and Dr. Jack Losso thank you for your time and conversations regarding my research progress and

completion of the many milestones throughout my matriculation. Dr. William K. Adeniyi, my Master's thesis advisor, it is because of your faith in me that pushed me to pursue a Ph.D. For that, I must thank you!

To the Warner Research Group past and present, thank you for the camaraderie. I have so many memories to reflect on for years to come. The many laughs, lunches, conversations, constructive criticisms, and helpful suggestions have been a fundamental part of my growth at LSU. Each one of you has taught me so much scientifically and culturally and are permanently etched into my memory.

To my wonderful classmates from 2007, I could not have asked for a great group of people with whom to go through this process. I pray that we cherish the times we have shared hanging out, shopping, venting, crying, working, stressing, and relaxing. You are all friends for life.

I also acknowledge Rev. and Mrs. Remus Harper, Jr. and the Mt. Carmel A.M.E. Church family for your love and encouragement. Mrs. Alma, Mrs. Flora, Mrs. Clara, Mrs. Evelyn thank you for all the phone calls, cards, and encouraging words as I have grown up before your eyes.

Finally, to my personal support system, I love you all dearly. Mom, there are no words to fully express my gratitude for you. Thank you for exposing me to a variety of experiences socially, academically, and culturally. You have been a constant support for me in anything I have ever done. When things got difficult for me, I could always call you or remember your words of wisdom to keep me going. I hope I have made you a proud mother in all aspects of being your daughter. To my brothers Corey and Justin, thank you for being the most loving brothers a sister could ask for. I love that I am wedged between the two of you. No matter if I

reach in front or behind, one of you is always there. I love my niece, Sydney Nicole, and nephews Julian Carter, Jordan Emmanual, and Jeremiah Blaise dearly. To the rest of my family and friends, thank you for being supportive in my educational endeavors and I appreciate all of you!!

TABLE OF CONTENTS

ACKNOWLEDGEMENTS iii

LIST OF FIGURES ix

LIST OF TABLES xiii

ABSTRACT xiv

CHAPTER 1. INTRODUCTION 1
1.1 Group of Uniform Materials Based on Organic Salts (GUMBOS) 1
1.1.1 Ionic Liquids 1
1.1.2 Synthesis of Ionic Liquids 2
1.1.3 Functionality of Ionic Liquids 4
1.1.4 GUMBOS 7
1.2 Nanomaterials 10
1.2.1 NanoGUMBOS 10
1.2.2 Gold Nanomaterials 15
1.2.2.1 Synthesis of Gold Nanoparticles 15
1.2.2.2 Stabilization of Gold Nanoparticles 16
1.2.2.3 Gold Surface Chemistry 17
1.2.2.4 Ionic Liquids as Stabilizers for Gold Nanomaterials 20
1.2.2.5 Optical Properties of Gold Nanoparticles 20
1.2.2.6 Applications of Gold Nanoparticles 21
1.2.3 Core-Shell Nanoparticles 23
1.2.3.1 Gold Nanoshells 23
1.3 Gels 26
1.3.1 Hydrogels in Drug Delivery 28
1.3.2 Organogels in Drug Delivery 28
1.3.3 Ionogels in Drug Delivery 29
1.3.4 Liposomal Gels in Drug Delivery 29
1.3.4.1 Liposomes 29
1.3.4.2 Liposomal Gels for Drug Delivery 33
1.4 Scope of Dissertation 34
1.5 References 35

CHAPTER 2. ANALYTICAL TECHNIQUES 44
2.1 Ultraviolet-visible Spectroscopy 44
2.2 Transmission Electron Microscopy 45
2.3 Scanning Electron Microscopy 46
2.4 Cyclic Voltammetry 47
2.5 Rheology 49
2.6 Differential Scanning Calorimetry 52
2.7 References 53

CHAPTER 3. GUMBOS-GOLD CORE-SHELL NANOPARTICLES: SYNTHESIS AND CHARACTERIZATION 55
3.1 Introduction 55
3.2 Materials and Methods 56
3.2.1 Materials 56
3.2.2 Characterization Techniques 56
3.2.3 Synthesis of GUMBOS 57
3.2.4 Preparation of NanoGUMBOS 58
3.2.5 Preparation of Gold Seeds and Attachment of Gold Seeds to NanoGUMBOS 59
3.2.6 Preparation of Gold Nanoshells 60
3.2.7 NanoGUMBOS as Organic Solvent Sensors 61
3.3 Results and Discussion 61
3.3.1 Synthesis and Characterization of GUMBOS 61
3.3.2 Preparation and Characterization of Reprecipitation NanoGUMBOS 62
3.3.3 Preparation, Optimization, and Characterization of Reverse Micellar NanoGUMBOS 62
3.3.4 Synthesis of Nanoshell Formation 64
3.3.5 NanoGUMBOS-Gold Core-Shell Nanoparticles as Sensors for Organic Solvents 69
3.4 Conclusion 70
3.5 References 72

CHAPTER 4. TEMPLATED SYNTHESIS OF GUMBOS-GOLD CORE-SHELL NANORODS FOR ELECTRONIC APPLICATIONS 75
4.1 Introduction 75
4.2 Materials and Methods 77
4.2.1 Materials 77
4.2.2 Characterization Techniques 77
4.2.3 Preparation of 1D NanoGUMBOS 78
4.2.4 Preparation of Core-Shell 1D NanoGUMBOS 78
4.2.5 Cyclic Voltammetry 79
4.3 Results and Discussion 79
4.3.1 Microscopic Characterization of 1D NanoGUMBOS 79
4.3.2 Morphological and Optical Characterizations of Core-Shell 1D NanoGUMBOS 80
4.3.3 Electrochemical Analysis of [PyrProSH][TPB] GUMBOS 81
4.4 Conclusion 84
4.5 References 85

CHAPTER 5. SYNTHESIS AND CHARACTERIZATION OF LIPOSOMAL IONOGELS 87
5.1 Introduction 87
5.2 Materials and Methods 89
5.2.1 Materials. 89
5.2.2 Characterization Techniques 89
5.2.3 Synthesis of Choline Proline 90
5.2.4 Preparation of Liposomal Ionogels (LIGs) 90
5.3 Results 91
5.3.1 Synthesis and Characterization of [Cho][Pro] 91

5.3.2 Liposomal Ionogels 91
5.3.3 Rheological Examination of LIGs 92
5.3.3.1 Viscoelastic Behavior of LIGs and [Cho][Pro]. 94
5.3.3.2 Viscosity of DPPC and POPC LIGs 98
5.3.4 Thermal Analyses 99
5.4 Conclusions 102
5.5 References 103

CHAPTER 6. CONCLUSIONS AND FUTURE STUDIES 106
6.1 Conclusions 106
6.2 Future Studies 108

VITA 110

LIST OF FIGURES

Figure 1.1: Common cation and anion structures for ILs. 2

Figure 1.2: Representative reaction scheme of quaternization synthesis for ILs. 3

Figure 1.3: Synthesis of 1-hexyl-3-methylimidazolium hexafluorophosphate. 4

Figure 1.4: Synthesis of ethylammonium nitrate using Bronstead acid-base neutralization. 4

Figure 1.5: Synthesis of chloroaluminate ionic liquids. 4

Figure 1.6: Second generation anion structures. 6

Figure 1.7: Representative third generation molecules and salts. 7

Figure 1.8: Melting point ranges for room temperature (R.T) ILs, frozen ILs, and GUMBOS. ... 8

Figure 1.9: Ionic structures of cyanine-based GUMBOS: (i) HMT (ii) PIC (iii) NTf_2 (iv) TFP4B (v) TFPB (vi) AOT (vii) BF_4 (viii) BETI. 9

Figure 1.10: Diagram of (A) normal micelle and (B) reverse micelle. 12

Figure 1.11: Representation of reverse micelle method preparation of nanoGUMBOS. 12

Figure 1.12: Diagram of reprecipitation procedure for the preparation of nanoGUMBOS. (A). 1mM acetone solution of GUMBOS, (B) addition of 100 µL (A) to 5 mL of water, and (C) TEM micrograph of nanoGUMBOS. 14

Figure 1.13: Diagram of (A) electrostatic and (B) steric stabilized Au nanoparticles. 17

Figure 1.14: Self-assembled monolayer of alkanethiols on gold substrate. 18

Figure 1.15: Color changes of gold colloidal solutions with respect to size. 21

Figure 1.16: Gold nanoparticles used as colorimetric biosensor. 22

Figure 1.17: Spectral profile of silica-gold core-shell nanoparticles with increasing core:shell ratios inspired by reference 76. 25

Figure 1.18: Colors of gold nanoshell solutions with various shell thicknesses inspired by reference 76. 25

Figure 1.19: Representation of hydrogel system with various chemical and physical interactions. 27

Figure 1.20: Diagram of a phospholipid structure. 30

Figure 1.21: Representation of lipid bilayers (a) below and (b) above the phase transition temperature. 31

Figure 1.22: Diagram of (a) multilamellar vesicles (MLVs) (b) large unilamellar vesicles (LUVs) and (c) small unilamellar vesicles (SUVs). 32

Figure 2.1: Representation of double beam UV-Vis spectrophotometer. 45

Figure 2.2: Diagrams of a (A) transmission electron microscope and (B) scanning electron microscope. 47

Figure 2.3: Diagram of cyclic voltammeter. 48

Figure 2.4: Representative excitation signal produced from CV reaction. 49

Figure 2.5: Representative cyclic voltammogram. 50

Figure 2.6: Newton's law of viscosity plot. 51

Figure 2.7: Depiction of (a) cone-plate and (b) parallel plate geometries of rotational rheometers. 52

Figure 2.8: Diagram of heat-flux differential scanning calorimeter. 53

Figure 3.1: Synthesis mechanism of [PyrProSH][TPB] GUMBOS. 58

Figure 3.2: Ionic structures of thiol-functionalized GUMBOS: (A) 1-methyl-4-propylthiol-pyridinium, (B) 1-methyl-3-propylthiol-l-imidazolium, and (C) tetraphenylborate. 58

Figure 3.3: Schematic of the reverse micelle procedure for the preparation of [MImProSH][NTf2] nanoGUMBOS. 60

Figure 3.4: (A) UV-vis absorption spectrum of bulk GUMBOS with a λmax of 209 nm and nanoGUMBOS with a λmax of 265 nm and (B) TEM micrograph of [PyrProSH][TPB] nanoGUMBOS formed through the reprecipitation procedure with an average diameter of 98 ± 17 nm. 62

Figure 3.5: TEM micrographs of [MImProSH][TPB] nanoGUMBOS prepared using TX-100 reverse micelle procedure. 63

Figure 3.6: Representative TEM micrograph of thiol-functionalized nanoGUMBOS prepared using the reverse micelle methods with average diameters of (A) 157 ± 47 nm and (B) 20 ± 5 nm. 64

Figure 3.7: (A) TEM micrograph and (B) UV absorbance spectrum of gold seeds. 65

Figure 3.8: Absorption spectra of Au seeds before (solid) and after (dotted) attachment to nanoGUMBOS. 66

Figure 3.9: (A) Normalized UV/vis absorption spectrum for growth of (i) gold nanoshell on 157 ± 47 nm nanoGUMBOS, and (ii) magnified absorption maxima (B) Evolution of gold nanoshell with increasing ratios of Au hydroxide solution to Au-seeded nanoGUMBOS (i) 1:1, (ii) 2:1, (iii) 4:1, (iv) 8:1. 67

Figure 3.10: Solutions of nanoGUMBOS with increasing coverage of gold nanoshell. 68

Figure 3.11: (A) Normalized UV/vis spectrum of gold nanoshell growth on (i) 21 ± 5 nm nanoGUMBOS, and (ii) magnified absorption maxima (B) TEM micrograph for nanoshell progression on Au-seeded nanoGUMBOS with increasing ratios from (i) 1:1 (ii) 2:1. 69

Figure 4.1: Chemical structure of [PyrProSH][TPB]. 76

Figure 4.2: SEM micrographs of (A) free and (B) array 1D nanoGUMBOS. 80

Figure 4.3: TEM micrographs of (A) bare (B) seeded and (C) coated 1D nanoGUMBOS. 80

Figure 4.4 (A) Side and (B) top view of gold-coated 1D nanooGUMBOS. 81

Figure 4.5: Absorption spectrum of bare (blue trace) and gold-coated 1D nanoGUMBOS. 81

Figure 4.6: Cyclic voltammogram of ferrocene. 82

Figure 4.7: Cyclic voltammogram of [PyrProSH][TPB] GUMBOS. 83

Figure 4.8: Negative cyclic voltammogram for [PyrProSH][TPB]. 84

Figure 4.9: Positive cyclic voltammograms for [PyrProSH][TPB]. 85

Figure 5.1: Chemical structure of DPPC. 89

Figure 5.2: Chemical structure of POPC. 89

Figure 5.3: Synthesis scheme of [Cho][Pro]. 90

Figure 5.4: DPPC LIGs with 0, 5, 10, 25, and 50% (w/w) cholesterol concentrations. 92

Figure 5.5: POPC LIGs with 0, 5, 10, 25, and 50% (w/w) cholesterol concentrations. 92

Figure 5.6: Linear viscoelasticity plot for DPPC LIG. 93

Figure 5.7: Linear viscoelasticity plot for POPC LIG. 94

Figure 5.8: Elasticity (G') (closed symbols) and viscosity (G") (open symbols) for DPPC LIGs. 96

Figure 5.9: Elasticity (G') (closed symbols) and viscosity (G") (open symbols) for POPC LIGs. 96

Figure 5.10: Viscoelastic properties of [Cho][Pro]. 97

Figure 5.11: Loss tangent plot for DPPC LIGs. 98

Figure 5.12: Loss tangent plot for POPC LIGs. 98

Figure 5.13: Viscosity rheogram for DPPC LIGs. 99

Figure 5.14: Viscosity rheogram for POPC LIGs. 100

Figure 5.15: Decomposition thermograms for DPPC LIGs. 101

Figure 5.16: Decomposition thermograms for POPC LIGs. 101

LIST OF TABLES

Table 3.1: Absorption maxima of nanoGUMBOS coated at a 2:1 ratio of Au hydroxide after exposure to various organic solvents. The third column is the difference between the absorbance shift values after exposure to the respective organic solvent and nanoGUMBOS in water. 70

Table 3.2: Absorption maxima of nanoGUMBOS coated at a 4:1 ratio of Au hydroxide after exposure to various organic solvents. The third column is the difference between the absorbance shift values after exposure to the respective organic solvent and nanoGUMBOS in water. 71

Table 3.3: Absorption maxima of nanoGUMBOS coated at an 8:1 ratio of Au hydroxide after exposure to various organic solvents. The third column is the difference between the absorbance shift values after exposure to the respective organic solvent and nanoGUMBOS in water. 72

Table 5.1: Thermal decomposition temperatures of [Cho][Pro] and LIGs. 101

Table 5.2: Phase transition temperatures of DPPC and POPC LIGs. 102

ABSTRACT

The work presented in this dissertation is a description of novel core-shell nanomaterials derived from a group of uniform materials based on organic salts (GUMBOS) and the synthesis and characterizations of novel liposomal ionogels (LIGs). These GUMBOS are an extension of ionic liquids (ILs) which are organic salts with melting points between 25 °C and 100 °C. Ionic liquids have high thermal stability, low vapor pressure, and tunable physiochemical and functional properties. All of the properties of ILs are controlled by the chosen cation and anion pair. Similarly to ILs, GUMBOS possess the same qualities; however, they have melting points up to 250 °C. The first section is a discussion of core-shell nanomaterials composed of GUMBOS and gold. Chapter 3 is a description of the synthesis of thiol-functionalized GUMBOS and their corresponding nanoparticles (nanoGUMBOS). NanoGUMBOS were prepared using non-templated and templated methods. Non-templated nanoparticles were obtained through ionic self-assembly using a reprecipiation procedure. A reverse micellar method was utilized in the preparation of templated nanoGUMBOS. NanoGUMBOS were used as core components for the core-gold shell nanoparticles. The optical and morphological properties of nanoGUMBOS were monitored throughout the gold-coating process. Although gold-coated nanoGUMBOS have potential uses in biomedical applications, they were investigated as organic solvent sensors. In chapter 4, 1D core-shell nanoGUMBOS were prepared using a porous anodic alumina template. The corresponding optical and morphological characteristics of the nanorods were also determined along with the gold-coating procedure. With interest in electrochemical applications, cyclic voltammetry measurements were performed to determine the electronic properties of bulk GUMBOS. The second section is a description of a new type of ionogel that utilizes liposomes as the gelation matrix which we have named

liposomal ionogels (LIGs). The ionogels developed in this dissertation are composed of a biocompatible IL which is prepared from choline and the amino acid proline along with dipalmitoylphosphatidylcholine (DPPC) and 1-palmitoyl-2-oleoyl-*sn*-glycero-3-phosphocholine (POPC) phospholipids. These LIGs offer two tunable components, phospholipids and ILs, and have potential as topical drug delivery tools.

CHAPTER 1

INTRODUCTION

1.1 Group of Uniform Materials Based on Organic Salts (GUMBOS)

1.1.1 Ionic Liquids

Ionic liquids (ILs) are organic salts that melt below 100 °C.[1] Within this definition, there are two subcategories of ILs: room temperature and frozen.[2] Though separated by melting point, room temperature ILs are viscous liquids near and below room temperature while frozen ILs are in the solid form at room temperature and melt between 25 °C and 100 °C. The type of IL is determined by the size and arrangement of ions within the lattice structure. The size asymmetry between the bulky cation or anion restricts the ability of the ions to organize within the lattice, which decreases the crystallization energy (i.e. melting point).[3] Careful selection of the cation and anion determines other properties of the salt such as viscosity, solubility, density, and polarity.[3,4,5] For example, increasing the alkyl chain on the heterocyclic cation results in a more hydrophobic IL. Likewise, as displayed in Figure 1.1, the choice of anion can determine the level of hydrophobicity. Other attractive properties of ILs include low volatility, negligible vapor pressure, recyclability, ionic conductivity, and high thermal stability, which has made them useful as alternative solvents for organic syntheses.[1] Common cations for ILs are alkylammonium, alkylphosphonium, *N*,*N*-dialkylimidazolium, and *N*-alkylpyridinium structures and common anions include hexafluorophosphate (PF_6), tetrafluoroborate (BF_4), nitrate (NO_3), and tetraphenylborate (TPB) as shown in Figure 1.1.

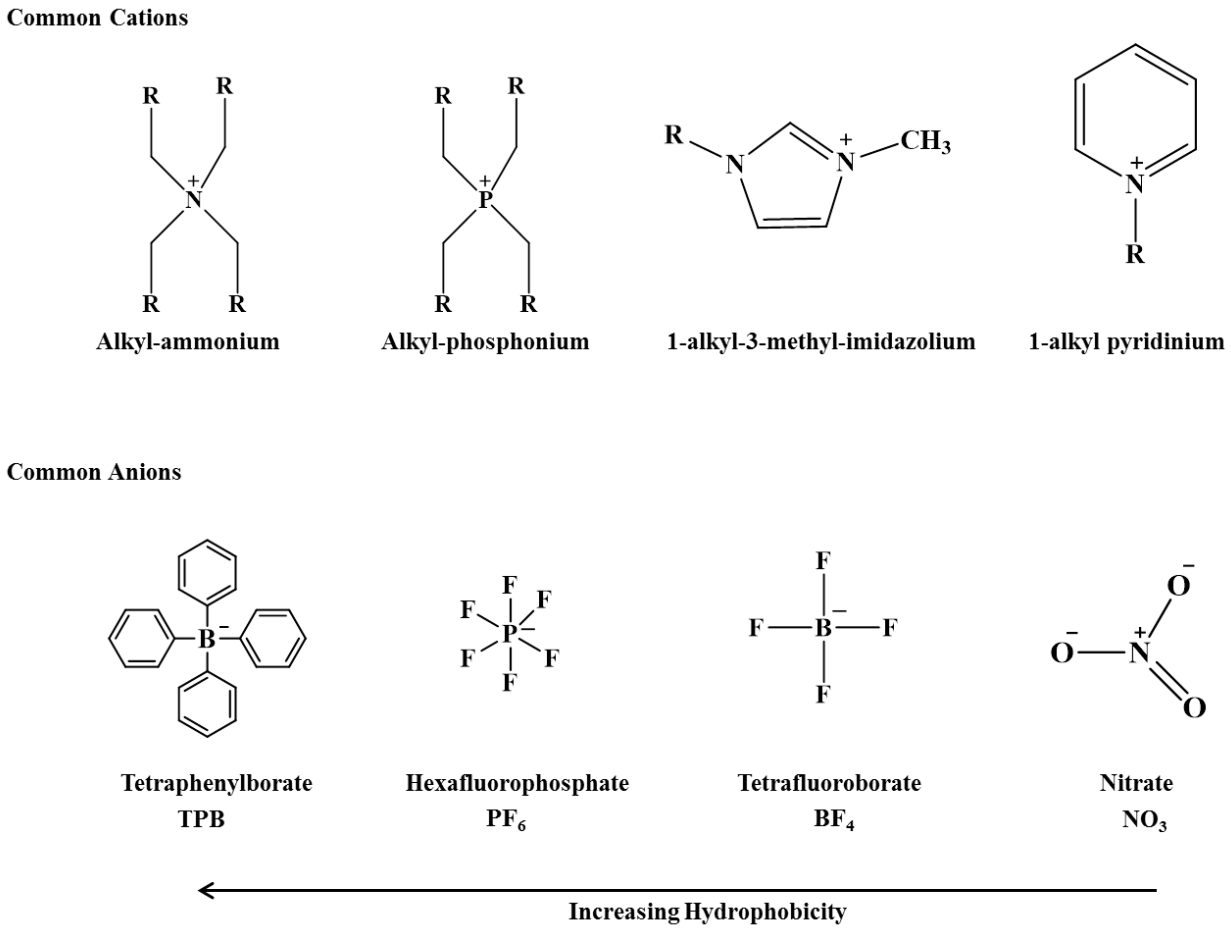

Figure 1.1: Common cation and anion structures for ILs.

1.1.2 Synthesis of Ionic Liquids

The preparation methods of ILs are fairly simple and do not require laborious synthetic procedures which take long periods of time. Some ILs can be synthesized within hours. There are various synthetic routes that can be used in combination for the preparation of ILs: quaternization, anion metathesis, and neutralization. Quaternization is the alkylation of tertiary amines, sulfides, or phosphines using an alkyl halide.[6] The conditions of the reaction are dependent on the chosen alkyl halide. The reactivity of halogens increases down the periodic table allowing in reaction conditions that are less harsh. For example, alkylation using alkylchlorides require temperatures of 80 °C for several days; whereas, alkyl bromide reactions

occur within 24 h at 60 °C and alkyliodide reactions can be performed at room temperature.[6] A representative quaternization synthesis of 1-hexyl-3-methylimidazolium bromide [HMIM][Br] is shown in Figure 1.2. The reaction occurs between 1-methyl imidazole and 1-bromohexane in isopropanol at 60 °C for 24 h. The product, 1-hexyl-3-methylimidazolium bromide [HMIM][Br], is a hygroscopic, viscous liquid. The unreacted starting materials and by-products can be washed with diethyl ether or ethyl acetate. Finally, any remaining organic solvent is removed under vacuum.

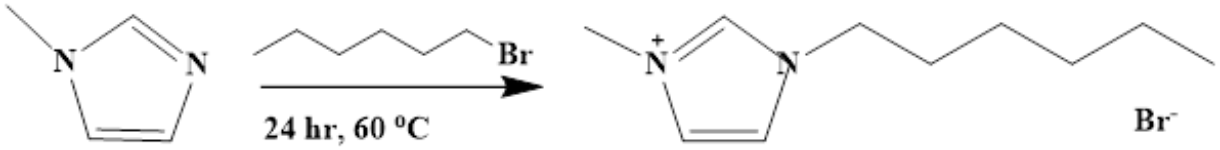

Figure 1.2: Representative reaction scheme of quaternization synthesis for ILs.

Anion metathesis, or ion exchange, is performed to replace the halide anion with an organic anion. This replacement occurs following alkylation or with other previously quaternized compounds. Ion exchange is typically takes place within a biphasic mixture. The ionic liquid is extracted from the aqueous phase into the organic phase. The salt by-product is easily removed with water rinses.[7] For the preparation of [HMIM][PF_6], represented by Figure 1.3, [HMIM][Br] is dissolved in dichloromethane while a slight molar excess of [Na][PF_6] is dissolved in minimal amounts of H_2O. The mixture is stirred for 48 h. The [Na][Br] by-product is removed using aqueous rinses in minimal amounts. The hydrophobic IL, [HMIM][PF_6] is extracted by removing dichloromethane under vacuum. Occasionally, exchanges with highly hydrophobic anions can be occurred in a one-system aqueous medium in which the IL immediately precipitates out of solution. The by-product is washed with copious amounts of water as in exchanges with bis(triflyl)imide and TPB anions.[8]

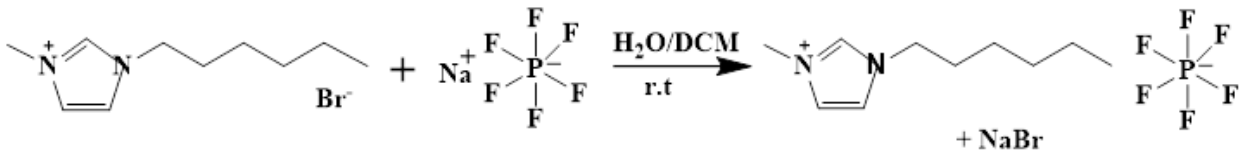

Figure 1.3: Synthesis of 1-hexyl-3-methylimidazolium hexafluorophosphate.

Neutralization reactions for the synthesis of ILs can occur between Brønstead and Lewis acids and bases. In the case of the first IL reported by Walden in 1914, ethylammonium nitrate,[9] ethylamine is mixed with nitric acid inducing a proton transfer as shown in Figure 1.4. Alternatively, haloaluminate ILs are prepared with quaternized-based cations and aluminum Lewis acids (AlX_3; X= Cl, Br) such as the chloroaluminate ILs reported by Hurley and Weir in 1951 (Figure 1.5).[10, 11]

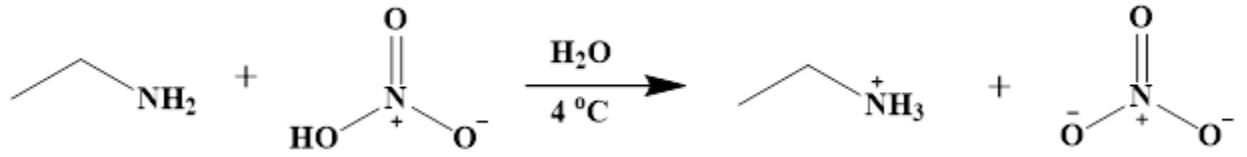

Figure 1.4: Synthesis of ethylammonium nitrate using Bronstead acid-base neutralization.

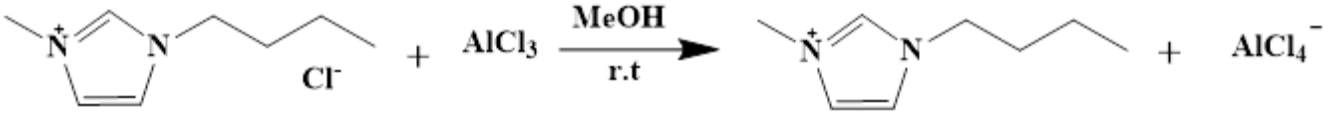

Figure 1.5: Synthesis of chloroaluminate ionic liquids.

1.1.3 Functionality of Ionic Liquids

The development of IL functionality is classified into three generations. First-generation ILs are composed of imidazolium and pyridinium cations with halogenated anions such as the chloroaluminate solvents initially reported by Hurley and Weir.[11] Haloaluminate ILs were used

as solvents or catalysts for organic syntheses. A major drawback to first generation ILs was the high reactivity with air and water. Therefore, had to be handled very carefully and under dry, inert conditions.

Second-generation ILs were initially reported by Wilkes and Zaworotko in the early 1990's and were composed of weakly coordinating anions such as PF_6^- and BF_4^-.[12] Although stable in air and water, they have the tendency to undergo hydrolysis, producing toxic hydrofluoric acid (HF) by-products. In 1996, Bonhôte reported the synthesis of imidazolium-based ILs with the hydrophobic, fluoride-free anion bis((trifluoromethyl)sulfonyl)amide, NTf_2^-.[8] These anions are safer because of the elimination of HF byproducts. The use of imidazolium and pyridinium cations remain in second generation ILs, and ammonium and phosphonium cations are added. Ammonium and phosphonium ILs yield lower melting points, and different viscosities and solubilities in organic solvents in comparison to the imidazolium and pyridinium ILs.[13] These developments within second-generation ILs led to the investigation of other cation and anion pairs in order to tailor not only the physical properties, but also the chemical properties.[13,14] Instead of solely being used for solvents in organic reactions, the use of ILs was now being explored in areas such as sensors,[15] batteries,[16] and lubricants.[17] Structures of second generation anions are displayed in Figure 1.6.

Third-generation ILs are among the more nontoxic and environmentally-friendly salts and are generally known as "task-specific ionic liquids" because they have functional groups inherent to its structure specific for a particular application. In 2001, Rogers *et al.* designed ILs with amine and thiol (thiourea, thioether, and urea) functional groups for the extraction of mercury and cadmium heavy metals.[18]

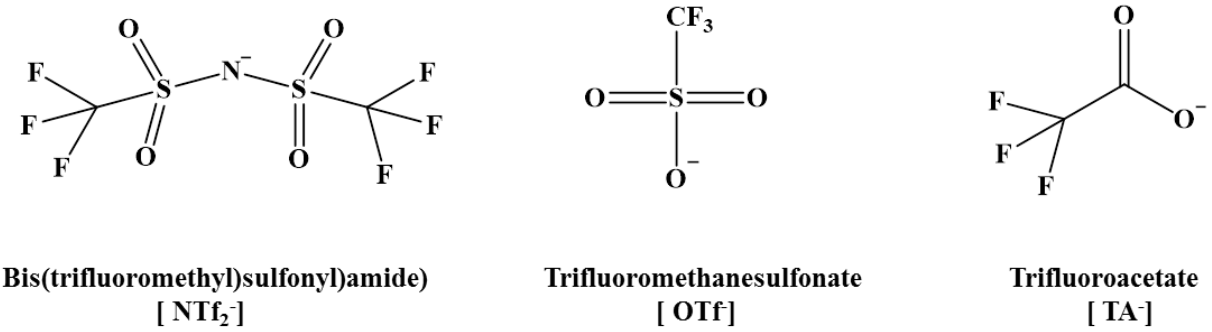

Figure 1.6: Second generation anion structures.

This generation of ILs also incorporated biological properties with the chemical and physical properties of first and second generation ILs. Examples of third generation ions are sugars, amino or organic acids, choline, or drugs. In 2007, Rogers *et al.* developed a series of ILs focused on biological properties which were composed of active pharmaceutical ingredients (API). The ILs were formed using lidocaine hydrochloride (LHCl) and ranitidine hydrochloride (RHCl) cations with a sodium docusate (dioctylsulfosuccinate) (NaD) anion, and didecyldimethylammonium bromide cation with sodium ibuprofen anion. The structures of the named ions are displayed in Figure 1.7. Lidocaine hydrochloride is a topical pain reliever; RHCl is an anti-histamine more commonly known as Zantac and had also been of concern for its tendency to undergo crystallization. Didecylmethylammonium bromide has antibacterial properties, NaD behaves as an emollient and has dispersion capabilities, and sodium ibuprofen has anti-inflammatory properties. It was determined that these salts in pure IL form possessed identical characteristics of traditional ILs such as increased hydrophobicity and hygroscopic in nature. In addition, the IL-APIs circumvented the possibility of crystallization. Biological assays were performed on lidocaine docusate (LD) in which the IL maintained its pain relief functionality as a topical antinociceptive drug over an extended period of time. At the cellular

level, LD demonstrated increased membrane permeability which was attributed to the docusate anion. Essentially, Rogers *et al.* introduced ILs that were multifunctional and biocompatible.

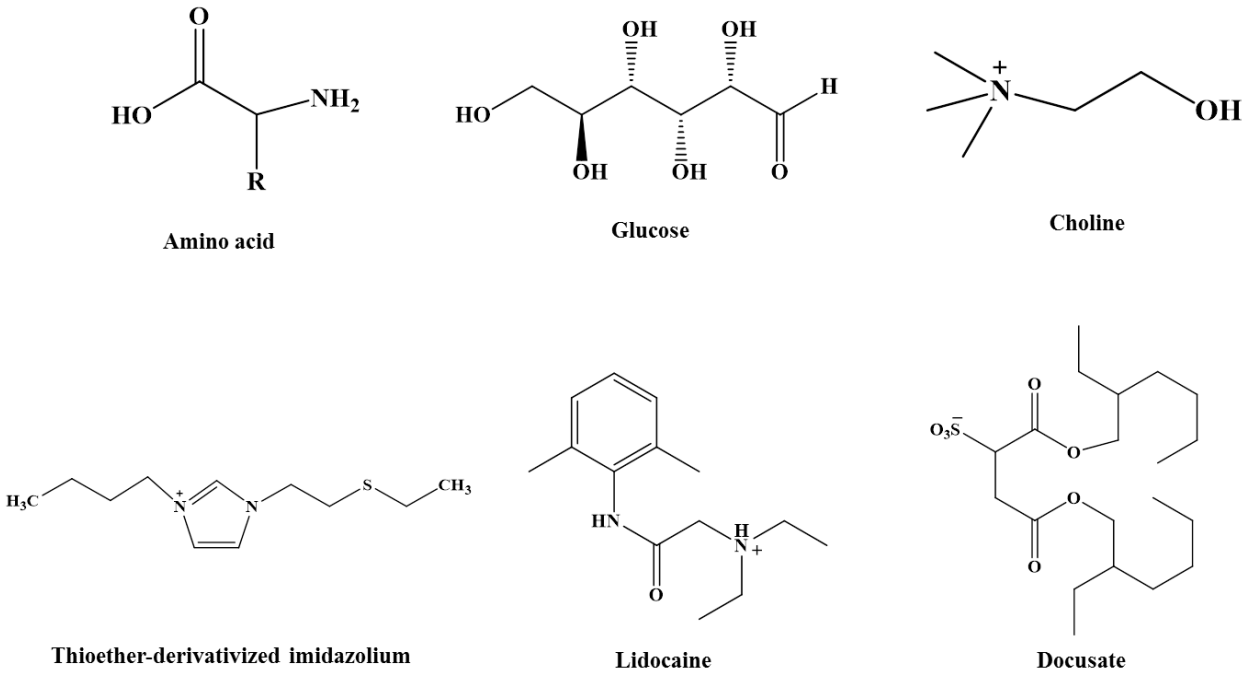

Figure 1.7: Representative third generation molecules and salts.

1.1.4 GUMBOS

Significant progression has been made on the physiochemical properties, functionality, biocompatibility, and applicability of ILs up to this point. However, many salts of similar properties were dismissed over the years due to the strict limitation of the IL melting point of 100 °C. As a result, the Warner research group developed a new class of organic materials which encompasses salts above the melting temperature threshold of traditional ILs. This new class has been termed a *group of uniform materials based on organic salts* or using the acronym, GUMBOS. GUMBOS are an extension of (frozen) ILs and cover a melting point range of 25 °C to 250 °C (Figure 1.8). These GUMBOS possess the same attractive, tunable properties of

traditional ILs with functional properties similar to TSILs. An increase in the melting point exponentially expands the library of functional materials.

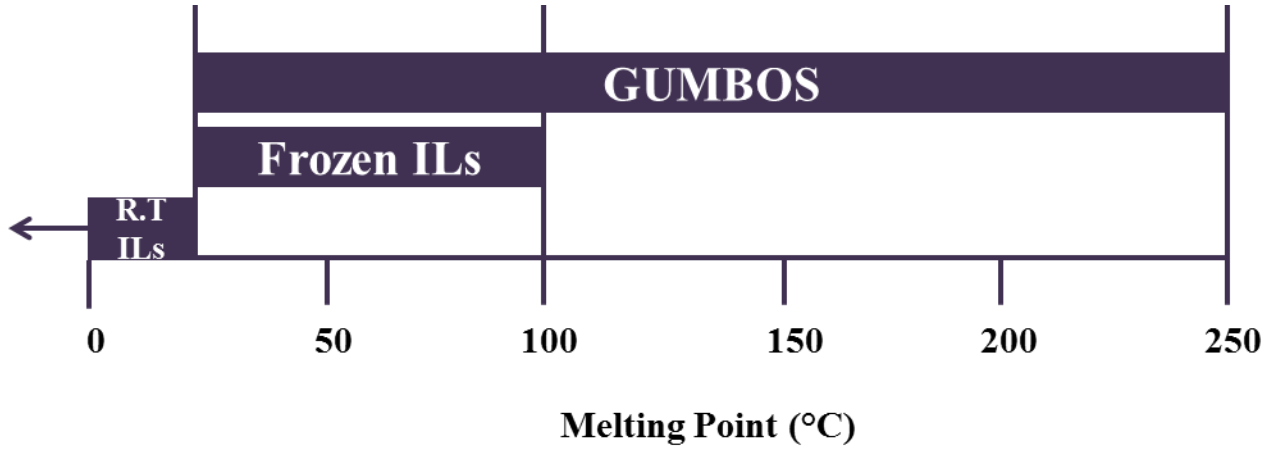

Figure 1.8: Melting point ranges for room temperature (R.T) ILs, frozen ILs, and GUMBOS.

The first report of GUMBOS was published by Tesfai *et al.* in 2009.[19] Magnetic GUMBOS composed of a tradition cation 1-butyl-2,3-dimethylimidazolium and a magnetic anion, tetrachloroferrate ($[Bm_2Im][FeCl_4]$), and nonmagnetic GUMBOS $[Bm_2Im][BF_4]$ were synthesized by ion exchange. The magnetic susceptibility of these GUMBOS was measured using a superconducting quantum interference device (SQUID) and was determined as 34.3×10^{-6} emu/g. This susceptibility was identical to similar ILs prepared with $FeCl_4^-$. In the same year, Bwambok *et al.* prepared series of GUMBOS utilizing a cyanine-based, near infrared (NIR)-emitting dye, 1,1',3,3,3',3'-hexamethylindotricarbocyanine (HMT) cation with anions: BF_4, NTf_2, bis(2-ethylhexyl)sulfosuccinate (AOT), and 3,5-bis(trifluoromethyl)-phenyltrifluoro-borate ($3,5CF_3PheB$). The melting points of the GUMBOS were tuned based on the chosen anion from 58 °C to 220 °C. Ethanolic solutions of the GUMBOS displayed NIR emissions at 765 nm attributed to the HMT cation. The use of other cyanine-based dyes

for the preparation of GUMBOS was also investigated. Das *et al.* synthesized HMT dyes with NTf_2, AOT, bis(pentafluoroethanesulfonimide) (BETI), and tetrakis[3,5-bis-(1,1,1,3,3,3-hexafluoro-2-methoxy-2-propyl)phenyl]borate (TFP4B) anions.[20] Similarly, Jordan *et al.* synthesized pseudoisocyanine (PIC)-based GUMBOS with NTf_2 and BETI anions for solar cell and photosensitizer applications.[21] These two reports were investigations of the tunable spectral properties of GUMBOS which was attributed to the aggregation of molecules (J and H aggregation) within the dye structure. Structures for cyanine-based GUMBOS are shown in Figure 1.9. In addition to magnetic and fluorescent functionalities, GUMBOS and ILs have been prepared by the Warner research group with luminescent,[22,23] chiral,[24,25,26] and biological[23,27] properties.

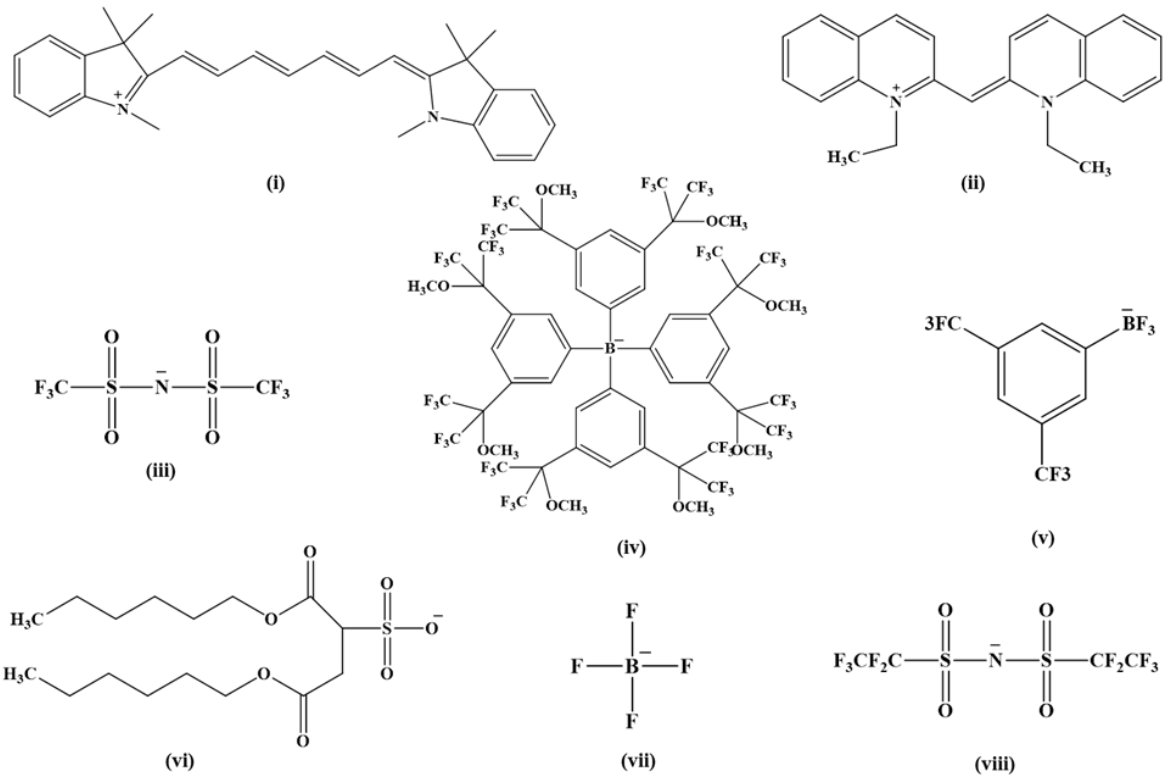

Figure 1.9: Ionic structures of cyanine-based GUMBOS: (i) HMT (ii) PIC (iii) NTf_2 (iv) TFP4B (v) TFPB (vi) AOT (vii) BF_4 (viii) BETI.

The continuously growing field of nanomaterials has been of great interest for years. The properties that were noticed in GUMBOS in comparison their respective parent ions led to the investigation of GUMBOS at the nanoscale. Nanomaterials derived from GUMBOS (nanoGUMBOS) have been shown to possess similar if not more interesting characteristics than those in the bulk form. The preparations of nanoGUMBOS and some of their applications will be further discussed in the next section.

1.2 Nanomaterials

Nanomaterials are structures that have at least one dimension that is less than 100 nm. These materials are reported to have interesting electronic, catalytic, mechanical, and optical properties in comparison to the macroscale. Nanomaterials have a higher surface area to volume ratio and an increased number of interfacial atoms than the bulk material which results in the enhancement of their properties. These properties are also dependent on their size and shape (spherical particles, rods, tubes, and cubes). Likewise, the composition of the nanomaterials also provides task-specific utility. As a result, there are an abundance of nanomaterials that are composed of organic and inorganic materials such as carbon nanotubes,[28] polymers,[29] and metals.[30,31] Recently, nanoGUMBOS were developed, and their physical, electronic, and optical properties studied. Particularly, the properties of nanoGUMBOS and gold (Au) nanomaterials are the scope of this dissertation and will be discussed in the following sections.

1.2.1 NanoGUMBOS

The first report of nanoparticles formed from ionic liquids was reported by Tesfai *et al.* of the Warner research group.[32] Nano- and microparticles of frozen IL, $[Bm_2Im][PF_6]$ (m.p. 42 °C), were prepared by a melt-emulsion-quench procedure. In this preparation method, $[Bm_2Im][PF_6]$ was heated to 70 °C to melt the solid. The solution was then subjected to probe or bath

sonication (at 70 °C), then quickly cooled in an ice bath. The sizes of the nanoparticles were dependent on the type, speed, and duration of sonication. Nanoparticles with diameters ~89 ± 33 nm were formed with 10 min homogenization (30000 rpm), followed by 10 min probe sonication, and quenching in an ice bath. Alternatively, microparticles with diameters ~3 μm were formed with 3 s homogenization (30000 rpm) followed by quenching without probe sonication. Since this initial report, attention has been given to preparation techniques and unique physiochemical and functional properties of nanostructures in the classes of ILs and GUMBOS.

As previously described, Tesfai *et al.* synthesized magnetic and nonmagnetic GUMBOS.[19] The synthesis of the GUMBOS and preparation of the nanoGUMBOS occurred simultaneously using a reverse micellar technique. Reverse micelles have been used for the synthesis of inorganic and organic nanoparticles.[33] Micelles are typically formed from surfactant monomers above their respective critical micelle concentration (CMC). Normal micelles are formed in aqueous medium wherein the hydrophilic heads face the external medium and the tails face inward. Alternatively, reverse micelles form in organic medium causing the tails to be directed toward the environment, while the heads face inward forming central water pools. Reverse micelles are suitable for hydrophobic nanoGUMBOS since the aqueous pool serves as templates for monodispersed nanoparticles. An illustration of normal and reverse micelles is shown in Figure 1.10.

The mechanism behind the formation of nanoGUMBOS by the reverse micelle method is illustrated in Figure 1.11. Initially, aqueous solutions of reactant salts are added to separate reverse micelle emulsions (A and B). The two emulsions are mixed together, (C), and the micelles coalesce and form dimer droplets. During the mixing process, the reactant salts undergo

anion metathesis. Finally, the micelles decoalesce into single droplets wherein, the hydrophobic nanoparticles remain suspended within the aqueous core.[33]

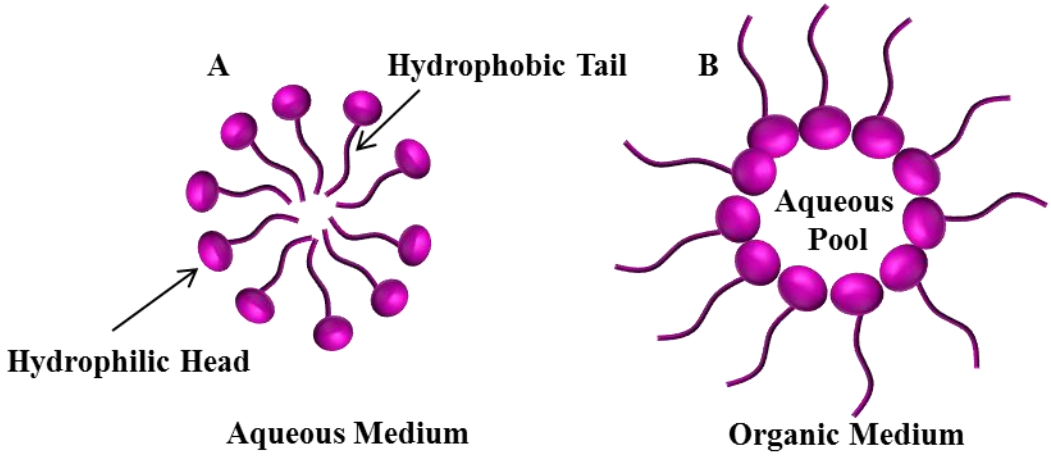

Figure 1.10: Diagram of (A) normal micelle and (B) reverse micelle.

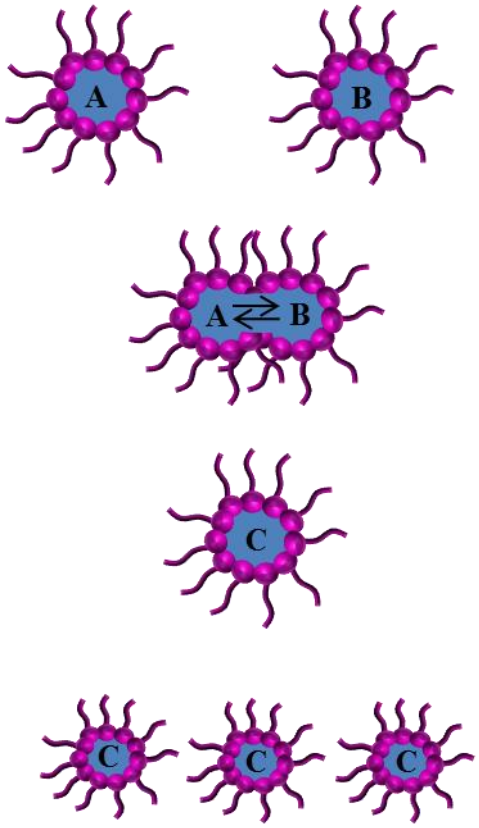

Figure 1.11: Representation of reverse micelle method preparation of nanoGUMBOS.

In the case of the magnetic GUMBOS, aqueous solutions of the parent salts $[Bm_2Im][Cl]$ and $[Fe][Cl_3]\cdot 6H_2O$ were separately added to NaAOT/*n*-heptane emulsions. When the two solutions were mixed, ion exchange and nanoGUMBOS formation occurred. The sizes of the nanoGUMBOS were tuned from ~98 nm to ~200 nm by varying the concentration of the parent ions. Interestingly, the magnetic susceptibility of the nanoGUMBOS was identical to that of the bulk solution.

The cyanine-based GUMBOS described above utilized a reprecipitation method. Nakanishi and coworkers developed the reprecipiation method for the fabrication of organic nanocrystals.[34] In the reprecipitation method, a sample material is dissolved in an alcohol or acetone. The resulting solution is rapidly injected into a solvent that is miscible with the injected solvent but which the target sample is insoluble (usually water). As illustrated in Figure 1.12, (A) a polar solution (*i.e.* ethanol, methanol, acetone) of hydrophobic GUMBOS is (B) added to water under bath sonication resulting in (C) nanoGUMBOS suspended in water. The polar solution is miscible with water while the GUMBOS, which are hydrophobic, precipitate as nanoparticles and remain suspended in the aqueous medium. This procedure is a template-free, additive-free, facile, and reproducible alternative for the synthesis of nanoGUMBOS.

The [HMT]-derived GUMBOS reported by Bwambok *et al.* was the first to be prepared as nanoGUMBOS using the reprecipitation method. The absorption and emission profiles of these NIR-emitting nanoGUMBOS differed from the spectral profiles of the GUMBOS in bulk. The absorbance and fluorescence spectra possessed similar shapes with slight differences due to the different anions that were used. However, the intensities at the same molar concentrations, decreased with anions of increasing molecular weights. The [HMT][AOT] nanoGUMBOS were also used as contrast agents for the imaging of Vero cells. Fluorescence microscopy studies were

performed to monitor efficient cellular uptake, which indicated that nanoGUMBOS have potential in biological applications.

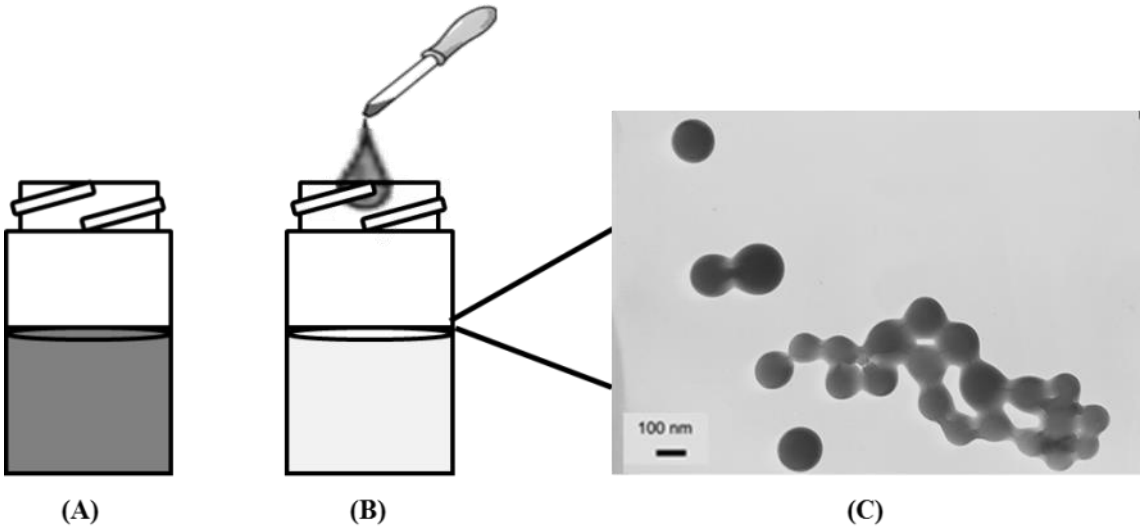

Figure 1.12: Diagram of reprecipitation procedure for the preparation of nanoGUMBOS. (A). 1mM acetone solution of GUMBOS, (B) addition of 100 µL (A) to 5 mL of water, and (C) TEM micrograph of nanoGUMBOS.

Jordan *et al.* was the first to report self-assembled morphological changes with varying anions of cyanine dye nanoGUMBOS.[21] Using the reprecipitation procedure, diamond-like nanostructures were formed for [PIC][NTf_2] GUMBOS and rod-like structures were formed for [PIC][BETI] GUMBOS. The morphological changes were attributed to the stacking orientations of the dye molecules. The head-to-tail pattern (J-aggregation) of the molecules led to the diamond shape of [PIC][NTf_2], whereas, the parallel molecular orientation (H-aggregation) induced the rod-like structures of [PIC][BETI]. The J and H aggregations were also responsible for the changes in the spectral properties of the nanoGUMBOS. A decrease in absorption intensity and red shift in the monomer absorption maximum, and an increase in the fluorescence intensity and red shift in the fluorescence spectra of [PIC][NTF_2] were characteristic of J-type aggregation. Likewise, a decrease in the absorption intensity with a blue shift of the monomer

maximum is characteristic of H-type aggregation of [PIC][BETI]. Furthermore, electrochemical studies were also performed on the [PIC] GUMBOS for their potential use in dye-sensitized solar cells. In addition to melt-emulsion-quench, reverse micelle, and reprecipitation methods, nanoGUMBOS have been synthesized by other techniques such as aerosol[22] and hydrogels.[35]

1.2.2 Gold Nanomaterials

The use of Au nanoparticles or Au colloids dates back to ancient Roman days, and they were used as a method to stain glass.[36] However, it was not until the 1850's that Au nanoparticles were well understood scientifically. In 1857, Michael Faraday observed that the reduction of tetrachloroauric acid, $HAuCl_4$, (Au^{3+}) to Au^0 with phosphorus resulted in a ruby red colloidal suspension which was drastically different than the yellow solution of $HAuCl_4$.[37] Thereafter, several other methods for preparing Au nanoparticles in aqueous and organic media were developed.[38]

1.2.2.1 Synthesis of Gold Nanoparticles

Gold nanoparticles are synthesized using two major mechanisms: reduction and stabilization. Gold (III) salt is reduced to Au^0 atoms by the addition of a reducing agent. As the number of Au^0 atoms that form in solution increase, sub-nanometer particles precipitate. These precipitates then attach to each other and form uniform nanoparticles. This process is called nucleation. Highly monodisperse gold nanoparticles are achieved by rapid nucleation which occurs when the synthesis takes place at high temperatures or with rapid addition of the reducing agent.[39] Stabilization prevents aggregation of the nanoparticles from occurring and will be discussed in the following section.

In 1951, John Turkevich developed an aqueous preparation of colloidal gold by the reduction of gold (III) chloride with sodium citrate.[40] According to this protocol, nanoparticles

are formed by the addition of the reducing agent, sodium citrate ($C_6H_8O_7$), to a boiling $HAuCl_4$ solution. The solution undergoes a color change from yellow to red indicating the formation of gold nanoparticles with diameters approximately 200 nm. Later, in 1973, Frens modified the method by investigating the ratiometric effects of $HAuCl_4$ and sodium citrate on particle size, wherein, higher Au:S ratios resulted in larger nanoparticles and smaller ratio, decreased nanoparticle sizes.[41] Since then, other procedures using reducing agents such as hydroquinone[42] and tetrakis(hydroxymethyl)phosphonium chloride (THPC)[43,44] in aqueous solution have been reported.

Brust *et al.* introduced the preparation of gold nanoparticles in organic media using a two-phase system involving toluene and water. A surfactant, tetraoctylammonium bromide (TOABr) was used to transfer $AuCl_4^-$ ions from the lower aqueous phase to toluene to mix with dodecanethiol where the Au(III) salt is initially reduced to Au(I). Sodium borohydride, $NaBH_4$, was then added to reduce Au(I) in the presence of dodecanethiol to Au^0 and form stable colloidal gold with diameters ≤ 5 nm in toluene.[45]

1.2.2.2 Stabilization of Gold Nanoparticles

The stabilization of nanoparticles is imperative to prevent aggregation of nanoparticles in solution. Stabilization can either occur by electrostatic or steric interactions. Sodium citrate and $NaBH_4$ are common reducing agents as well as surfactants, polymers, and alkanes.[38] Sodium citrate and sodium borohydride serve as reducing agents and electrostatic stabilizers. Equation 1.1 shows that the chloride ions (Cl^-) produced from the reduction process of sodium citrate creates a negatively charged repulsion layer to keep sufficient distance between dispersed nanoparticles. In the Brust method, dodecanethiol was added as a steric stabilizer.[45] The reduction of Au (III) in the presence of the alkane chains allowed for the simultaneous

adsorption onto nanoparticle surfaces and stabilization. Steric stabilizers such as alkane chains, polymers, and surfactants typically have long alkyl chains that are used to keep sufficient distance between particles and prevent aggregation. Additionally, alkane steric stabilizers usually contain thiol or amine head groups because of the affinities of these groups for Au. Figure 1.13 displays a representation of gold nanoparticles stabilized electrostatically and sterically.

$$6AuCl_4^- + C_6H_8O_7 + 5H_2O \longrightarrow 6CO_2 + 24Cl^- + 6Au^0 + 18H^+ \qquad \text{Equation 1.1}$$

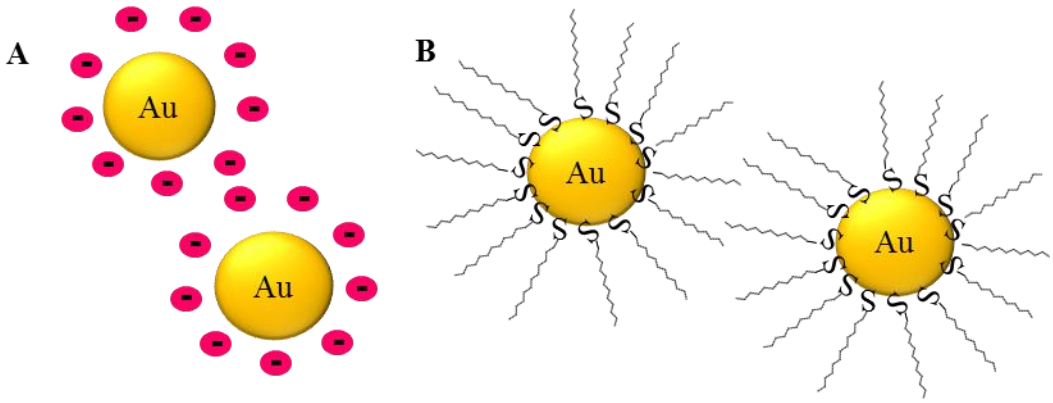

Figure 1.13: Diagram of (A) electrostatic and (B) steric stabilized Au nanoparticles.

1.2.2.3 Gold Surface Chemistry

In 1983, Nuzzo and Allara were the first to report the adsorption of well-defined organic disulfides on planar gold substrates.[46] These self-assembled monolayers or SAMs were part of initial studies to control wetting properties of amphiphile monolayers on metal surfaces.[47] The use of gold as substrates is beneficial in the formation of SAMs because gold is inert, do not form oxides, resist contamination, and has a strong, specific interaction with sulfur (S), disulfides (S-S), and thiols (SH).[46,48] Thiol-derivatized hydrocarbons [$HS(CH_2)_nX$; X= CH_3, OH, COOH, c-C_6H_5] are typically used in SAMs. The preparation of SAMS occurs upon the immersion of a

cleaned gold surface (Au(111)) in a dilute thiol/disulfide solution at room temperature followed by washing in the same solvent and drying under a stream of argon. During immersion, the sulfur-derivatized molecules lie parallel to the gold substrate. As the surface coverage increases, the molecules transition to a standing up (θ= 30°) configuration forming dense thiol lattices.[49] This orientation is specific for alkanethiols; however, the orientations are dependent on the length of the hydrocarbon chain and end groups. A representation of SAMs of alkanethiols is displayed in Figure 1.14.

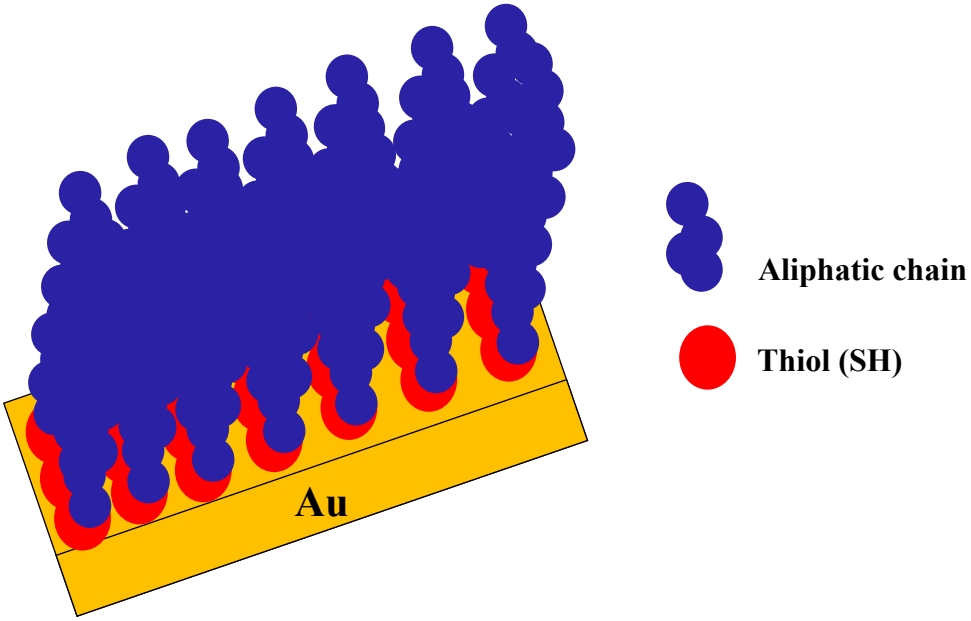

Figure 1.14: Self-assembled monolayer of alkanethiols on gold substrate.

The exact chemistry between sulfur and gold remains a controversial topic, however, it is believed that sulfur atoms chemisorb to gold surfaces forming a strong thiolate-gold bond (S-Au; 40-50 kcal · mol^{-1}). The three main factors that affect the construction of a stable monolayer include the adsorption of sulfur to gold, the interactions between adjacent hydrocarbon chains, and interactions of terminal functional groups with the external medium.[48]

The sulfur chemistry on gold nanoparticles has also been studied.[50,51] Similar to the planar gold substrates, nanoparticles exhibit an increased number of atoms which creates enhanced synergy between SAMs and gold nanoparticles. The alkyl chains of SAMs serve as physical barriers between neighboring particles. However, alkanethiols differ due to the chemical reactivity between the thiol and gold surface.[51] Data from X-ray photoelectron spectroscopy (XPS) of thiol-capped gold nanoparticles has shown signals characteristic of thiolate-gold bonds.[49,52] Differences between Au(111) and gold nanoparticles were attributed to chain orientation on the nanoparticle surfaces. Small particles (< 4 nm) displayed higher binding energies which were attributed to the defects on the nanosurface since thiolates strongly bond in the defect areas.[49]

Contrary to thiols, amines (NH_2) do not form ordered, stable, packed monolayers on planar Au surfaces from solution. Bigelow *et al.* investigated the spontaneous adsorption of amines onto Au(111) surfaces in ethanol similar to the formation of thiol-based SAMs.[53] It was determined that the Au-N interaction was not strong enough to overcome solvent interactions. However, amines are able to form SAMs in low polarity[53] solvents and the vapor phase. Xu *et al.* utilized in situ Fourier transform infrared-external reflectance spectroscopy (FTIR-ERS) and found that vapor phase SAMs of amines remained stable for hours through Au-N and interchain van der Waals interactions. A few years later, Leff *et al.* stabilized gold nanocrystals with primary alkylamines with diameters ranging from 25-70 Å (2.5 nm – 7 nm) in the solution phase. Through a variety of characterization techniques, they concluded nanocrystal stability was due to weak covalent bonds between charge-neutral gold/amine interactions and finite size effect.

1.2.2.4 Ionic Liquids as Stabilizers for Gold Nanomaterials

Thiol-functionalized imidazolium-based ILs have been used to form and stabilize gold,[54,55,56] platinum,[54] and palladium[57] nanoparticles. Stable, monodispersed nanoparticles ranging from 2 nm to 10 nm were prepared by reducing $HAuCl_4$ in the presence of the ILs. The tailoring advantages of ILs played a role in the preparation of gold nanoparticles, wherein, nanoparticle size was tuned by changing the Au:S molar ratio,[56] increasing the amount of thiol groups on the imidazolium cation,[54] or exchanging the anion.[55,57] Kim *et al.* reported other advantages of ionic liquid stabilization such as the solvation and stabilization of metal ionic species is more favorable in ionic liquids rather than conventional solvents, and the removal of ionic liquids is easier because of the difference in solubility.[54,57]

1.2.2.5 Optical Properties of Gold Nanoparticles

The optical properties of gold nanoparticles make them useful as facile and economical sensors in environmental, electrochemical,[58] and biological applications. The optical properties are a result of the localized surface plasmon resonances (LSPR) produced by the particles upon exposure to light. This phenomenon is unique to metallic nanomaterials involving the free conduction electrons surrounding the material and an incident electromagnetic wave.[59] It is strongly dependent on shape,[59,60] size,[61] aggregation,[62] and surrounding medium.[63] Upon irradiation, the electrons oscillate (plasmon resonance) in response to the electromagnetic field. For smaller nanoparticles, the oscillation frequency is higher which yields a lower wavelength of absorption, while the larger nanoparticles red shift to longer wavelengths due to electromagnetic retardation of the oscillation frequency. Hence, for particles ~20 nm, the absorption maximum is approximately 520 nm and larger particles (~100 nm) absorb at longer wavelengths. In the same manner, the blue-green absorption of smaller nanoparticles transmit red which gives rise to the

deep red color of the colloidal solution. The colors of colloidal gold solutions strongly depend on the sizes of the nanoparticles as illustrated in Figure 1.15.

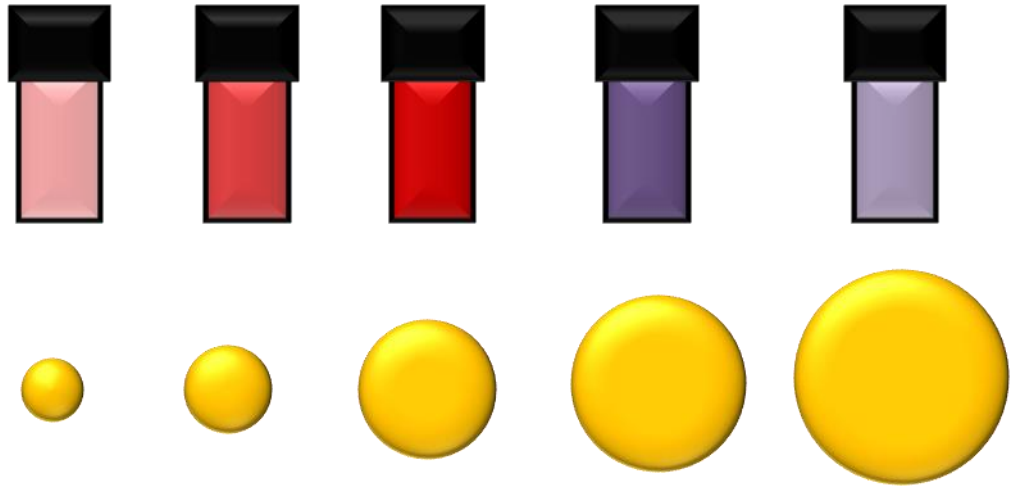

Figure 1.15: Color changes of gold colloidal solutions with respect to size.

1.2.2.6 Applications of Gold Nanoparticles

The unique properties of gold nanoparticles are suitable for a range of applications in fields such as catalysis,[38] sensors,[58,36] and medicine.[39] Mirkin *et al.* have extensively studied DNA and protein-modified gold nanoparticles.[52] For example, DNA-modified gold nanoparticles were used to target complementary DNA. Once the complementary DNA was detected, a polymeric network was formed inducing a subsequent color change of the DNA-modified gold nanoparticle solution from red to purple as illustrated in Figure 1.16. The color change also resulted in an absorbance shift from 520 nm to 574 nm suggesting surface modification induced aggregation.

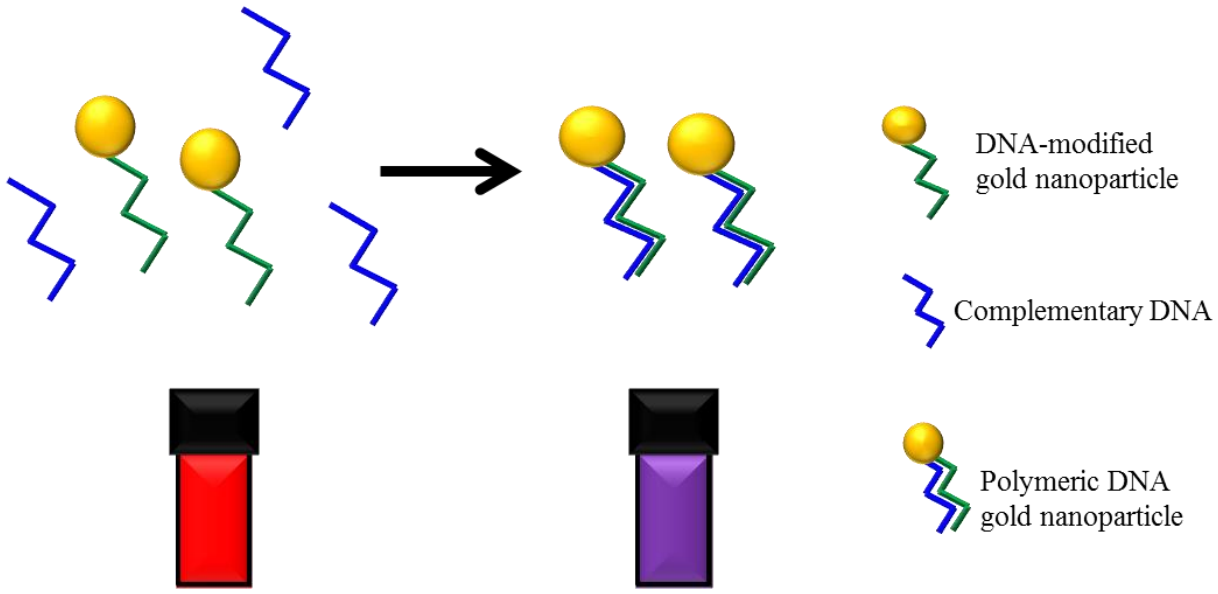

Figure 1.16: Gold nanoparticles used as colorimetric biosensor.

El Sayed *et al.* also utilized the scattering and absorption properties of gold nanoparticles as contrast agents for the *in vitro* detection[64] and photothermal treatment[65,66] of cancer cells. Gold nanoparticles were modified with cancer biomarker epidermal growth factor receptor (EGFR) antibodies. Dark-field imaging techniques were used to locate anti-EGFR conjugated gold nanoparticles that attach to cancer cells. Malignant oral cancer cells were distinguished from adjacent normal cells due to the strong scattering of gold nanoparticles. The same conjugated gold nanoparticles were also exposed to a visible argon laser for selective *in vitro* photothermal therapy, requiring less than half of the laser power in comparison to benign cancer cells.

A limitation of using gold nanoparticles in biological systems is that the gold nanoparticles are unable to scatter or absorb beyond the visible region of the electromagnetic spectrum. On the other hand, wavelengths into the NIR region increase biological applications since tissues are optically transparent in this region.[67] Therefore, *in vivo* studies through deeper

layers of the skin the tissues become impossible to investigate. One way researchers have overcome this limitation has been the use of core-shell nanoparticles.

1.2.3 Core-Shell Nanoparticles

Core-shell nanoparticles are composite nanoparticles composed of two different materials. One material is the inner core and the other material consists of a thin (~ 1-20 nm) outer shell. Core-shell nanoparticles can be designed to have multiple properties representative of the chosen materials for each component. Core-shell combinations can be classified as organic-organic, organic-inorganic, inorganic-inorganic, inorganic-organic.[68,69] Shell layers may serve purposes such as surface functionalization, increased functionality, stability, and controlled release of the core.[69] These composite materials can be synthesized in different morphologies by coating a core material of a different shape such as rod, tube, or cube. Current applications for core-shell nanomaterials include catalysis,[70,71] electronics,[72,73] and medicine.[74,75]

1.2.3.1 Gold Nanoshells

Gold nanoshells are a type of the core-shell nanomaterial in which a homogenous layer of gold is adsorbed onto the surface of the core material. Pioneered by Oldenburg *et al.*, the preparation of silica-gold core-shell particles can be summarized in four steps: 1) synthesis of amine-functionalized silica particles, 2) synthesis of 2 nm gold seeds,[43,44] 3) attachment of seeds to silica surface, and 4) growth of gold nanoshells.[76] Nanoshell growth occurs in the presence of K_2CO_3/$HAuCl_4$ solution with formaldehyde as a reducing agent. The attached seeds grow and coalesce while excess gold within the solution fills voids to form a complete monolayer around the core material. This protocol has proven successful for the synthesis of silver, palladium, and alloy shells on silica cores,[77,78] and gold and silver shells on polystyrene cores.[79]

An attractive feature of gold nanoshells is the optical sensitivity and tunability they possess. Unlike gold nanoparticles, gold nanoshells absorb within the NIR region of the electromagnetic spectrum (700-1100 nm). This characteristic of gold nanoshells overcome the absorption limitation presented by gold nanoparticles and allows for use *in vivo* studies. The optical tunability can be customized by varying the ratio of the shell thickness and core diameter as illustrated in Figure 1.17. Experimentally, nanoshell thickness can be adjusted by controlling the relative amounts of gold-seeded silica particles and $K_2CO_3/HAuCl_4$ solution. In this case, larger core to shell ratios yield absorption maxima that shift to longer wavelengths. Alternatively, smaller shell to core ratios yield blue-shifted absorption maxima. Similar to gold nanoparticle suspensions, the colors of nanoshell suspensions occur with varying shell thickness of a fixed core diameter as shown in Figure 1.18.

Gold nanoshells are useful tools for biomedical applications such as photothermal therapy[80,81] or drug delivery[50] primarily because of the characteristics of gold. Gold is the most biologically inert metal, rendering it biocompatible and non-cytotoxic. The photothermal applications of gold are due to its strong absorption cross section as well as its ability to transform optical irradiation into heat (hyperthermia).[66,82] When tumor-targeted gold nanoshells accumulate with the cells, a NIR laser is applied inducing a temperature increase within the cell. An increase of 30-35 °C is considered significant enough to result in cellular death.[83] Photothermal therapy is a non-invasive procedure that is specific to cancerous cells, leaving healthy tissues unaffected.[84]

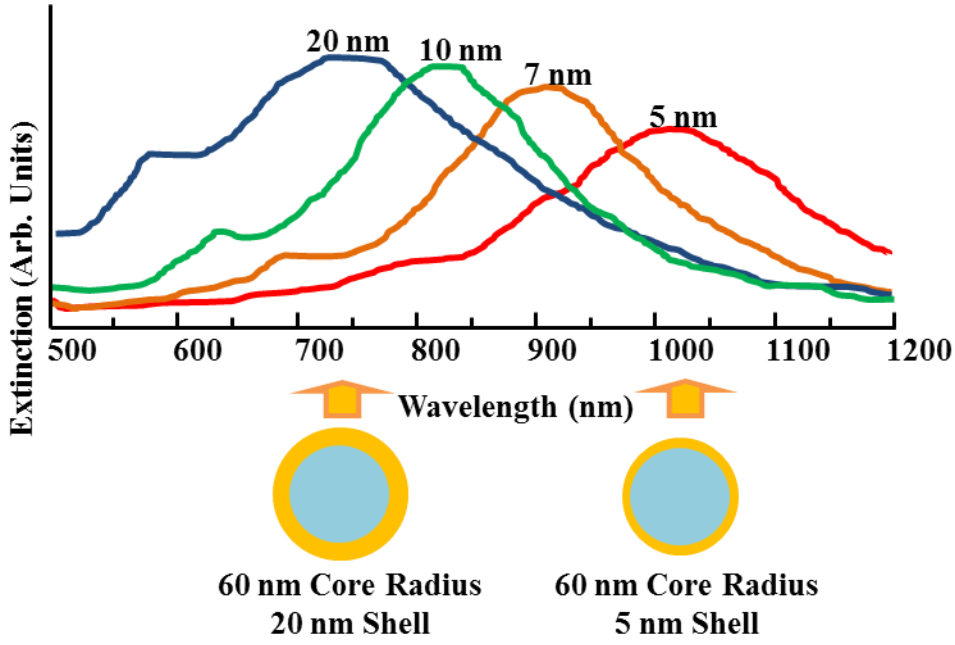

Figure 1.17: Spectral profile of silica-gold core-shell nanoparticles with increasing core:shell ratios inspired by reference 76.

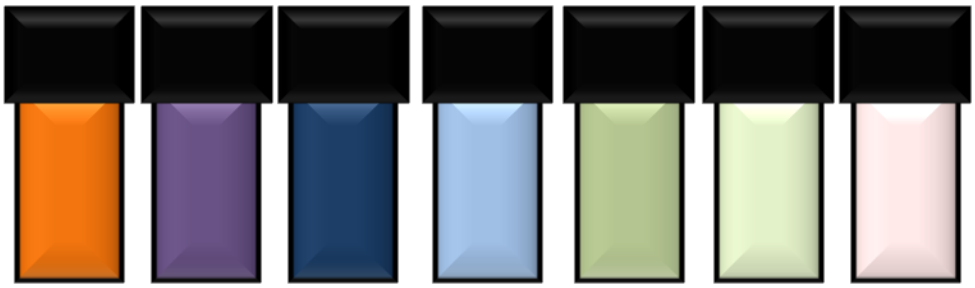

Figure 1.18: Colors of gold nanoshell solutions with various shell thicknesses inspired by reference 76.

There are a few reports of gold nanoshells as potential drug delivery vehicles. In most cases, the gold nanoshells were incorporated within a polymeric hydrogel which undergoes structural changes as a function of systemic thermal adjustments.[50,85] For example, Sershen *et al.* encapsulated gold nanoshells within a polymer hydrogel, poly(N-isopropylacrylamide-co-acrylamide) exhibits a lower critical solution temperature (LCST).[86] The polymer contracts

above the LCST and expands below its LCST. The studies demonstrated that upon irradiation with a NIR, diode laser, the hydrogel-coated gold nanoshells generate heat causing a reduction of its size. The structural transition is reversible once the irradiation is complete and the heat has dissipated. In principle, drug release occurs upon the contraction of the hydrogel-coated gold nanoshells. Berkstein *et al.* applied this concept by monitoring the release of insulin, methylene blue, and lysozyme as model drug molecules before and after irradiation.[87]

Gel systems have also been utilized for drug delivery applications. The next section will describe the characteristics of different types of gels and the significance of gels for efficient drug delivery.

1.3 Gels

Gels are semisolid materials in which a liquid is constrained by a 3D network created by a solid phase (gelator) which are able to absorb and retain significant amounts of solvent. They are jelly-like materials that are mostly liquid but have no mobility in the steady state. Gels are usually named based on the hydrating solvent. Hydrogels are composed of water, organogels involve the use of organic solvents, ILs form ionogels, and liposome solutions create liposomal gels. The term "gels" is understood as hydrogels unless otherwise specified. Gelators are obtained from a class of synthetic or natural polymers. Synthetic polymers include polymethylmethacrylate (PMMA), polyacrylic acid (PAA), or polyethylene glycol (PEG). Chitin/chitosan, starch, pectin, and cellulose are naturally-occurring polymers. Inorganic gelators such as carbon nanotubes and silica/silica nanomaterials can also be utilized. Furthermore, the cross-linking mechanism of the 3D network is classified as physical or chemical. Physical networks are reversible and occur when the network is held together by hydrogen bonding, electrostatic interactions, hydrophobic forces, junctions, or entanglements.

The networks are disrupted when the physical conditions (pH, temperature) of the gel are changed or when stress is applied. Chemical networks are irreversible and the networks are covalently cross-linked. Figure 1.19 displays a few of the physical and chemical cross-linking possibilities within a gel network.

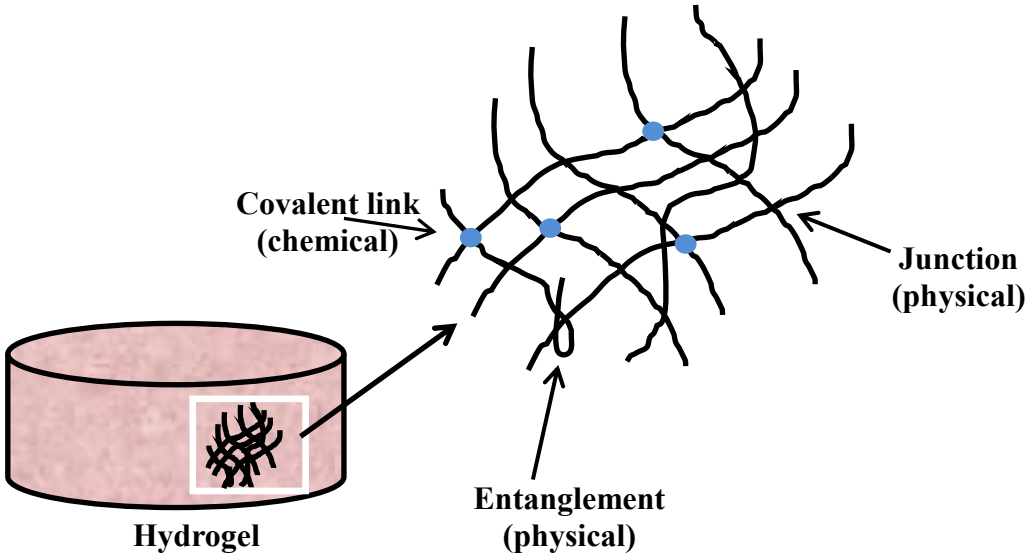

Figure 1.19: Representation of hydrogel system with various chemical and physical interactions.

Gels have been applied to an array of fields such as wound care, dental materials, tissue engineering, cosmetics, food/agriculture, and drug delivery.[88] For drug delivery, gels should be inert, biocompatible, stable, economical, washable with water, ineffective towards the biological nature of the drug, and they should maintain their rheological properties.[89] The properties of gels and their release rates can be tuned by the polymer or combination of polymers,[90] or the nature of liposomes and ILs[91] used in gel preparation.

Gels are favored over creams for drug delivery, particularly as topical agents because they are non-invasive, avoid gastrointestinal complications (pH, absorption, and enzymatic activity), economical, offer controlled release rates, dosage reduction, and minimal side effects.[89]

The following sections will briefly summarize hydrogels and organogels in drug delivery systems; however a more detailed discussion on ionogels and liposomal gels is provided since they are relevant to the work presented in this dissertation.

1.3.1 Hydrogels in Drug Delivery

Hydrogels are the most common gels investigated for drug delivery. The mechanism of action is based on their physical response (*i.e* swelling, shrinking) to environmental stimuli such as pH or temperature. The nature of the polymer determines the type of response for the hydrogel. Polymers often used in pH-sensitive gels are PMMA, PEG, or PAA. These polymers, although hydrophobic, respond by swelling according to changes in pH of the external environment resulting in release of the encapsulated drug.[90] In cases such as PDEAEMA (poly dimethylaminoethylmethacrylate), at pH's above 6.6, the polymer shrinks inducing drug release.[90] Thermo-sensitive gels can be classified as positive or negative thermo-sensitive gels. Negative thermo-sensitive gels contract or shrink at temperatures above their LCST and swell below the LCST. Positive thermo-sensitive gels have upper critical solution temperatures (UCST) and contract when cooled above their UCST.[90] Poly(N-isopropylacrylamide (PNIAA) is a polymer responsible for negative thermo-sensitive gels[85] and polymer PAA is used for positive thermo-sensitive gels.[92]

1.3.2 Organogels in Drug Delivery

The number of organogels reported as drug delivery tools is low. This scarcity is largely due to the limited number of gelators capable of gelling organic solvents and toxicology information on such gelators. Also, there are few pharmaceutically-suitable solvents that can be used.[93] In contrast to hydrogels which use polymers as gelators, organogels utilize low molecular weight organogelators. Organogelators that have been investigated for drug delivery

include lecithin, glyceryl fatty acid esters, poly(ethylene), sorbitan monosterate, *N*-stearoyl l-alanine methyl ester, and acrylic acid-based polymers.[93,94]

1.3.3 Ionogels in Drug Delivery

Ionogels have an advantage over hydrogels and organogels because the use of ILs as the liquid phase adds a second source of tunability to the system since ILs maintain their characteristic properties under the constraints of the 3D network. Therefore, thermally stable and highly conductive ionogels can be synthesized. As a drug delivery system, ionogels are advantageous since ILs can be designed to solubilize hydrophilic or hydrophobic molecules. This feature of ILs circumvents a common problem of low solubility among active pharmaceutical ingredients.[91] As the interest in ILs in biological applications has increased, there has been much attention on the development of biocompatible and biodegradable ILs.[95] These ILs incorporate a biologically-friendly cation or anion into its structure resulting in an IL innate to its structure. Viau *et al.* synthesized an ionogel using an imiadazolium-ibuprofenate IL and silica via a one-step sol-gel process and monitored the release of ibuprofen from the ionogels as well as other non-gel systems.[96] The release rates from the ionogel were more controlled than pure ibuprofen or ibuprofen IL.

1.3.4 Liposomal Gels in Drug Delivery

1.3.4.1 Liposomes

Similar to ILs to ionogels, liposomes add another dimension of tunability to drug delivery of liposomal gels. Liposomes, or lipid vesicles, are spherical, amphiphilic vesicles composed of phospholipid bilayers that form in aqueous solution. Phospholipids mimic the cell membrane and have been used as model drug carrier systems.[97] As previously stated, liposomes are made up of phospholipids. These amphiphilic molecules have two hydrophobic tails per hydrophilic

head. The hydrophilic head is comprised of glycerol, phosphate, and choline groups as shown in the schematic diagram of phosphatidylcholine lipid in Figure 1.20. The choline group may be substituted for other groups such as ethanolamine, glycerol, or serine.[98]

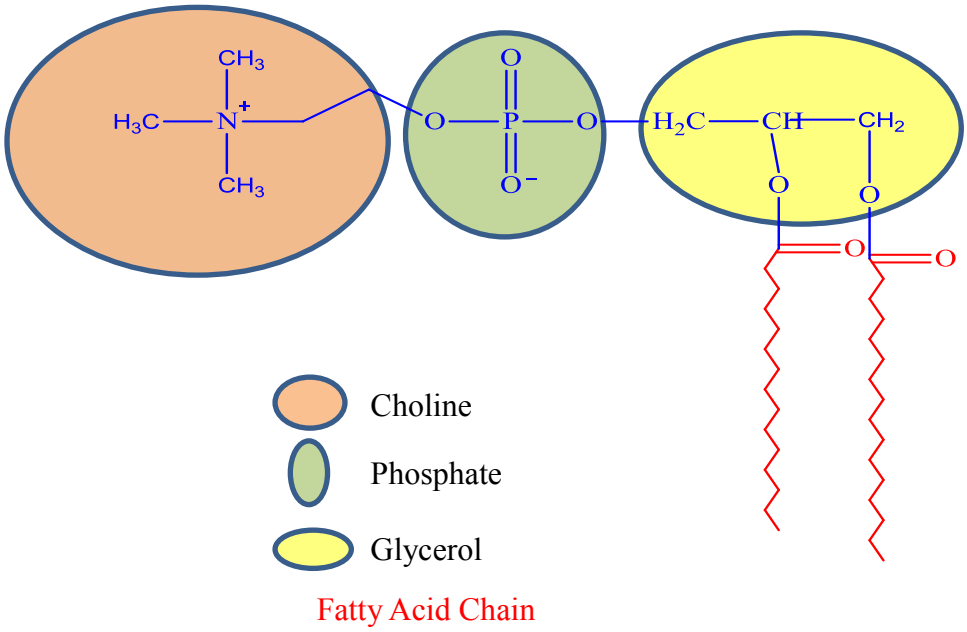

Figure 1.20: Diagram of a phospholipid structure.

The physical properties of phospholipids can be tuned by modifications to the structure and composition. For example, glycerol head groups result in a net negative charge of the phospholipid. Additionally, double bonds within the hydrocarbon chain form unsaturated lipids. Many of these modifications affect the phase transition temperature (T_p) of the phospholipid. The phospholipid hydrocarbon chains are rigid and tightly packed below their T_p and transition to a fluid, liquid-crystalline gel state above its T_p. Figure 1.21 illustrates a representation of the arrangement of the hydrocarbon chains below and above the T_p. The T_p of alkyl chains with double bonds, branches, or bulky side groups is dramatically reduced, in some cases, below room

temperature.[99] The tunable capabilities of phospholipids enable liposomes to be tailored for specific applications.[97,99]

Figure 1.21: Representation of lipid bilayers (a) below and (b) above the phase transition temperature.

In the presence of aqueous medium, phospholipids form spherical structures (liposomes or vesicles) in which the hydrophobic tails orient tail-to-tail forming lipid bilayers as the hydrophilic heads are oriented toward the aqueous medium forming an aqueous core. The lipid bilayer is used for the solubilization of hydrophobic molecules (Figure 1.22). Vesicles are classified based on their size and number of bilayers. Small unilamellar vesicles (SUVs) have diameters from 20 nm to 100 nm and large unilamellar vesicles have diameters between 100 nm and 200 nm. Both SUVs and LUVs consist of a single bilayer. Liposomes with 2 or more bilayers are called multilamellar vesicles (MLVs) and the diameters range from 100 nm to 500 nm.[100]

Several approaches have been developed to prepare liposomes such as lipid film hydration and emulsion.[100] In the hydration procedure, the phospholipid is dissolved in an organic solvent (*i.e.* methylene chloride, chloroform or methanol) or mixture of organic solvents. Thereafter, the solvent is removed by vacuum, evaporation, or lyophilization. The resulting film is hydrated with aqueous-based medium to produce MLV liposomes. For the emulsion protocol,

phospholipids are dissolved in an organic solvent or solvent mixture before addition to the aqueous-based medium under vigorous agitation.

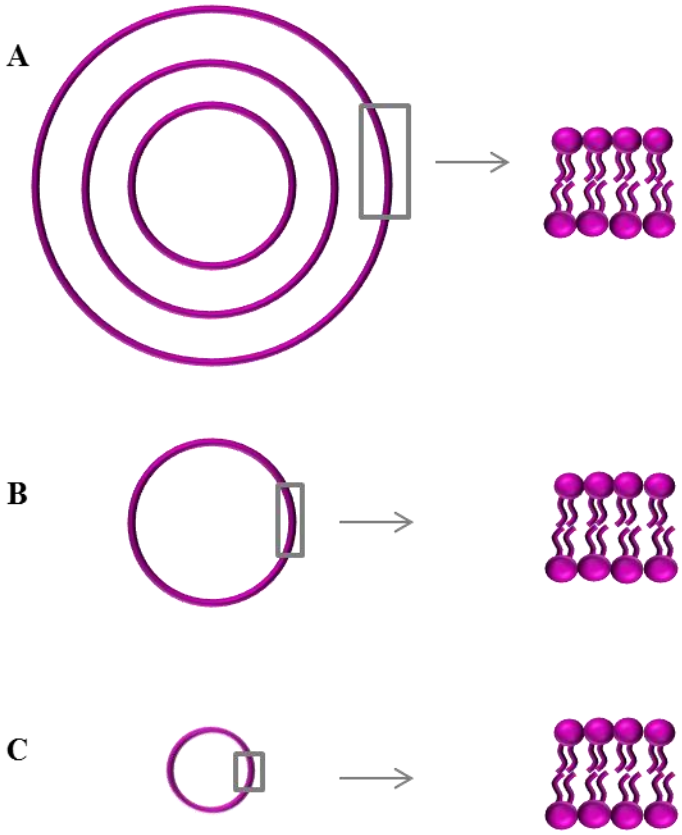

Figure 1.22: Diagram of (a) multilamellar vesicles (MLVs) (b) large unilamellar vesicles (LUVs) and (c) small unilamellar vesicles (SUVs).

High pressure vacuum is used to remove the organic solvent from the biphasic phospholipid mixture with MLVs remaining in aqueous solution. To create LUVs or SUVs from MLVs techniques such as extrusion, sonication and homogenization are utilized.[99,100] All mechanical treatments of liposomal preparation (hydration, sonication, homogenization and extrusion) must occur above the T_p of the higher melting phospholipid comprising the liposome.[100]

Liposomes are quite versatile molecules and may be prepared using single or multiple phospholipids, or additives. Cholesterol is a waxy steroid produced by the liver, and plays an essential role in cell membrane permeability. In liposomes, cholesterol wedges its hydroxyl

group within liposome bilayer facing the aqueous pockets while the steroid and alkyl chain groups lie parallel to the lipid tails. The inclusion of cholesterol has been reported to increase the stability of liposomes for *in vivo* drug delivery applications.[97,100]

The amphiphilic nature of liposomes enables the solubilization of a range of drug molecules regardless of their polarities. The simplicity in preparing various liposomal vesicles permits efficient uptake and delivery of drug molecules. The encapsulation of hydrophilic drugs can be achieved by including the drug in the aqueous component of the preparation procedure. Likewise, dissolving hydrophobic drugs in the organic phases allow for the drug to permeate the liposome bilayers upon hydration once the organic solvent is removed. Specific to the lipid film hydration preparation method of liposomes water-soluble drugs can be dissolved in the aqueous medium. Upon hydration of the film, the drug will be entrapped within the water pockets of the bilayers.

Liposomes are biocompatible, can protect the encapsulated drug from the external environment, increase drug circulation lifetimes, and be designed to be stimuli-responsive (*i.e.* pH, temperature) which has a greater impact on the drug delivery and pharmacokinetic properties of the encapsulated drug. The advantages have rendered liposomes suitable in the areas of pharmaceuticals, medicine, and cosmetics. However, a disadvantage of using liposomes for drug delivery is the rapid leakage of the drug. Leakage is problematic because the effectiveness of the drug dramatically decreases for treatment while drug administration is increased. To compensate for these limitations, liposomal gels have been investigated.

1.3.4.2 Liposomal Gels for Drug Delivery

Liposomal gels have been developed to improve the effectiveness of liposomal drug delivery systems by reducing the release rates of drugs from the liposome and increasing drug or

liposome stability. Liposomes are usually embedded within carbopol or cellulose-based hydrogels.[101] Pavelić *et al.* extensively studied liposomal gels for the treatment of vaginitis.[102,103,104] The bacterial vaginosis medications metronidazole, clotrimazole and chloramphenicol entrapped in phosphatidylcholine-based liposomes were implanted in Carbopol 947P NF gel and studied *in vitro* for controlled release under vaginal conditions. Liposomal gels were ideal due to the limitations associated with vaginosis medications. Metronidazole has a short life time when administered vaginally due to the liquid nature of preparation and produces severe side-effects. Mitkari *et al.* prepared liposomal gels with fluconazole, an antifungal agent, for topical treatments reporting increased skin permeation in gel dispersions versus controls.[105]

1.4 Scope of Dissertation

This dissertation is a discussion of composite materials prepared using nanoGUMBOS with a gold outer layer. NanoGUMBOS and GUMBOS are materials that have similar properties and functionalities of ILs, except that GUMBOS have melting limits of 250 °C. The introduction provides the foundation of the ILs, GUMBOS, nanomaterials, gold nanoparticles, and gels. The first two-thirds of this dissertation outline the preparation, spectral, morphological, and electrochemical properties of GUMBOS and gold-coated nanoGUMBOS. Chapter 3 is a description of 0D nanomaterials which were prepared using reprecipitation and reverse micelle techniques. The reverse micelle method was able to produce nanoparticles of two distinct sizes. The two particle sizes (21 nm and 157 nm) were used to spectroscopically and morphologically monitor the gold-coating process. As the gold layer nears completion, the absorbance maximum red-shifts, followed by a blue shift which is indicative of gold monolayer completion. The application of gold-coated nanoparticles that is discussed herein is the behavior of particles after exposure to organic solvents of various polarities. It was determined that the nanoparticles

spectrally responded to organic solvents based on their densities and boiling points. Chapter 4 is a description of gold-coated 1D nanoGUMBOS. The optical properties of these nanorods were greatly increased which has not been noticed for other gold-coated nanorods or gold nanorods. The electrochemical properties of GUMBOS are also discussed in this chapter since nanorods have increased electron efficiency for electroanalytical applications.

Chapter 5 is a discussion of liposomal ionogel systems that utilize liposomes are gelators rather than polymers as in traditional gels. Saturated and unsaturated phospholipids, DPPC and POPC, respectively, were utilized to investigate the viscoelastic properties of the resulting gels. The mechanical strength of gels prepared using DPPC was similar to crosslinked polymers; whereas, unsaturated POPC gels were not as strong. However, POPC is pH responsive and weakens are low pHs (~4) which is useful for applications such as cancer drug delivery since cancer cells have acidic environments.

1.5 References

1. Welton, T., Room-Temperature Ionic Liquids. Solvents for Synthesis and Catalysis. *Chem. Rev.* **1999,** *99* (8), 2071-2084.

2. Plechkova, N.; Seddon, K., Applications of Ionic Liquids in the Chemical Industry. *Chem. Soc. Rev.* **2008,** *37*, 123-150.

3. Earle, M. J.; Seddon, K., Ionic Liquids. Green Solvents for the Future. *Pure Appl. Chem.* **2000,** *72* (7), 1391-1398.

4. Ngo, H. L.; LeCompte, K.; Hargens, L.; McEwen, A. B., Thermal Properties of Imidazolium Ionic Liquids. *Thermochim. Acta* **2000,** *357–358* (0), 97-102.

5. Hu, Y.-F.; Xu, C.-M., Effect of the Structures of Ionic Liquids on their Physical-Chemical Properties and the Phase Behavior of Mixtures Involving Ionic Liquids. *Chem. Rev.* **2005**.

6. Xu, C.; Sun, L.; Kepley, L. J.; Crooks, R. M., Molecular Interactions Between Organized, Surface-Confined Monolayers and Vapor-Phase Probe Molecules. 6. In-Situ FTIR External Reflectance Spectroscopy of Monolayer Adsorption and Reaction Chemistry. *Anal. Chem.* **1993,** *65*, 2102-2107.

7. Wasserchеid, P.; Welton, T., *Ionic Liquids in Synthesis*. 2nd ed.; Wiley-Vch: 2007.

8. Bonhote, P.; Dias, A.-P.; Papageorgiou, N.; Kalyanasundaram, K.; Gratzel, M., Hydrophobic, Highly Conductive Ambient-Temperature Molten Salts. *Inorg. Chem.* **1996,** *35*, 1168-1178.

9. Walden, P., *Bull Acad. Imper. Sci. (St. Petersburg)* **1914**, 405-422.

10. Hurley, F. H.; Wier, T. P., Electrodeposition of Metals from Fused Quaternary Ammonium Salts. *J. Electrochem. Soc.* **1951,** *98* (5), 203-206.

11. Hurley, F. H.; Wier, T. P., The Electrodeposition of Aluminum from Nonaqueous Solutions at Room Temperature. *J. Electrochem. Soc.* **1951,** *98* (5), 207-212.

12. Wilkes, J. S.; Zaworotko, M. J., Air and Water Stable 1-Ethyl-3-Methylimidazolium Based Ionic Liquids. *J. Chem. Soc., Chem. Commun.* **1992,** *13*, 965-967.

13. Smiglak, M.; Metlen, A.; Rogers, R. D., The Second Evolution of Ionic Liquids: From Solvents and Separations to Advanced Materials—Energetic Examples from the Ionic Liquid Cookbook. *Acc. Chem. Res.* **2007,** *40* (11), 1182-1192.

14. Fei, Z.; Geldbach, T. J.; Zhao, D.; Dyson, P. J., From Dysfunction to Bis-function: On the Design and Applications of Functionalised Ionic Liquids. *Chem. Eur. J.* **2006,** *12* (8), 2122-2130.

15. Jin, X.; Yu, L., Ionic Liquid High-Temperature Gas Sensor Array. *Anal. Chem.* **2006,** *78*, 6980-6989.

16. Nakagawa, H.; Izuchi, S.; Kuwana, K.; Nukuda, T.; Aihara, Y., Liquid and Polymer Gel Electrolytes for Lithium Batteries Composed of Room-Temperature Molten Salt Doped by Lithium Salt. *J. Electrochem. Soc.* **2003,** *150*, A695-A700.

17. Sanes, J.; Carrion-Vilches, F.-J.; Bermudez, M.-D., New Epoxy-Ionic Liquid Dispersions. Room Temperature Ionic Liquid as Lubricant of Epoxy Resin-Stainless Stell Contacts. *e-Polymers* **2007,** *005*, 1-12.

18. Visser, A. E.; Swatloski, R. P.; Reichert, W. M.; Mayton, R.; Sheff, S.; Wierzbicki, A.; Davis, J. J. H.; Rogers, R. D., Task-Specific Ionic Liquids for the Extraction of Metal Ions from Aqueous Solutions. *Chem. Comm.* **2001,** (1), 135-136.

19. Tesfai, A.; El-Zahab, B.; Kelley, A. T.; Li, M.; Garno, J. C.; Baker, G. A.; Warner, I. M., Magnetic and Nonmagnetic Nanoparticles from a Group of Materials Based on Organic Salts. *ACS Nano* **2009,** *3* (10), 3244-3250.

20. Das, S.; Bwambok, D.; El-Zahab, B.; Monk, J.; de Rooy, S. L.; Challa, S.; Li, M.; Hung, F. R.; Baker, G. A.; Warner, I. M., Nontemplated Approach to Tuning the Spectral Properties of Cyanine-Based Fluorescent NanoGUMBOS. *Langmuir* **2010,** *26* (15), 12867-12876.

21. Jordan, A. N.; Das, S.; Siraj, N.; de Rooy, S. L.; Li, M.; El-Zahab, B.; Chandler, L.; Baker, G. A.; Warner, I. M., Anion-Controlled Morphologies and Spectral Features of Cyanine-Based NanoGUMBOS - an Improved Photosensitizer. *Nanoscale* **2012,** *4* (16), 5031-5038.

22. Dumke, J. C.; El-Zahab, B.; Challa, S.; Das, S.; Chandler, L.; Tolocka, M.; Hayes, D. J.; Warner, I. M., Lanthanide-Based Luminescent NanoGUMBOS. *Langmuir* **2010,** *26* (19), 15599-15603.

23. Li, M.; Ganea, G. M.; Lu, C. F.; De Rooy, S. L.; El-Zahab, B.; Fernand, V. E.; Jin, R. Y.; Aggarwal, S.; Warner, I. M., Lipophilic Phosphonium-Lanthanide Compounds with Magnetic, Luminescent, and Tumor Targeting Properties. *J. Inorg. Biochem.* **2012,** *107* (1), 40-46.

24. Bwambok, D. K.; Marwani, H. M.; Fernand, V. E.; Fakayode, S. O.; Lowry, M.; Negulescu, I.; Strongin, R. M.; Warner, I. M., Synthesis and Characterization of Novel Chiral Ionic Liquids and Investigation of their Enantiomeric Recognition Properties. *Chirality* **2008,** *20*, 151-158.

25. Li, M.; De Rooy, S. L.; Bwambok, D. K.; El-Zahab, B.; DiTusa, J. F.; Warner, I. M., Magnetic Chiral Ionic Liquids Derived from Amino Acids. *Chem. Comm.* **2009,** (45), 6922-6924.

26. de Rooy, S. L.; Li, M.; Bwambok, D. K.; El-Zahab, B.; Challa, S.; Warner, I. M., Ephedrinium-Based Protic Chiral Ionic Liquids for Enantiomeric Recognition. *Chirality* **2011,** *23* (1), 54-62.

27. Cole, M. R.; Min, L.; El-Zahab, B.; Janes, M. E.; Hayes, D.; Warner, I. M., Design, Synthesis, and Biological Evaluation of β-Lactam Antibiotic-Based Imidazolium- and Pyridinium-Type Ionic Liquids. *Chem. Biol. Drug Des.* **2011,** *78* (1), 33-41.

28. Kamalha, E.; Shi, X. Y.; Mwasiagi, J. I.; Zeng, Y. C., Nanotechnology and Carbon Nanotubes; A Review of Potential in Drug Delivery. *Macromol. Res.* **2012,** *20* (9), 891-898.

29. Lu, X. F.; Zhang, W. J.; Wang, C.; Wen, T. C.; Wei, Y., One-Dimensional Conducting Polymer Nanocomposites: Synthesis, Properties and Applications. *Prog. Polym. Sci.* **2011,** *36* (5), 671-712.

30. Huang, Z. H.; Jiang, X. L.; Guo, D. W.; Gu, N., Controllable Synthesis and Biomedical Applications of Silver Nanomaterials. *J. Nanosci. Nanotechnol.* **2011,** *11* (11), 9395-9408.

31. Kumar, C.; Mohammad, F., Magnetic Nanomaterials for Hyperthermia-Based Therapy and Controlled Drug Delivery. *Adv. Drug Deliv. Rev.* **2011,** *63* (9), 789-808.

32. Tesfai, A.; El-Zahab, B.; Bwambok, D. K.; Baker, G. A.; Fakayode, S. O.; Lowry, M.; Warner, I. M., Controllable Formation of Ionic Liquid Micro- and Nanoparticles Via a Melt-Quench-Emulsion Approach. *Nano Lett.* **2008,** *8* (3), 897-901.

33. Qi, L., Synthesis of Inorganic Nanostructures in Reverse Micelles. *Encyclopedia of Surface and Colloid Science* **2006**.

34. Pensa, E.; Cortés, E.; Corthey, G.; Carro, P.; Vericat, C.; Fonticelli, M. H.; Benítez, G.; Rubert, A. A.; Salvarezza, R. C., The Chemistry of the Sulfur–Gold Interface: In Search of a Unified Model. *Acc. Chem. Res.* **2012,** *45* (8), 1183-1192.

35. Das, S.; de Rooy, S. L.; Jordan, A. N.; Chandler, L.; Negulescu, I. I.; El-Zahab, B.; Warner, I. M., Tunable Size and Spectral Properties of Fluorescent NanoGUMBOS in Modified Sodium Deoxycholate Hydrogels. *Langmuir* **2011,** *28* (1), 757-765.

36. Sperling, R. A.; Gil, P. R.; Zhang, F.; Zanella, M.; Parak, W. J., Biological Applications of Gold Nanoparticles. *Chem. Soc. Rev.* **2008,** *37*, 1896-1908.

37. Faraday, M., Experimental Relations of Gold (and Other Metals) to Light. *Phil. Trans. Roy. Soc London* **1857,** *147*, 145-181.

38. Daniel, M.-C.; Astruc, D., Gold Nanoparticles: Assembly, Supramolecular Chemistry, Quatum-Size Related Properties, and Applications toward Biology, Catalysis, and Nanotechnology. *Chem. Rev.* **2004,** *104*, 293-346.

39. Huang, X.; Jain, P. K.; El-Sayed, I. H.; El-Sayed, M. A., Gold Nanoparticles: Interesting Optical Properties and Recent Applications in Cancer Diagnostics and Therapy. *Nanomedicine* **2007,** *2* (5), 681-693.

40. Turkevich, J.; Stevenson, P. C.; Hillier, J., Nucleation and Growth Process in the Synthesis of Colloidal Gold. *Discuss. Faraday Soc.* **1951,** *11*, 55-75.

41. Frens, G., Controlled Nucleation for the Regulation of the Particle Size in Monodispersed Gold Suspensions. *Nature* **1973,** *241*, 20-22.

42. Perrault, S. D.; Chan, W. C. W., Synthesis and Surface Modification of Highly Monodispersed, Spherical Gold Nanoparticles of 50−200 nm. *J. Am. Chem. Soc.* **2009,** *131* (47), 17042-17043.

43. Duff, D. G.; Baiker, A.; Edwards, P. P., A New Hydrosol of Gold Clusters. 1. Formation and Particle Size Variation. *Langmuir* **1993,** *9* (9), 2301-2309.

44. Duff, D. G.; Baiker, A.; Gameson, I.; Edwards, P. P., A New Hydrosol of Gold Clusters. 2. A Comparison of Some Different Measurement Techniques. *Langmuir* **1993,** *9* (9), 2310-2317.

45. Brust, M.; Walker, M.; Bethell, D.; Schiffrin, D. J.; Whyman, R., Synthesis of Thiol-Derivatized Gold Nanoparticles in a Two-Phase Liquid-Liquid System. *J. Chem. Soc., Chem. Comm.* **1994**, 801-802.

46. Nuzzo, R. G.; Allara, D. L., Adsorption of Bifunctional Organic Disulfides on Gold Surfaces. *J. Am. Chem. Soc.* **1983,** *105* (13), 4481-4483.

47. Poirer, G. E., Characterization of Organosulfur Molecular Monolayers on Au(111) Using Scanning Tunneling Microscopy. *Chem. Rev.* **1997,** *97*, 1117-1127.

48. Xu, J.; Li, H.-L., The Chemistry of Self-Assembled Long-Chain Alkanethiol Monolayers on Gold. *J. Colloid Interface Sci.* **1995,** *176*, 138-149.

49. Pensa, E.; Cortés, E.; Corthey, G.; Carro, P.; Vericat, C.; Fonticelli, M. H.; Benítez, G.; Rubert, A. A.; Salvarezza, R. C., The Chemistry of the Sulfur–Gold Interface: In Search of a Unified Model. *Acc.Chem. Res.***2012,** *45* (8), 1183-1192.

50. Erickson, T. A.; Tunnell, J. W., Gold Nanoshells in Biomedical Applications. In *Nanomaterials for the Life Sciences: Mixed Metal Nanomaterials*, Kumar, C. S. S. R., Ed. WILEY-VCH Weinheim, 2009; Vol. 3.

51. Love, J. C.; Estroff, L. A.; Kriebel, J. K.; Nuzzo, R. G.; Whitesides, G. M., Self-Assembled Monolayers of Thiolates on Metals as a Form of Nanotechnology. *Chem. Rev.* **2005,** *105* (4), 1103-1170.

52. Thaxton, C. S.; Georganopoulou, D. G.; Mirkin, C. A., Gold Nanoparticle Probes for the Detection of Nucleic Acid Targets. *Clinica Chimica Acta* **2006,** *363* (1–2), 120-126.

53. Bigelow, W. C.; Pickett, D. L.; Zisman, W. A., Oleophobic Monolayers. Films Adsorbed from Solution in Non-Polar Liquids. *J. Colloid Sci.* **1946,** *1*, 513-538.

54. Kim, K.-S.; Demberelnyamba, D.; Lee, H., Size-Selective Synthesis of Gold and Platinum Nanoparticles Using Novel Thiol-Functionalized Ionic Liquids. *Langmuir* **2004,** *20*, 556-560.

55. Itoh, H.; Naka, K.; Chujo, Y., Synthesis of Gold Nanoparticles Modified with Ionic Liquid Based on the Imidazolium Cation. *J. Am. Chem. Soc.* **2004,** *126*, 3026-3027.

56. Jin, Y.; Wang, P.; Yin, D.; Liu, J.; Qin, L.; Yu, N.; Xie, G.; Li, B., Gold Nanoparticles Prepared by Sonochemical Method in Thiol-Functionalized Ionic Liquid. *Colloid Surf., A: Physicochem. and Eng. Aspects* **2007,** *302*, 366-370.

57. Kim, K.-S.; Demberelnyamba, D.; Yeon, S.-W.; Choi, S.; Cha, J.-H.; Lee, H., One-Phase Preparation of Palladium Nanoparticles Using Thiol-Functionalized Ionic Liquid. *Korean J. Chem. Eng.* **2005,** *22* (5), 717-720.

58. Guo, S.; Wang, E., Synthesis and Electrochemical Applications of Gold Nanoparticles. *Anal. Chim. Acta* **2007,** *598*, 181-192.

59. Myroshnychenko, V.; Rodriguez-Fernandez, J.; Pastoriza-Santos, I.; Funston, A. M.; Novo, C.; Mulvaney, P.; Liz-Marzan, L. M.; Garcia de Abajo, F., Modelling the Optical Response of Gold Nanoparticles. *Chem. Soc. Rev.* **2008,** *37*, 1792-1805.

60. Jana, N. R.; Gearheart, L.; Murphy, C. J., Wet Chemical Synthesis of High Aspect Ratio Cylindrical Gold Nanorods. *J. Phys. Chem. B* **2001,** *105* (19), 4065-4067.

61. Kreibig, U.; Genzel, U., Optical-Absorption of Small Metallic Particles. *Surf. Sci.* **1985,** *156*, 678-700.

62. Elghanian, R.; Storhoff, J. J.; Mucic, R. C.; Letsinger, R. L.; Mirkin, C. A., Selective Colorimetric Detection of Polynucleotides Based on the Distance-Dependent Optical Properties of Gold Nanoparticles. *Science* **1997,** *277*, 1078-1081.

63. Underwood, S.; Mulvaney, P., Effect of the Solution Refractive Index on the Color of Gold Colloids. *Langmuir* **1994,** *10* (10), 3427-3430.

64. El-Sayed, I. H.; Huang, X.; El-Sayed, M. A., Surface Plasmon Resonance Scattering and Absorption Anti-RGFR Antibody Conjugated Gold Nanoparticles in Cancer Diagnostics: Application in Oral Cancer. *Nano Lett.* **2005,** *5* (5), 829-834.

65. El-Sayed, I. H.; Huang, X.; El-Sayed, M. A., Selective Laser Photo-Thermal Therapy of Epithelial Carcinoma Using Anti-EGFR Antibody Conjugated Gold Nanoparticles. *Cancer Lett.* **2006,** *239* (1), 129-135.

66. Huang, X.; Jain, P. K.; El-Sayed, I. H.; El-Sayed, M. A., Determination of the Minimum Temperatre Required for Selective Photothermal Destruction of Cancer Cells Using Immunotargeted Gold Nanoparticles. *Photochem. Photobiol.* **2006,** *82* (2), 412-417.

67. Bashkatov, A. N.; Genina, E. A.; Kochubey, V. I.; Tuchin, V. V., Optical Properties of Human Skin, Subcutaneous and Mucous Tissues in the Wavelength Range from 400-2000 nm. *J. Phys. D: Appl. Phys.* **2005,** *38*, 2543-2555.

68. Kalele, S.; Gosavi, S. W.; Urban, J.; Kulkarni, S. K., Nanoshell Particles: Synthesis, Properties, and Applications *Current Science* **2006,** *91* (8), 1038-1052.

69. Chaudhuri, R. G.; Paria, S., Core/Shell Nanoparticles: Classes, Properties, Synthesis Mechanisms, Characterization, and Applications. *Chem. Rev.* **2011,** *112* (4), 2373-2433.

70. Park, J.-I.; Cheon, J., Synthesis of "Solid Solution" and "Core-Shell" Type Cobalt−Platinum Magnetic Nanoparticles via Transmetalation Reactions. *J. Amer. Chem. Soc.* **2001,** *123* (24), 5743-5746.

71. Park, J.-I.; Kim, M. G.; Jun, Y.-w.; Lee, J. S.; Lee, W.-r.; Cheon, J., Characterization of Superparamagnetic "Core−Shell" Nanoparticles and Monitoring Their Anisotropic Phase Transition to Ferromagnetic "Solid Solution" Nanoalloys. *J. Amer. Chem. Soc.* **2004,** *126* (29), 9072-9078.

72. Maliakal, A.; Katz, H.; Cotts, P. M.; Subramoney, S.; Mirau, P., Inorganic Oxide Core, Polymer Shell Nanocomposite as a High K Gate Dielectric for Flexible Electronics Applications. *J. Amer. Chem. Soc.* **2005,** *127* (42), 14655-14662.

73. White, M. A.; Maliakal, A.; Turro, N. J.; Koberstein, J., "Click" Dielectrics: Use of 1,3-Dipolar Cycloadditions to Generate Diverse Core-Shell Nanoparticle Structures with Applications to Flexible Electronics. *Macromol. Rapid Commun.* **2008,** *29* (18), 1544-1548.

74. Katii, K. S., Biomaterials in Total Hip Replacement. *Colloids Surf. B* **2004,** *39*, 133-142.

75. Wang, X.; Yang, T.; Jiao, K., Electrochemical Sensing the DNA Damage *in situ* Induced by a Cathodic Process Based on Fe@Fe_2O_3 Core-Shell Nanonecklace and Au Nanoparticles Mimicking Metal Toxicity Pathways *in vivo*. *Biosens. Bioelectron.* **2009,** *25*, 668-673.

76. Oldenburg, S. J.; Averitt, R. D.; Westcott, S. L.; Halas, N. J., Nanoengineering of Optical Resonances. *Chem. Phys. Lett.* **1998,** *288* (2–4), 243-247.

77. Kim, J.-H.; Chung, H.-W.; Lee, T. R., Preparation and Characterization of Palladium Shells with Gold and Silica Cores. *Chem. Mater.* **2006,** *18* (17), 4115-4120.

78. Kim, J. H.; Bryan, W. W.; Lee, T. R., Preparation, Characterization, and Optical Properties of Gold, Silver, and Gold-Silver Alloy Nanoshells Having Silica Cores. *Langmuir* **2008,** *24* (19), 11147-11152.

79. Yong, K.-T.; Sahoo, Y.; Swihart, M. T.; Prasad, P. N., Synthesis and Plasmonic Properties of Silver and Gold Nanoshells on Polystyrene Cores of Different Size and of Gold-Silver Core-Shell Nanostructures. *Colloid Surf., A: Physicochem. and Eng. Aspects* **2006,** *290* (1-3), 89-105.

80. Gobin, A.; Lee, M. H.; Halas, N.; James, W.; Drezek, R. A.; West, J. L., Near-Infrared Resonant Nanoshells for Combined Optical Imaging and Photothermal Cancer Therapy. *Nano Lett.* **2007,** *7* (7), 1929-1934.

81. Cole, J. R.; Mirin, N. A.; Knight, M. W.; Goodrich, G. P.; Halas, N. J., Photothermal Efficiencies of Nanoshells and Nanorods for Clinical Therapeutic Applications. *J. Phys. Chem. C* **2009,** *113*, 12090-12094.

82. Huang, X.; Jain, P. K.; El-Sayed, I. H.; El-Sayed, M. A., Plasmonic Photothermal Therapy (PPTT) Using Gold Nanoparticles. *Lasers Med. Sci.* **2008,** *23*, 217-218.

83. Hirsch, L. R.; Stafford, R. J.; Bankson, J. A.; Sershen, S. R.; Rivera, B.; Price, R. E.; Hazle, J. D.; Halas, N. J.; West, J. L., Nanoshell-Mediated Near-Infrared Thermal Therapy of Tumors under Magnetic Resonance and Guidance *Proc. Natl. Acad. Sci. U.S.A.* **2003,** *100* (23), 13549-13554.

84. O'Neal, D. P.; Hirsch, L. R.; Halas, N. J.; Payne, J. D.; West, J. L., Photothermal Tumor Ablation in Mice Using Near Infrared-Absorbing Nanoparticles. *Cancer Lett.* **2004,** *209*, 171-176.

85. Kim, J.-H.; Lee, T. R., Thermo-Responsive Hydrogel-Coated Gold Nanoshells for *In Vivo* Drug Delivery. *J. Biomed. Pharm. Eng.* **2008,** *2* (1), 29-35.

86. Sershen, S. R.; Westcott, S. L.; Halas, N. J.; West, J. L., Indeppendent Optically Addressable Nanoparticle-Polymer Optomechanical Composites. *Appl. Phys. Lett.* **2002,** *80*, 4609-.

87. Bikram, M.; Gobin, A. M.; Whitmire, R. E.; West, J. L., Temperature-Sensitive Hydrogels with SiO2-Au Nanoshells for Controlled Drug Delivery. *J. Control Release* **2007,** *123*, 219-227.

88. Gulrez, S.; Al-Assaf, S.; Phillips, G. O., Hydrogels: Methods of Preparation, Characterisation and Applications in Molecular and Environmental Bioengineering. In *Analysis and Modeling to Technology Applications*, Capri, A., Ed. 2011.

89. Bharadwaj, S.; Gupta, G. D.; Sharma, V. K., Topical Gel: A Novel Approach for Drug Delivery. *J. Chem. Bio. Phy. Sci. Sec. B* **2012,** *2* (2), 856-867.

90. Amin, S.; Rajabnezhad, S.; Kohli, K., Hydrogels as Potential Drug Delivery Systems. *Sci. Res. Essays* **2009,** *3* (11), 1175-1183.

91. Bideau, J. L.; Viau, L.; Vioux, A., Ionogels, Ionic Liquid Based Hybrid Materials. *Chem. Soc. Rev.* **2011,** *40*, 907-925.

92. Soppimath, K. S.; Aminabhavi, T. M.; Dave, A. M.; Kumbar, S. G.; Rudzinski, W. E., Stimulus-Responsive Smart Hydrogels as Novel Drug Delivery Systems. *Drug Dev. Ind. Pharm.* **2002,** *28* (8), 957-974.

93. Vintiloiu, A.; Leroux, J.-C., Organogels and Their Use in Drug Delivery-A Review. *J. Controlled Release* **2008,** *125*, 179-192.

94. Murdan, S., Organogels in Drug Delivery. *Expert Opin. Drug Deliv.* **2005,** *2* (3), 1-17.

95. Hough, W. L.; Smiglak, M.; Rodriguez, H.; Swatloski, R. P.; Spear, S. K.; Daly, D. T.; Pernak, J.; Grisel, J. E.; Carliss, R. D.; Soutullo, M. D.; Davis, J. J. H.; Rogers, R. D., The Third Evolution of Ionic Liquids: Active Pharmaceutical Ingredients. *New J. Chem.* **2007,** *31*, 1429-1436.

96. Viau, L.; Tournae-Peteilh, C.; Devoisselle, J.-M.; Vioux, A., Ionogels as Drug Delivery System: One-Step Sol-Gel Synthesis Using Imidazolium Ibuprofenate Ionic Liquid. *Chem. Commun.* **2010,** *46*, 228-230.

97. Mauer, N.; Fenske, D. B.; Cullis, P., Developments in Liposomal Drug Delivery Systems. *Exper Opin. Biol. Ther.* **2001,** *1*, 1-25.

98. Philippot, J. R.; Schuber, F., *Liposomes as Tools in Basic Research and Industry*. CRC Press, Inc.: Boca Raton, 1994.

99. Szoka Jr., F.; Papahadjopoulos, D., Comparative Properties and Methods of Preparation of Lipid Vesicles (Liposomes). *Ann. Rev. Biophys. Bioeng.* **1980,** *9*, 467-508.

100. Walde, P.; Ichikawa, S., Enzymes inside lipid vesicles: preparation, reactivity and applications. *Biomol. Eng.* **2001,** *18* (4), 143-177.

101. Hoare, T.; Kohane, D. S., Hydrogels in Drug Delivery: Progress and Challenges. *Polymer* **2008,** *49*, 1993-2007.

102. Pavelić, Ž.; Škalko-Basnet, N.; Schubert, R., Liposomal Gels for Vaginal Drug Delivery. *Int. J. Pharm.* **2001,** *219* (1–2), 139-149.

103. Pavelić, Ž.; Skalko-Basnet, N.; Jalsenjak, I., Liposomal Gel with Chloramphenicol: Characterisation and *in vitro* Release. *Acta. Pharm.* **2004,** *54*, 319-330.

104. Pavelić, Ž.; Skalko-Basnet, N.; Jalsenjak, I., Characterisation and *in vitro* Evaluation of Bioadhesive Liposome Gels for Local Therapy of Vaginitis. *Int. J. Pharm.* **2005,** *301*, 140-148.

105. Mitkari, B. V.; Korde, S. A.; Mahadik, K. R.; Kokare, C. R., Formulation and Evaluation of Topical Liposomal Gel for Fluconazole. *Indian J. Pharm. Educ. Res.* **2010,** *44* (4), 324-333.

CHAPTER 2

ANALYTICAL TECHNIQUES

2.1 Ultraviolet-visible Spectroscopy

Ultraviolet-visible (UV-vis) spectroscopy is a technique which measures the amount of light an analyte absorbs upon its exposure to a light source. This exposure excites the molecules within the analyte from a ground state to an excited state. A double beam spectrophotometer, represented in Figure 2.1 is used to measure the amount of light transmitted through the sample. The light which does not transmit is absorbed by the analyte. Different types of light sources produce continuous light over a broad range of wavelengths. Deuterium lamps are utilized for UV wavelengths, whereas, tungsten-halogen lamps are used for vis and NIR wavelengths.[1] The arrays of resulting wavelengths are passed through a monochromator which selects the optimal wavelength for the analyte. The monochromatic beam is split to direct a portion of the beam through the sample as the other portion of the beam goes through the reference cell, which consists of all components of the sample cell except the analyte. The intensity of both beams is measured by detectors which then send the data to a computer with the corresponding absorbance spectrum.

Equation 2.1 describes the relationship between the intensity of light that is directed through the reference (I_o) and the intensity of light which passes through the sample (I). The transmittance (T) is related to absorbance by Equation 2.2, where ϵ is the molar absorption coefficient of the analyte, b represents the path length of the cuvette that holds the sample, and c is the concentration. In a typical UV-vis measurement, a reference solution containing all components of the sample solution except the analyte is measured as a blank. Therefore, the reading given by the sample solution is representative of the analyte only. The direct

relationship between absorbance and concentration is the Beer-Lambert Law (Equation 2.2) which is used for quantitative determination of analyte concentration.[1]

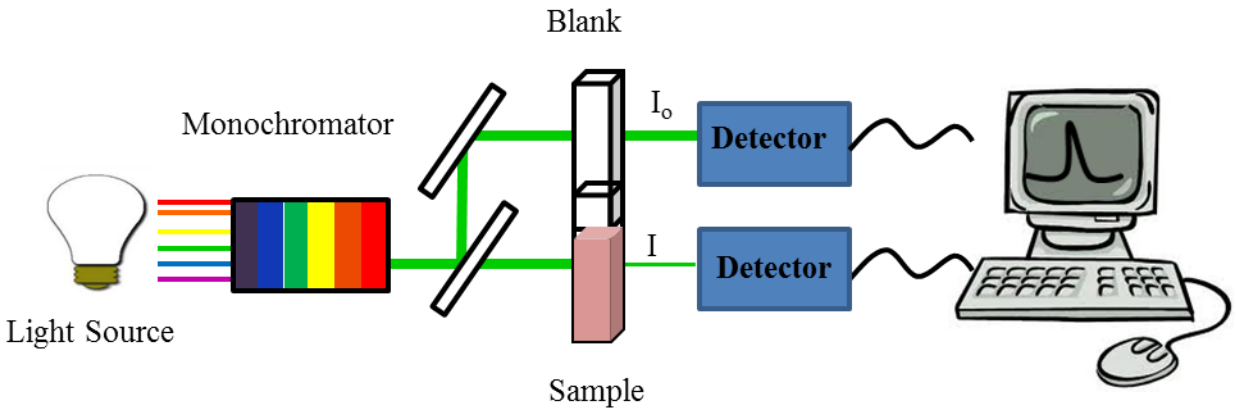

Figure 2.1: Representation of double beam UV-Vis spectrophotometer.

$$T = \frac{I}{I_o} \qquad \text{Equation 2.1}$$

$$\mathrm{A} = -\log T = \epsilon bc \qquad \text{Equation 2.2}$$

2.2 Transmission Electron Microscopy

Transmission electron microscopy (TEM) (Figure 2.2A) uses electrons visualize the morphology of sub-micron structures. Transmission electron microscopes contain four main components: light (electron) source, illumination system, sample, and imaging system all of which are under vacuum. The electron source is usually a tungsten gun which produces a stream of electrons which are then focused through two condenser lenses. This focused beam is further restricted by the condenser aperture, which eliminates high angle electrons, and directed toward the sample. Once the beam reaches the sample, a portion is transmitted and then passed through an objective lens which converts the electrons into an image. The image is then enlarged by the projector lens and displayed on the phosphor screen. The interior of the microscope is placed

under vacuum to minimize scattering of electrons by air molecules. The samples are prepared on carbon-coated copper grids. The darker structures produced by the microscope represent areas in which less electrons are transmitted and are more dense, whereas, the lighter areas depict where more electrons are transmitted and are less dense. Typically, electron sources are accelerated at 80 kV which produces a substantial amount of heat that may damage or melt less rigid materials. Therefore, there are microscopes with lower accelerating voltages (~ 5 kV) which are more suitable for low-melting materials such as nanoGUMBOS.

2.3 Scanning Electron Microscopy

Scanning electron microscopy (SEM) also uses electrons to produce an image, and produce three-dimensional morphological images of sub-micron structures. In addition to providing three dimensional 3D images, SEM offers large depth field and high spatial resolution which enables for a larger area to be magnified with less than 5 nm resolution.[2] Conductive materials are required for SEM samples; therefore, non-conductive samples undergo sputter coating with a conductive material (*i.e* platinum or gold) prior to analysis. Samples are then placed on a metal stub and adhered with conductive tape. A diagram of a scanning electron microscope is illustrated in Figure 2.2B. An electron gun generates a beam of divergent electrons that are then focused using a series of condenser and magnetic lenses. Scanning coils pass the focused beam of electrons along the sample, and the objective lens focuses the beam on the sample. Once in contact with the sample, the electrons are reflected as secondary electrons and captured by the photomultiplier tube detector. The secondary electrons produce the image.[3] A vacuum is maintained to avoid scattering of electrons by air molecules and contamination of the electron guns.

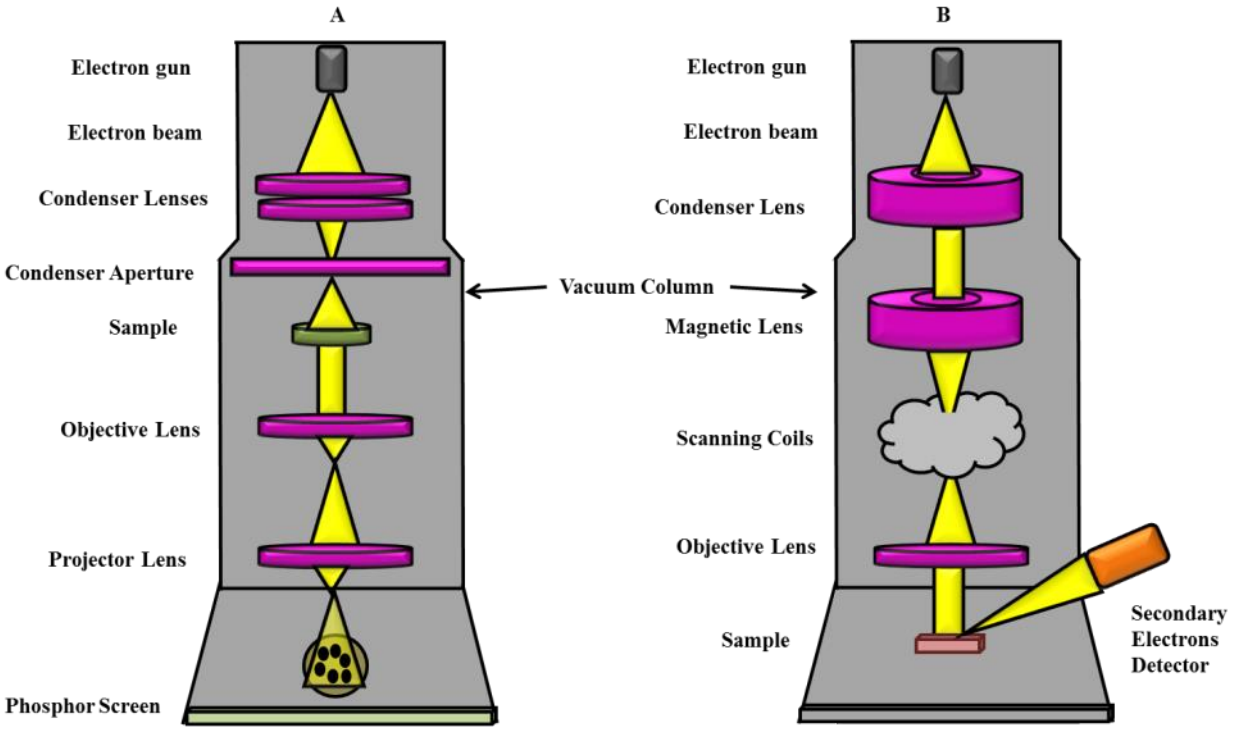

Figure 2.2: Diagrams of a (A) transmission electron microscope and (B) scanning electron microscope.

2.4 Cyclic Voltammetry

Cyclic voltammetry (CV) is a potentiodynamic method used in the determination of formal potentials that occur during electrochemical reactions. It is the most widely used electroanalytical technique because of its simplicity and versatility in determining reduction-oxidation (redox) behavior over a wide potential range.[4] A cyclic voltammeter is composed of four major components: electrochemical cell, potentiostat, current-to-voltage converter, and a data acquisition system as illustrated in Figure 2.3. The electrochemical cell contains the working, reference, and counter electrodes that are submerged in a supporting electrolyte solution. The working electrode is typically made of platinum, gold, silver, or glassy carbon. Common reference electrodes include the normal hydrogen electrode (NHE), Ag/AgCl electrode, or calomel electrode. The counter (auxiliary) electrode is often a platinum wire responsible for

conducting current from the signal source through the solution and to the electrodes. The supporting electrolyte solution contains the analyte and excess non-reactive ions.[1]

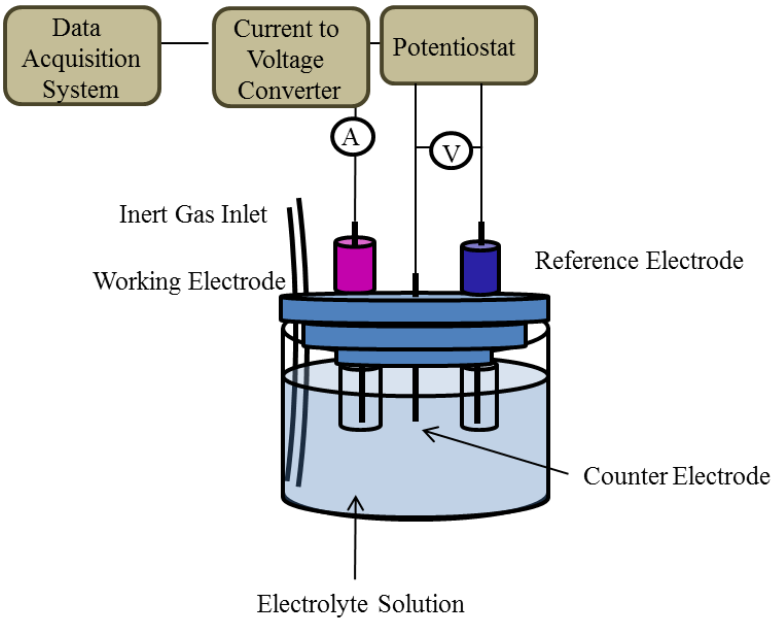

Figure 2.3: Diagram of cyclic voltammeter.

In a typical CV experiment, voltage from a signal source is routed to a potentiostat which maintains a constant potential between the working and reference electrodes while adjusting the current at the counter electrode. The current is converted to voltage via the aptly named current-voltage converter and recorded as a function of time by the data acquisition system.[1] The potential is varied linearly with time between the working electrode and reference electrode which has a known and constant potential. The potential scan produces a triangular waveform excitation signal as shown in Figure 2.4. The potential increases to a maximum or switching potential wherein the analyte obtains sufficient voltage to undergo an oxidation or reduction process (a to b). A scan in the opposite direction occurs decreasing the potential to the original value (b to c). The direction of the initial scan can be negative of positive depending on the

analyte. Scans in the more negative direction are described as forward scans, and scans in the more positive direction are considered reverse scans.[1] The complete scan (a-c) can be repeated several times.

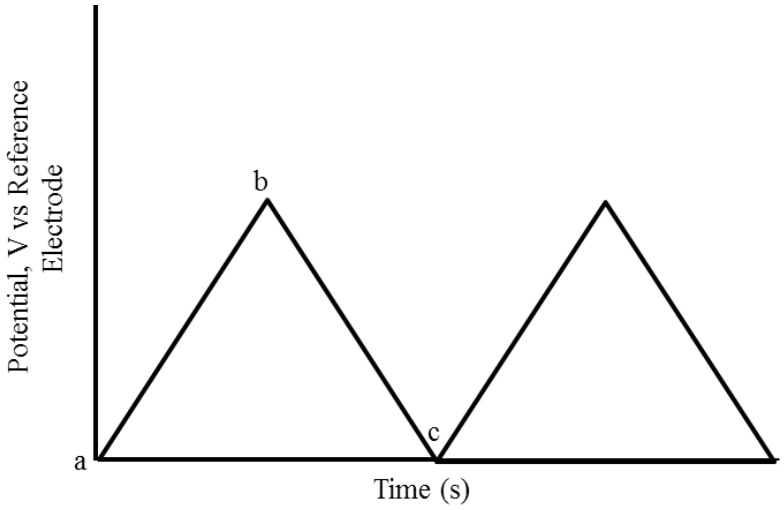

Figure 2.4: Representative excitation signal produced from CV reaction.

The current measured between the working electrode and the counter electrode resulting in a cyclic voltammogram (Figure 2.5). The cyclic voltammogram represents the reversible electrode reaction of ferrocene. E_{pc} and E_{pa} are indicative of the cathodic and anodic peak potentials, respectively. The formal potential for ferrocene electron transfers can be deduced from the half-reaction potentials by using Equation 2.3.

2.5 Rheology

Rheology studies the changes in flow and strain of a material under an applied stress. Stress can be described as the force acting per unit area while strain is the change in dimension per unit length of the material.[5] More specifically, rheology is dedicated to non-Newtonian materials such as polymers, biological fluids, food, gels and suspensions which will be discussed later. Newtonian materials (*i.e* air, water, ethanol, benzene) abide by Newton's law of viscosity.

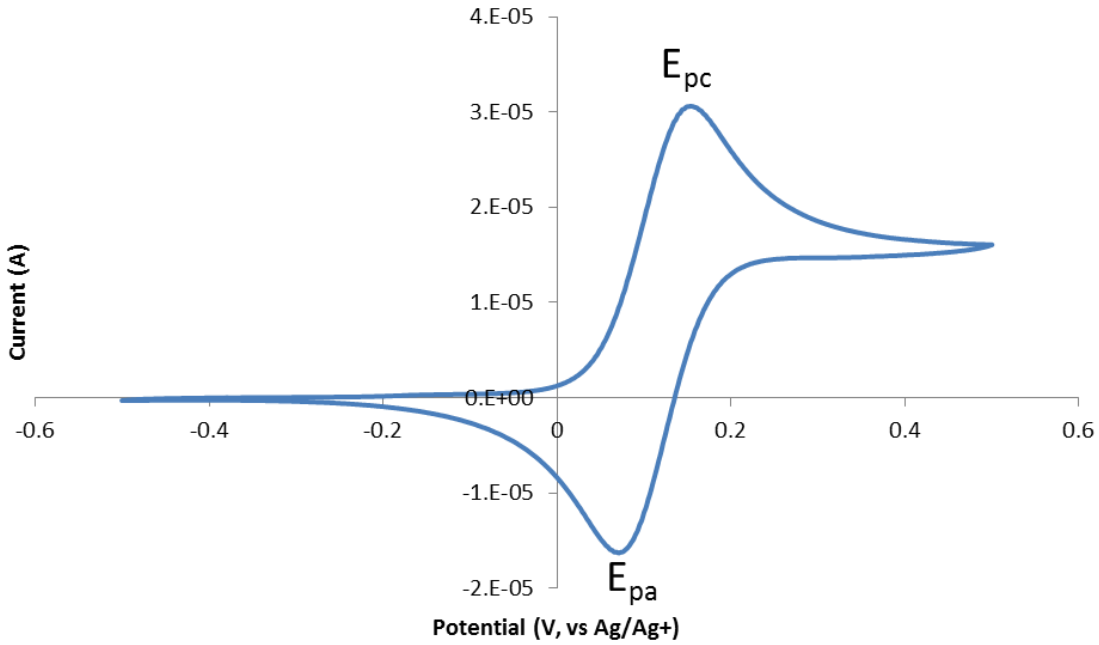

Figure 2.5: Representative cyclic voltammogram.

$$E^o = \frac{E_{pc}+E_{pa}}{2} \qquad \text{Equation 2.3}$$

There are three basic classifications for materials based on the manner its response to stresses or strains.. (i.e. elastic solids, viscous liquids, and viscoelastic materials). Elastic solids experience strain instantaneously and immediately recover to its original structure when the stress is removed. Elastic materials can be further characterized using Hooke's Law (Equation 2.4) which states that shear stress (τ) is directly proportional to shear strain (γ). The proportionality constant (G) is the storage modulus which measures the stored energy within the solid.

$$\tau = G\gamma \qquad \text{Equation 2.4}$$

Viscous liquids initially resist strain and do not fully recover to its original shape when a stress is removed. Liquids are described by Newton's Law of Viscosity (Equation 2.5) where shear stress is directly proportional to the shear stress rate. The proportionality constant, μ, represents Newtonian viscosity. Contrary to the ability of an elastic solid to store energy, viscous materials dissipate or lose energy. The viscosity of liquids is independent of the forces acting on it, the direction of the stress and the shear rate. As seen in Figure 1.29, for Newtonian liquids, when shear stress is plotted against shear strain, the slope (viscosity) is linear through the origin.

$$\tau = \mu \frac{\partial \gamma}{\partial t} \qquad \text{Equation 2.5}$$

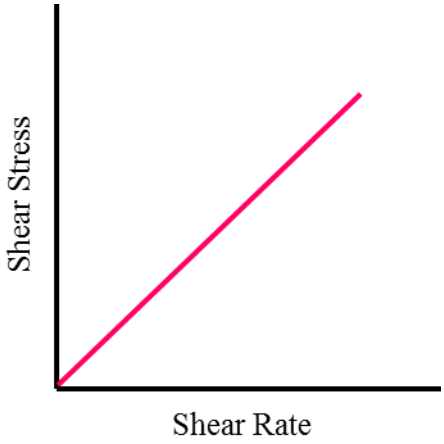

Figure 2.6: Newton's law of viscosity plot.

Viscoelastic materials are considered non-Newtonian materials and possess elastic and viscous characteristics. Under an applied stress, these materials initially resist strain, but will recover to its original shape if given enough time. Two components are used to characterize viscoelastic materials. The elastic portion (G') is the storage modulus which represents the elastic portion of the material, and the viscous portion is represented by the loss modulus (G"). Viscoelastic materials do not abide by Newton's Law of Viscosity; therefore, the viscosity increases or decreases under an applied stress. An increase in viscosity with increasing shear

rate describes the behavior of a shear thinning material; whereas, a decrease in viscosity with increasing shear rate is a shear thickening behavior. Viscoelastic materials exhibit non-Newtonian behaviors.

Rheometers are used to measure the flow behaviors of non-Newtonian materials when stress is applied. There are several configurations of rheometers; however, for the purposes of the studies described herein this dissertation, the cone-plate and parallel plate rheometers (Figure 2.7) will be described. Rheometers continually shear the sample between two surfaces in which either one or both rotate. Measurements can either be strain-controlled where torque is measured at a particular oscillation rate (strain), or stress-controlled where the oscillation rate remains constant and the resulting strain is measured. Cone-plate and parallel plate rheometers are advantageous because only a small amount of sample is required and the instrument is robust to handle highly viscous samples. The cone-plate configuration is designed with an inverted cone at a small angle (< 4°) that rotates just above the base surface. Parallel plate rheometers have an angle of 0° and constrain the sample within a small gap above the base.

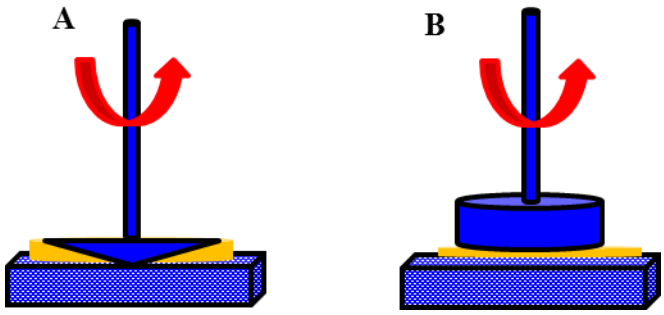

Figure 2.7: Depiction of (a) cone-plate and (b) parallel plate geometries of rotational rheometers.

2.6 Differential Scanning Calorimetry

Differential scanning calorimetry (DSC) is used to identify the types of thermal transitions that occur within polymeric materials. By monitoring the heat flow between the

sample and reference, energy changes such as melting, glass transitions, recrystallization or decompositions can be characterized. The heat flow is measured as a function of time or temperature in a controlled atmosphere.[1] Total heat flow can be written as in Equation 2.6 where H is the enthalpy, C_p is the specific heat capacity and $f(T,t)$ is the kinetic response of the sample.

$$\frac{dH}{dt} = C_p \frac{dT}{dt} + f(T,t) \qquad \text{Equation 2.6}$$

There are three types of DSC configurations: power-compensated DSC, heat flux DSC, and modulated DSC. Figure 2.8 illustrates is a schematic of a heat-flux instrument used in the studies in this dissertation. Heat-flux DSC measures the difference in heat flow between the sample and reference pans within a single furnace. The pans sit on thermoelectric disks which are an alloy of copper and nickel. Heat is transferred through the disks to the material either at a chosen rate (°C/min) or constant temperature. Thermocouples are formed at the Chromel disk and Chromel wire connection at the base of the pans. The sample temperature is monitored at the Chromel-alumel junction under the Chromel disk.[1]

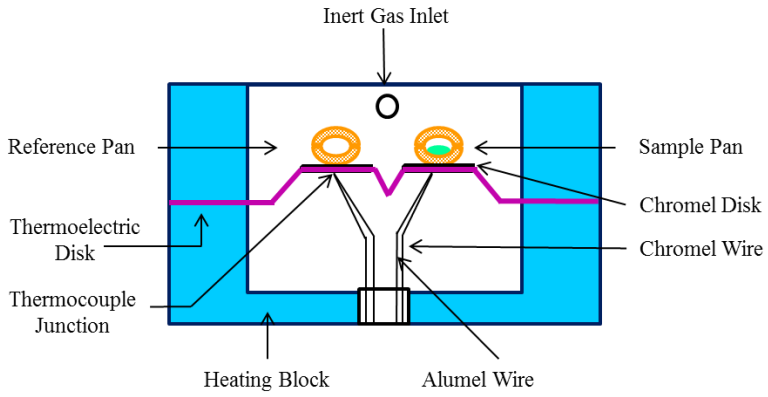

Figure 2.8: Diagram of heat-flux differential scanning calorimeter.

2.7 References

1. Skoog, D.; Holler, F. J.; Crouch, S., *Principles of Instrumental Analysis*. 6th ed.; Saunders College Pub: Philadpelphia, 2007.

2. Hayat, M. A., *Principles and Techniques of Scanning Microscopy*. Van Norstrand Reinhold: 1974

3. Goldstein, J.; Newbury, D. E.; Joy, D. C.; Lyman, C. E.; Echlin, P.; Lifshin, E.; Sawyer, L.; Michael, J. R., *Scanning Electron Microscopy and X-ray Microanalysis*. 3rd ed.; Springer: 2003.

4. Kissinger, P. T.; Heineman, W. R., Cyclic Voltammetry. *Journal of Chemical Education* **1983,** *60* (9), 702.

5. Askeland, D. R.; Fulay, P. P.; Wright, W. J., *The Science and Engineering of Materials*. 6th ed.; Cengage Learning: Stamford, 2011.

CHAPTER 3

GUMBOS-GOLD CORE-SHELL NANOPARTICLES: SYNTHESIS AND CHARACTERIZATION

3.1 Introduction

Core-gold nanoshells which consist of a dielectric core with a thin gold outer layer are known to have absorption and light scattering properties that extend into the NIR region of the electromagnetic spectrum.[1,2,3,4] This feature permits gold nanoshelled particles to be used for biological applications. Since gold nanoshells are highly absorbing in the NIR region where skin and tissues are optically transparent,[5] cancer cells loaded with core-gold shell nanoshells are selectively irradiated without harming surrounding tissues.[6,7,8] These qualities encourage the use of core-gold nanoshells as bifunctional photothermal/chemotherapeutic delivery vehicles.

Silica and polystyrene nanoparticles are commonly used as core materials; however, these materials have rigid physical properties which can limit their potential applications biologically or in other areas. Although silica and polystyrene can be easily functionalized for biocompatibility,[9] they have poor solvating properties,[10] size-dependent toxicity[11] and stability in aqueous media,[10] and have the tendency to accumulate within the body which can cause long-term health effects.[12] To overcome these disadvantages, we use an approach of involving nanomaterials that have tunable properties and can solvate a range of compounds with different polarities, are stable in aqueous environments, and can incorporate biocompatible components innate to its structure, which reduces the need for additional functionalization. This new class of nanomaterials is derived from a group of uniform material based on organic salts (GUMBOS).

Herein, we discuss the preparation and characterization of a number of thiol-functionalized nanoGUMBOS, 1-methyl-3-propylthiol-imidazolium [MImProSH] tetraphenylborate [TPB], 1-methyl-4-propylthiol-pyridinium [PyrProSH][TPB], and

[MImProSH] bis(trifluoromethylsulfonyl)amide [NTf_2] is discussed as proof-of-concept agents that demonstrate their potential use as thiol-functionalized biocompatible materials or drugs as core materials. In addition, the sensing capabilities of these agents were investigated in a series of organic solvents. Two separate techniques were used to prepare nanoGUMBOS prior to monitoring the optical behaviors of gold nanoshell formation and their sensing capabilities. To date, ionic liquids have only been used as templates and stabilizers for gold nanoparticles.[13,14,15] To the best of our knowledge, this is the first report of gold acting as an external layer for ionic liquids/GUMBOS nanoparticles.

3.2 Materials and Methods

3.2.1 Materials

Reagents were purchased at the highest quality available and used as received. Lithium bis(trifluoromethylsulfonyl)amide ($LiNTf_2$), sodium tetraphenylborate (NaTPB), potassium carbonate (K_2CO_3), sodium hydroxide (NaOH), 4-picoline, 1-methylimidazole, tetrakis(hydroxylmethyl)phosphonium chloride (THPC, 80% in water), acetone, formaldehyde (37 wt. % solution in water), isopropyl alcohol (IPA), cyclohexane, Triton X-100, 3-chloro-1-propane thiol, 1-methylimidazole, hydrogen tetrachloroaurate trihydrate ($HAuCl_4$), were obtained from Sigma-Aldrich (St. Louis, MO, USA). Ultrapure water (18.2 MΩ · cm) was obtained using an Elga model PURELAB Ultra water filtration system.

3.2.2 Characterization Techniques

The GUMBOS were characterized using ^{1}H (400 MHz) and ^{13}C NMR (100 MHz) spectroscopies in deuterated dimethylsulfoxide (d_6-DMSO) on a Bruker DPX-400 instrument. The chemical shifts are provided in parts per million (ppm). The elemental compositions were

quantified by Atlantic MicroLab (Norcross, GA). The melting temperature was obtained using a DigiMelt MPA 160 capillary melting point system (Stanford Research Systems, Sunnyvale, CA).

Transmission electron micrographs of nanoGUMBOS were obtained with a LVEM5 microscope (Delong America, Montreal, Canada) with an operating accelerating voltage of 5 kV. A JEOL model 100CX operating at an accelerating voltage of 80 kV was used to collect TEM micrographs of the Au seeds and Au–coated nanoGUMBOS. Samples for TEM were prepared on 400 mesh copper grids coated with an ultrathin carbon support film (Ted Pella, Redding, CA). Specimens were prepared by placing a 2 μL drop of solution onto the grid and allowed to dry at room temperature before analysis.

Absorption analyses were measured in aqueous solution at room temperature using a Perkin Elmer LAMBDA 750 UV/Vis/NIR spectrometer with 10 mm reduced volume quartz cells (Starna Cells, Inc., Atascadero, CA).

3.2.3 Synthesis of GUMBOS

The synthesis of functionalized GUMBOS involved a quaternization reaction followed by anion metathesis as shown in Figure 3.1. A 1:1 molar ratio of 4-picoline and 3-chloro-1-propane thiol were mixed and purged under Ar (g) in the presence of approximately 15 mL of IPA for 20 min. The solution was then refluxed at 80°C for 48 h. Once completely cooled, the solvent was removed under vacuum leaving a slight yellow, hygroscopic residue. The resulting salt [PyrProSH][Cl] was purified by washing with ethyl acetate in triplicate and dried under vacuum. Anion methathesis consisted of separately dissolving [PyrProSH][Cl] and [Na][TPB] (1:1.1 molar ratio) in deionized water. Upon mixing the two solutions, a white precipitate, [PyrProSH][TPB], was immediately formed. Contrary to the hydrophilic reactants, exchange with TPB anion formed a hydrophobic product. The sodium chloride (NaCl) byproduct was

removed by washing in triplicate with deionized water. The same reaction procedures were applied for [MImProSH][TPB], replacing 4-picoline with 1-methylimidazole. The ionic structures of the GUMBOS synthesized in this study are displayed in Figure 3.2.

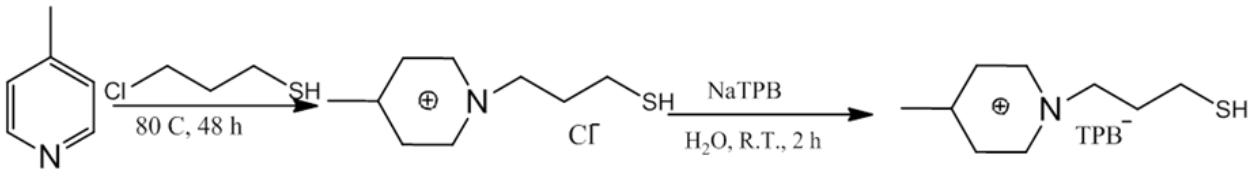

Figure 3.1: Synthesis mechanism of [PyrProSH][TPB] GUMBOS.

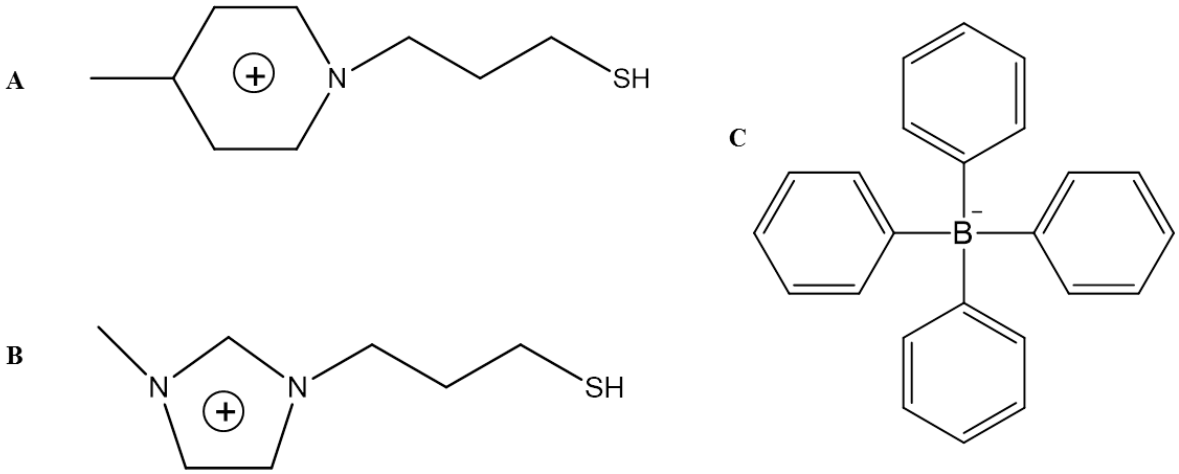

Figure 3.2: Ionic structures of thiol-functionalized GUMBOS: (A) 1-methyl-4-propylthiol-pyridinium, (B) 1-methyl-3-propylthiol-l-imidazolium, and (C) tetraphenylborate.

3.2.4 Preparation of NanoGUMBOS

NanoGUMBOS were prepared by two methods: reprecipitation and reverse micelle. In the reprecipitation procedure, a 100 µL (1mM acetone solution) aliquot of GUMBOS was added to 5 mL of deionized water under bath sonication for 5 min. NanoGUMBOS remained undisturbed to equilibrate for 1 hour and were used as prepared for further characterization.

NanoGUMBOS prepared via the reverse micellar approach (Figure 3.3) were formed in an oil-in-water microemulsion consisting of of 0.4 M Triton X-100 in cyclohexane. Two separate solutions of 3.0 M [MImProSH][Cl] and equimolar [Li][NTf_2] were prepared in water. A 0.040 mL aliquot of aqueous [MImProSH][Cl] solution was added to one of the 8 mL Triton X-100/cyclohexane solutions. Then, a 0.040 mL aliquot of aqueous [Li][NTf_2] solution was added to the other 8 mL Triton X-100/cyclohexane solution. The solutions were stirred separately for approximately 10 min. The two solutions were then combined and stirred for 24 h at room temperature. The resulting nanoGUMBOS were centrifuged at 3200 rpm for 10 min and washed twice with cyclohexane followed by a duplicate rinse with deionized water. Finally, the nanoGUMBOS were resuspended in 5 mL of deionized water for further use. NanoGUMBOS of smaller diameters were prepared using 1.0 M [MImProSH][Cl] and [Li][NTf_2].

3.2.5 Preparation of Gold Seeds and Attachment of Gold Seeds to NanoGUMBOS

Gold seeds of approximately 5 nm in diameter were prepared using a modified method of that previously reported by Duff *et al.*,[16,17] which describes the reduction of $HAuCl_4$ with THPC. A 1.0 mL aliquot of NaOH (0.06 mmol), 2 mL of THPC solution (24 μL of THPC in 2 mL of water), and 200 mL of deionized water were mixed in a 250 mL volumetric flask for 15 min. A 4 mL aliquot of 1% (w/v) aqueous $HAuCl_4$ solution was added to the mixture and continuously stirred for an additional 30 min. The color of the reaction mixture immediately changed from colorless to a dark red-yellow. The solution was aged for at least three days at 4 °C before further use. After aging, the gold colloid solution was observed as brown. Gold seeds were attached by stirring 1 mL of the nanoGUMBOS solution with 5 mL of gold seeds for two days. The mixture was then centrifuged three times and resuspended in water.

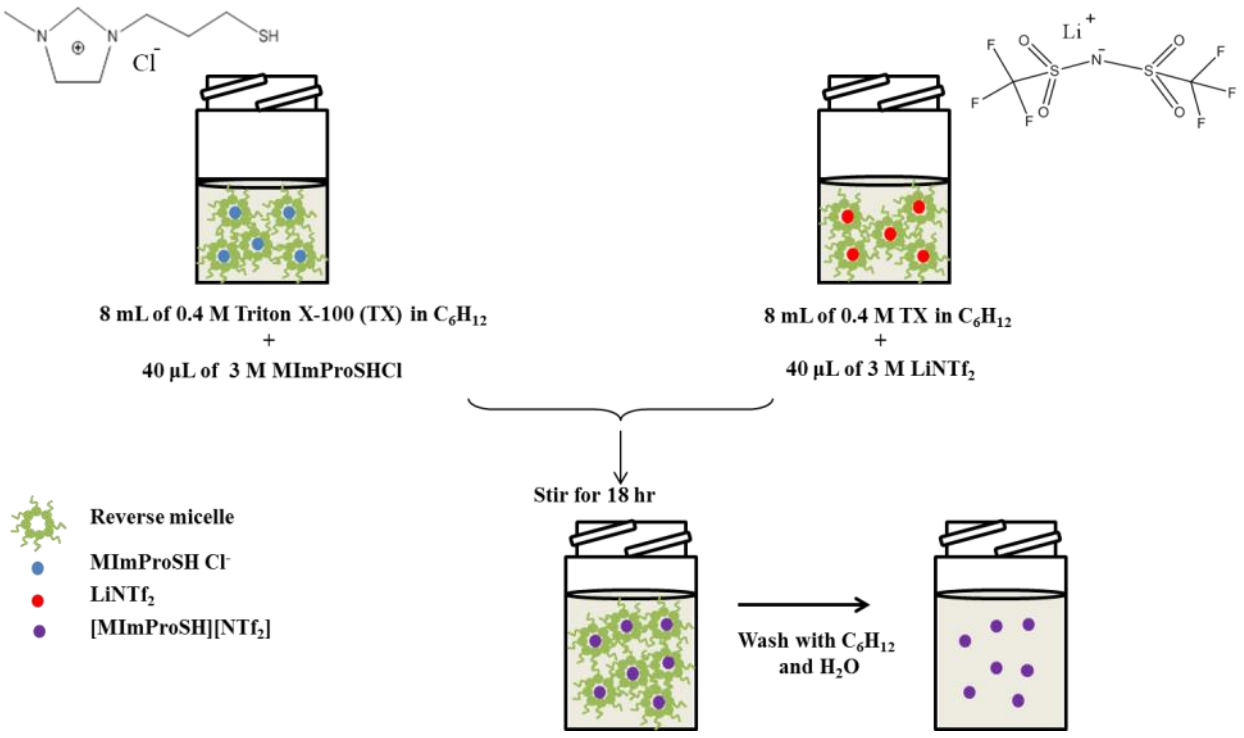

Figure 3.3: Schematic of the reverse micelle procedure for the preparation of [MImProSH][NTf2] nanoGUMBOS.

3.2.6 Preparation of Gold Nanoshells

Gold nanoshells were prepared following a method previously described by Kim *et al.*,[18] wherein a gold hydroxide solution was prepared by dissolving 0.05 g of K_2CO_3 into 200 mL of water and adding a 4 mL of 1% (w/v) $HAuCl_4 \bullet H_2O$ solution. The color of the mixture changed from yellow to colorless within 40 min. It was then aged for one day at 4 °C. Varying volumetric ratios of gold-seeded nanoGUMBOS and gold hydroxide solution were mixed. After 10 min, 0.025 mL of formaldehyde was added. Depending on the shell thickness, the color of the solutions changed from opaque to dark blue after approximately 40 min. The nanoshells were then centrifuged using previous conditions and resuspended in water.

3.2.7 NanoGUMBOS as Organic Solvent Sensors

Gold-coated nanoGUMBOS (1 mL aqueous solution) were separately added to 1 mL of acetonitrile, methanol, and dimethylsulfoxide (DMSO). The two solutions were allowed to equilibrate undisturbed overnight. NanoGUMBOS were separated by centrifugation (2000 rpm for 5 min) and resuspended in 1 mL of deionized water. The absorbance spectra before and after interaction with the organic solvents were measured.

3.3 Results and Discussion

3.3.1 Synthesis and Characterization of GUMBOS

The synthesis of thiol-functionalized GUMBOS was performed in two parts: quaternization of thiol-containing alkyl chain to the pyridinium or imidazolium ring, and anion exchange. By exchanging the chloride anion with the bulky TPB, a solid, hydrophobic salt was formed. Below are the structural and physical characterizations of the thiol-functionalized GUMBOS. The melting points for each GUMBOS are above 100 °C which is in agreement with the definition of GUMBOS.

- **[PyrProSH][TPB]**, white solid, m.p. 134 °C, ^{1}H (400 MHz, d_6-DMSO, δ (ppm): 8.84-8.82 (d, 2H); 7.93-7.91 (d, 2H); 7.13 (d, 1H); 6.89-6.86 (t, 1H); 6.76-6.72 (t, 1H); 4.55-4.52 (t, 2H); 3.31 (s, 1H); 2.54-2.52 (t, 2H); 2.50-2.39 (m, 2H); 2.16-2.09 (t,2H); ^{13}C (100 MHz, d_6-DMSO, δ (ppm): 163.7, 144.4, 136.2, 129.0, 125.9, 122.1, 59.3, 34.9, 22.0, 20.9. Elemental analysis (%) calculated for $[C_6H_{14}NS][B(C_6H_5)_4]$: C, 81.30; H, 7.03; N, 2.87. Found: C, 80.26; H, 7.08; N, 3.01.
- **[MImProSH][TPB],** white solid, m.p. 143 °C, ^{1}H (400 MHz, d_6-DMSO, δ (ppm): 8.45 (d, 2H); 7.54 (d, 2H); 6.77 (d, 1H); 6.36-6.53 (t, 1H); 6.36 (t, 1H); 4.15-4.18 (t, 2H); 2.93 (s, 1H); 2.08 (s, 3H); 2.04-2.14 (m, 2H); 1.74-1.77 (p, 2H); ^{13}C (100 MHz, d_6-DMSO, δ

(ppm): 162.9, 144.3, 136.0, 128.9, 125.8, 122.0, 59.2, 34.8, 21.8, 20.7. Elemental analysis (%) calculated for $[C_6H_{13}N_2S][B(C_6H_5)_4]$: C, 78.14; H, 6.98; N, 5.88. Found: C, 78.50; H, 7.04; N, 6.10.

3.3.2 Preparation and Characterization of Reprecipitation NanoGUMBOS

The reprecipitation method is a facile, additive-free preparation procedure that is reproducible under set conditions. Representative TEM micrographs of [PyrProSH][TPB] nanoGUMBOS achieved using the reprecipitation approach is shown in Figure 3.4A. In this case, spherical and monodisperse nanoGUMBOS were formed with average diameters of 98±11 nm. The absorption spectra of GUMBOS in acetone and nanoGUMBOS suspended in water is shown in Figure 3.4B. GUMBOS display a sharp absorbance maximum at 209 nm while at the nanoscale the absorption spectrum broadens and the maximum shifts to 265 nm.

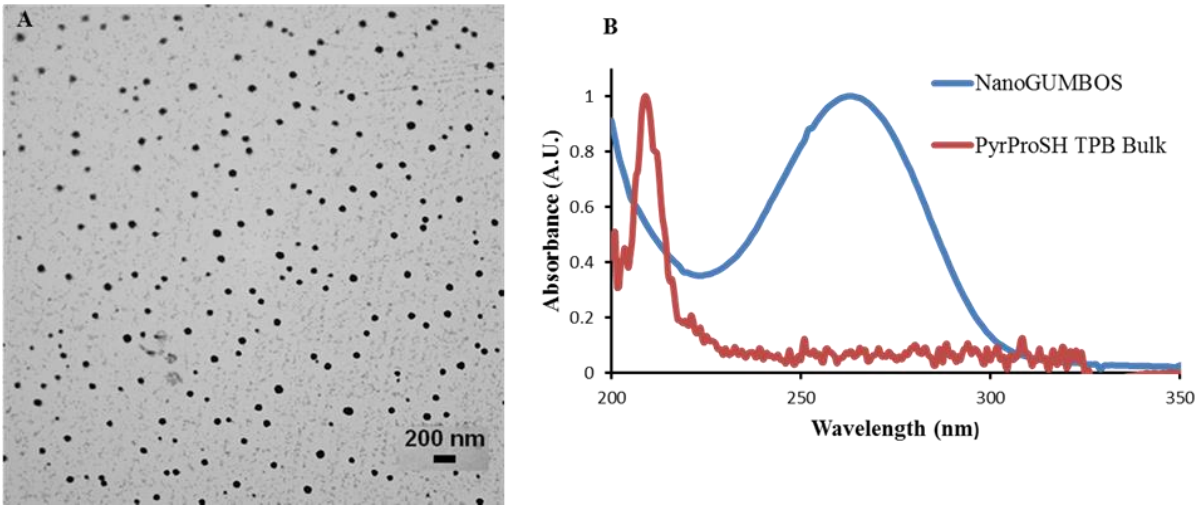

Figure 3.4: (A) UV-vis absorption spectrum of bulk GUMBOS with a λmax of 209 nm and nanoGUMBOS with a λmax of 265 nm and (B) TEM micrograph of [PyrProSH][TPB] nanoGUMBOS formed through the reprecipitation procedure with an average diameter of 98 ± 17 nm.

3.3.3 Preparation, Optimization, and Characterization of Reverse Micellar NanoGUMBOS

In the reverse micelle synthesis of nanoGUMBOS, anion metathesis occurs during nanoparticle preparation. Triton X-100 is a non-ionic surfactant and eliminates the possibility of

ion exchange of surfactant ions with the GUMBOS, which may occur with ionic surfactants such as NaAOT. Initial studies were performed using [MImProSH][TPB] at equimolar reactant ([MImProSH][Cl] and [Na][TPB) concentrations of 0.2 M. This concentration resulted in nanoGUMBOS with average diameters of 53 ± 11 nm. Reactant concentrations of 0.5 M resulted in nanoGUMBOS with average diameters of 74 ± 22 nm with a lesser population density than 0.2 M nanoGUMBOS. Figure 3.5 displays the TEM micrographs of [MImProSH][TPB] nanoGUMBOS at 0.2 M and 0.5 M reactant concentrations. Increasing the reactant concentrations by 2.5 times did not show a quantifiable increase in the nanoGUMBOS size. In addition, concentrations above 0.5 M yielded saturated solutions, which prohibited the dissolution of additional [Na][TPB], thus limiting the maximum size of [MImProSH][TPB] nanoGUMBOS within this system to approximately 74 nm. Therefore, a less hydrophobic anion, [NTf_2], was chosen.

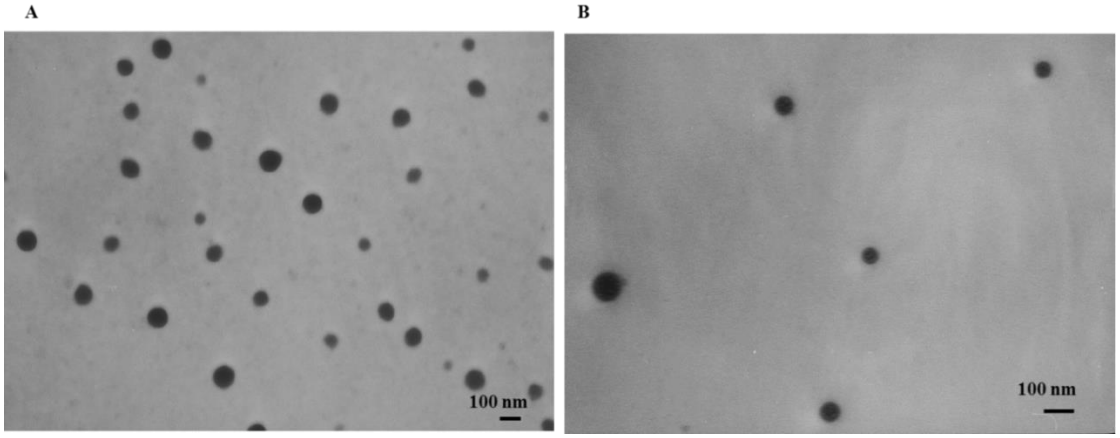

Figure 3.5: TEM micrographs of [MImProSH][TPB] nanoGUMBOS prepared using TX-100 reverse micelle procedure.

In contrast to [MImProSH][TPB], [MImProSH][NTf_2] formed liquid GUMBOS and thus droplets upon nanoformulation. Under the described conditions, nanoGUMBOS with average diameters of 157 ± 47 nm were formed as shown in Figure 3.6A. The size of the nanoGUMBOS can be controlled by adjusting the initial concentrations of the parent compounds

[MImProSH][Cl] and [Li][NTf_2]. Reactant concentrations of 1.0 M yielded nanoGUMBOS with average diameters of 21 ± 5 nm as shown in Figure 3.6B. The use of higher reactant concentrations reduced the polydispersity and the population density of the resulting nanoGUMBOS which can be observed from the two micrographs in Figure 3.6. The relative standard deviation (RSD) for nanoGUMBOS prepared with 3.0 M reactant concentrations shown in Figure 3.6A was over 9 times higher than the RSD for reactant concentration of 1.0 M. This behavior has been observed previously during reverse micelle preparation of [Bm_2Im][BF_4] and [Bm_2Im][$FeCl_4$] nanoGUMBOS. These observations were attributed to higher diffusion collision and ion exchange rates of reactants at higher concentrations which shift the coalescence and decoalescence equilibrium during nanoparticle synthesis.[19]

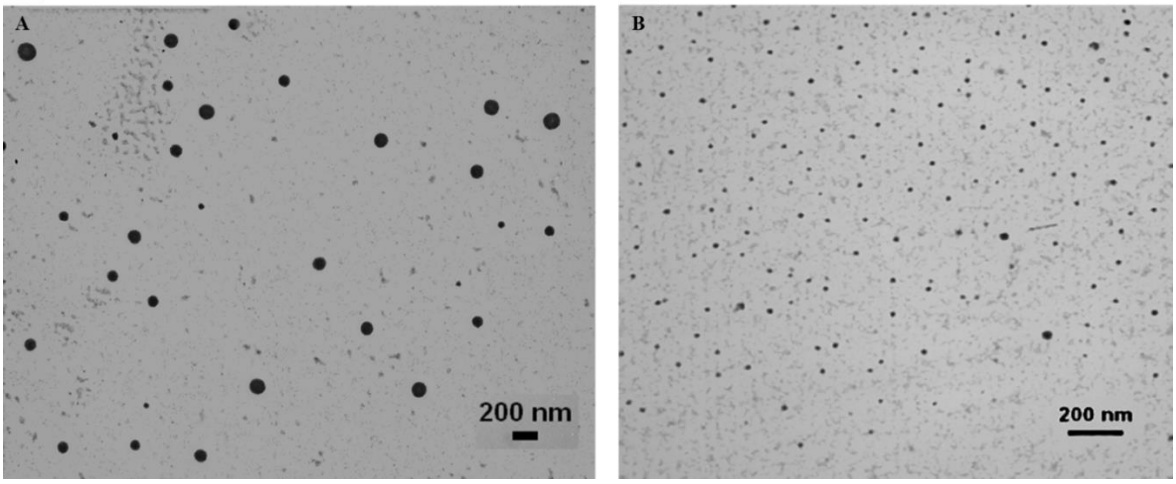

Figure 3.6: Representative TEM micrograph of thiol-functionalized nanoGUMBOS prepared using the reverse micelle methods with average diameters of (A) 157 ± 47 nm and (B) 20 ± 5 nm.

3.3.4 Synthesis of Nanoshell Formation

Nanoshell formation was prefaced with the attachment of gold seeds (~5 nm) onto the surfaces of the thiol-functionalized nanoGUMBOS (Au-seeded nanoGUMBOS) which serve as nucleation sites for the growth of the nanoshell. Figure 3.7 shows the TEM micrograph and UV

absorbance spectrum of Au seeds and 15 nm Au nanoparticles. The absorption of Au seeds has a maximum at 510 nm. There is also a noticeable suppression at 520 nm which is the characteristic absorbance maximum of Au nanoparticles. This behavior is typical of Au particles with diameters below 10 nm.[16,17] Once the Au seeds are attached to the nanoGUMBOS the absorbance plasmon is slightly red-shifted from 510 nm to 513 nm which is attributed to partial aggregation on the surface of the nanoGUMBOS (Figure 3.8).[18] This absorbance plasmon resonance at 513 nm is consistent with Au seeds with 5 nm diameter adsorbed on the surface of other core nanoparticles.[4, 18,20]

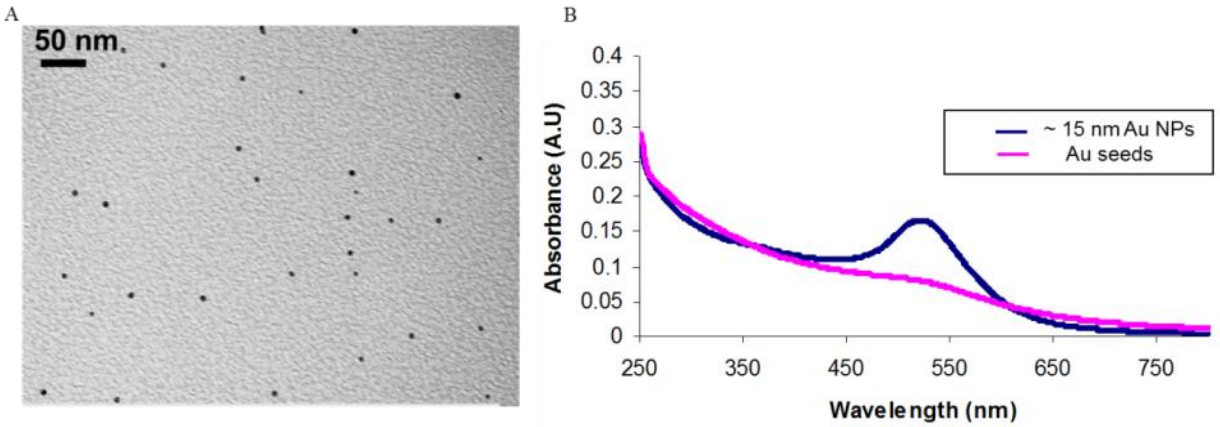

Figure 3.7: (A) TEM micrograph and (B) UV absorbance spectrum of gold seeds.

Nanoshell completion and the corresponding optical properties are dependent on the ratio of the gold hydroxide solution to Au-seeded nanoGUMBOS as explored previously in the literature.[1, 4,20] Ratios between gold hydroxide solution and Au-seeded nanoGUMBOS were investigated for both concentrations of [MImProSH][NTf_2] nanoGUMBOS. Figure 3.9A shows the absorption spectra for 1:1, 2:1, 4:1, 8:1, 20:1, 40:1 ratios of gold hydroxide to 157 nm Au-seeded nanoGUMBOS. Figure 3.9B displays the corresponding TEM micrograph which illustrates the growth process of the nanoshell formation. In the presence of gold hydroxide

solution and the "soft" reducing agent formaldehyde, the seeds adsorbed onto the surface grow and coalesce with adjacent seeds until a partial monolayer of gold covers the nanoGUMBOS.

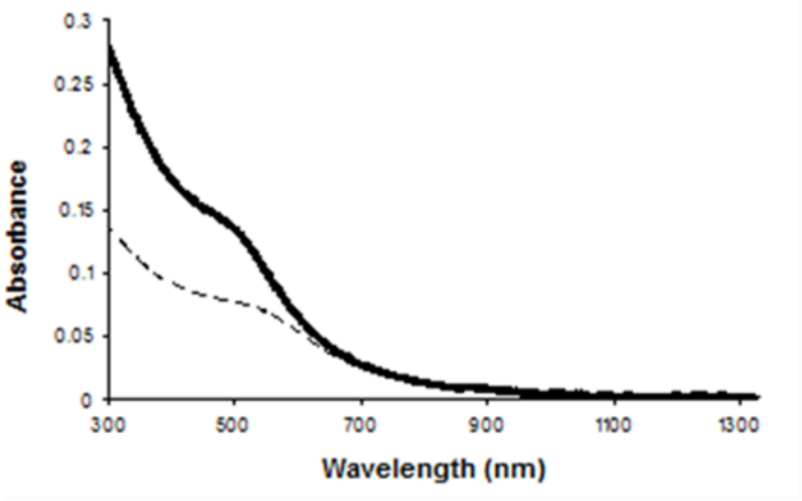

Figure 3.8: Absorption spectra of Au seeds before (solid) and after (dotted) attachment to nanoGUMBOS.

As the amount of gold hydroxide increases, additional gold from the gold hydroxide solution fills the void areas until a complete monolayer is formed. Figure 3.10 displays the solutions of nanoGUMBOS through nanoshell completion.

Spectroscopically, the absorption maxima continuously shifts to longer wavelengths and broadens as excess Au fills the voids on the core surface until coverage is completed. As the nanoshell thickens, the absorbance plasmons begin to shift to lower wavelengths. In the case of the 157 nm nanoGUMBOS, the absorbance maxima are as follows 619, 679, 757, 874, 773, and 715 nm for Au hydroxide : Au-seeded nanoGUMBOS ratios 1:1, 2:1, 4:1, 8:1, 20:1, and 40:1, respectively. This suggests that nanoshells are completely formed at an 8:1 ratio. In addition, the absorbance profile for the 8:1 ratio demonstrates a pronounced, broad peak from 900 to 1100 nm in comparison to the other ratios. The TEM micrographs in Figure 3.9B depict the completion of the nanoshell from ratios 1:1 to 8:1. The images are in agreement with the optical

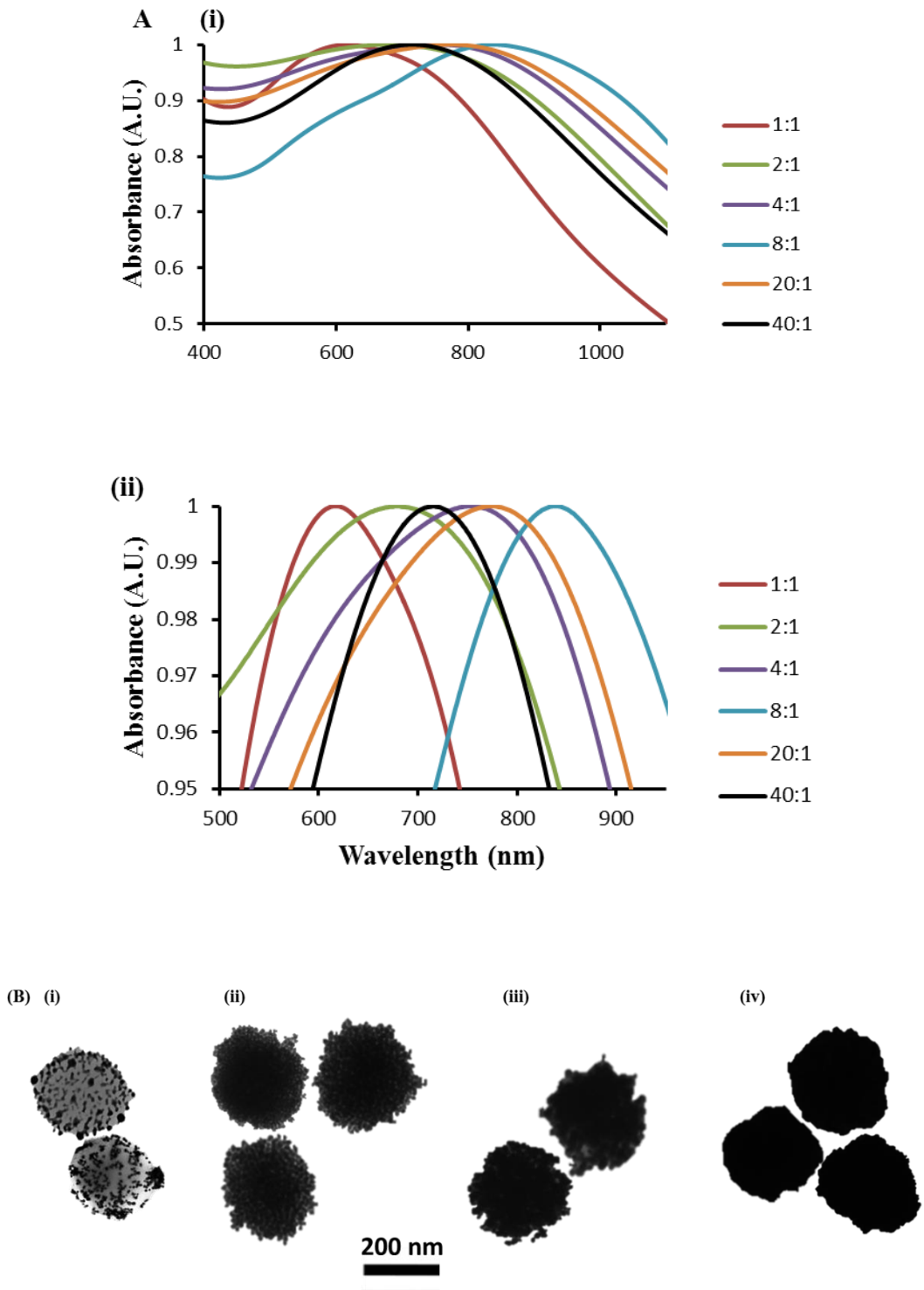

Figure 3.9: (A) Normalized UV/vis absorption spectrum for growth of (i) gold nanoshell on 157 ± 47 nm nanoGUMBOS, and (ii) magnified absorption maxima (B) Evolution of gold nanoshell with increasing ratios of Au hydroxide solution to Au-seeded nanoGUMBOS (i) 1:1, (ii) 2:1, (iii) 4:1, (iv) 8:1.

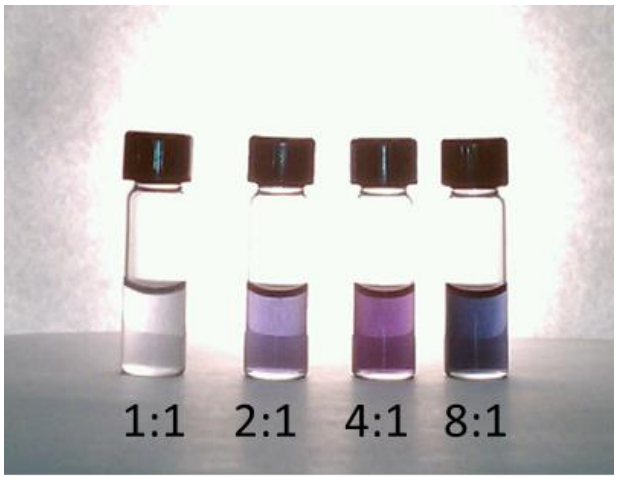

Figure 3.10: Solutions of nanoGUMBOS with increasing coverage of gold nanoshell.

data showing an increased gold coverage as the ratios increase with complete nanoshells at ratio 8:1.

The absorption profiles and related TEM images for 21 nm nanoGUMBOS are projected in Figure 2.11. As the ratio of gold hydroxide solution to nanoGUMBOS was increased from 1:1, 2:1, 4:1, 8:1, and 20:1 on 21 nm diameter cores, the absorbance maxima was recorded as 715, 813, 774, 759, and 733 nm, respectively, indicating that nanoshell formation was completed at the 2:1 ratio. The absorbance plasmon maximum for nanoshell completion on the smaller core nanoGUMBOS occurred 61 nm lower than that of the larger core size. Rasch *et al.* investigated the limitations of Au nanoshell tunability based on various core sizes.[20] It was determined that absorbance plasmon maximum decreases with decreasing core size based on limitations of the seeds' particle diameter. The core to shell ratio determines the absorbance plasmon peaks; thus, restricting the maxima to lower wavelengths for smaller core sizes. The TEM images for the 1:1 and 2:1 ratio display an agglomeration of the particles which contrasts that seen in larger core sizes.

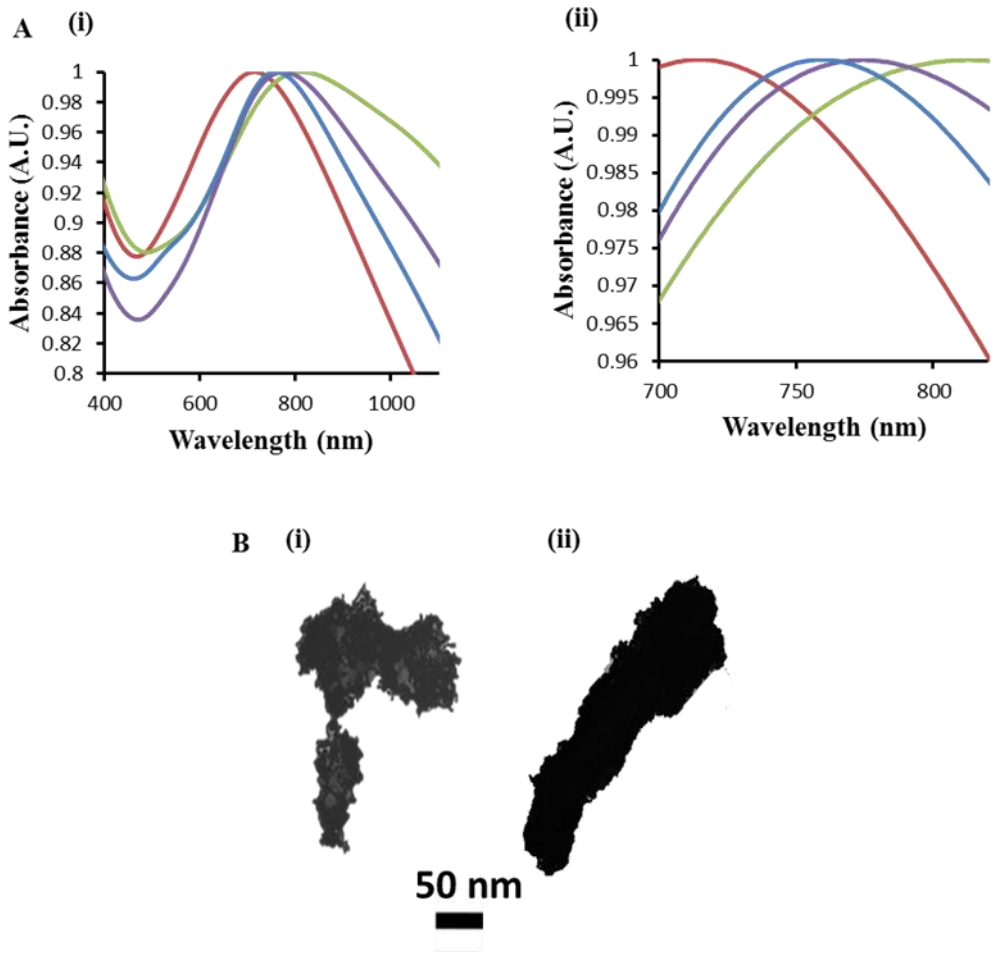

Figure 3.11: (A) Normalized UV/vis spectrum of gold nanoshell growth on (i) 21 ± 5 nm nanoGUMBOS, and (ii) magnified absorption maxima (B) TEM micrograph for nanoshell progression on Au-seeded nanoGUMBOS with increasing ratios from (i) 1:1 (ii) 2:1.

3.3.5 NanoGUMBOS-Gold Core-Shell Nanoparticles as Sensors for Organic Solvents

GUMBOS possess solvating properties that allow them to solubilize or to be solubilized by various solvents. Additionally, GUMBOS are characteristically more porous than other rigid materials such as silica. Therefore, they may absorb their surrounding environment and react by swelling or shrinking. Changes in the core size can be easily monitored by the plasmon resonances of the gold nanoshell. Methanol, acetonitrile, and DMSO were chosen as model solvents because of the range of their polarities. Tables 2.1, 2.2, and 2.3 display the absorbance

shifts observed by 157 nm nanoGUMBOS at various stages in nanoshell formation (2:1, 4:1, and 8:1 gold hydroxide : Au-seeded nanoGUMBOS ratios) after being exposed to the respective solvents. Note that original maximum wavelengths differ from those reported in section 2.3.2; however, the trend remains the same as the plasmon resonances red-shift into the NIR region of the electromagnetic spectrum with increasing ratio. The discrepancies can be attributed to the minor polydispersities from batch to batch preparation of nanoGUMBOS.

At each ratio, bathochromic shifts were observed from the respective original absorption maximum in the order of acetonitrile, methanol, and DMSO. This trend is in agreement with increasing boiling points and densities of the solvents. Furthermore, as the ratios increase to 8:1, the magnitude of the absorption shifts decrease between ratios (2:1 to 4:1, 4:1 to 8:1, or 2:1 to 8:1). The decrease in magnitude shifts with increasing ratios can be attributed to the completion of the gold monolayer. At lower ratios, the core nanoGUMBOS is more exposed to the surrounding and allowed to absorb more of the solvent which causes the nanoparticle to swell inducing a red shift in the absorption behavior. At larger ratios, the nanoshell nears completion and prevents the solvent from interacting with the nanoGUMBOS inducing a decrease in the magnitude of the spectral shifts.

3.4 Conclusion

To the best of our knowledge, this is the first report of core-shell nanoparticles consisting of a nanoGUMBOS core and a gold shell and their corresponding optical properties. Pyridinium and imidazolium thiol-functionalized GUMBOS were synthesized and characterized prior to forming nanoparticles. The reprecipitation technique provided an additive-free, reproducible method for spherical and relatively monodispersed nanoGUMBOS with sizes of 98 nm in diameter. Tunable

nanoparticle sizes were achieved with variable reactant concentrations using the reverse micellar technique.

Table 3.1: Absorption maxima of nanoGUMBOS coated at a 2:1 ratio of Au hydroxide after exposure to various organic solvents. The third column is the difference between the absorbance shift values after exposure to the respective organic solvent and nanoGUMBOS in water.

Solvent	λ_{max} (nm) nanoGUMBOS coated at a 2:1 ratio	Difference Between Organic Solvent Shifts and Water (nm)
Water	**541**	**------**
Acetonitrile	**683**	**142**
Methanol	**765**	**224**
DMSO	**880**	**339**

Table 3.2: Absorption maxima of nanoGUMBOS coated at a 4:1 ratio of Au hydroxide after exposure to various organic solvents. The third column is the difference between the absorbance shift values after exposure to the respective organic solvent and nanoGUMBOS in water.

Solvent	λ_{max} (nm) nanoGUMBOS coated at a 4:1 ratio	Difference Between Organic Solvent Shifts and Water (nm)
Water	**557**	**------**
Acetonitrile	**700**	**143**
Methanol	**760**	**203**
DMSO	**780**	**223**

Table 3.3: Absorption maxima of nanoGUMBOS coated at an 8:1 ratio of Au hydroxide after exposure to various organic solvents. The third column is the difference between the absorbance shift values after exposure to the respective organic solvent and nanoGUMBOS in water.

Solvent	λ_{max} (nm) nanoGUMBOS coated at a 8:1 ratio	Difference Between Organic Solvent Shifts and Water (nm)
Water	**722**	**------**
Acetonitrile	**797**	**75**
Methanol	**800**	**78**
DMSO	**830**	**108**

Gold shell nanoGUMBOS exhibited tunable optical properties relative to particle size and ratio of Au hydroxide solution and Au-seeded particles. Bathochromic shifts were observed for gold-coated nanoGUMBOS in different organic solvents ranging in order of increasing boiling points and densities. In addition, the magnitudes of the shifts decreased as the nanoshell completion increased due to the nanoshell acting as a protective layer for the absorbent nanoGUMBOS.

These materials are quite versatile and can be composed of an array of combinations. Although the GUMBOS discussed in this report are based on imidazolium and pyridinium cations, they can be prepared with multifunctional ions and with pharmaceutically active agents.

3.5 References

1. Oldenburg, S. J.; Averitt, R. D.; Westcott, S. L.; Halas, N. J., Nanoengineering of Optical Resonances. *Chem. Phys.Lett.* **1998,** *288* (2-4), 243-247.

2. Kim, K.-S.; Demberelnyamba, D.; Lee, H., Size-Selective Synthesis of Gold and Platinum Nanoparticles Using Novel Thiol-Functionalized Ionic Liquids. *Langmuir* **2003,** *20* (3), 556-560.

3. Shi, W.; Sahoo, Y.; Swihart, M. T.; Prasad, P. N., Gold Nanoshells on Polystyrene Cores for Control of Surface Plasmon Resonance. *Langmuir* **2005,** *21* (4), 1610-1617.

4. Yong, K.-T.; Sahoo, Y.; Swihart, M. T.; Prasad, P. N., Synthesis and Plasmonic Properties of Silver and Gold Nanoshells on Polystyrene Cores of Different Size and of Gold-Silver Core-Shell Nanostructures. *Colloid Surf.,A: Physicochem. Eng. Aspects* **2006,** *290* (1-3), 89-105.

5. Bashkatov, A. N.; Genina, E. A.; Kochubey, V. I.; Tuchin, V. V., Optical Properties of Human Skin, Subcutaneous and Mucous Tissues in the Wavelength Range from 400 to 2000 nm. *J. Phys. D: Appl. Phys.* **2005,** *38*, 2543-2555.

6. Cole, J. R.; Mirin, N. A.; Knight, M. W.; Goodrich, G. P.; Halas, N. J., Photothermal Efficiencies of Nanoshells and Nanorods for Clinical Therapeutic Applications. *J. Phys. Chem. C* **2009,** *113* (28), 12090-12094.

7. Lal, S.; Clare, S. E.; Halas, N. J., Nanoshell-Enabled Photothermal Cancer Therapy: Impending Clinical Impact. *Acc. Chem.Res.* **2008,** *41* (12), 1842-1851.

8. Loo, C.; Lowery, A.; Halas, N.; West, J.; Drezek, R., Immunotargeted Nanoshells for Integrated Cancer Imaging and Therapy. *Nano Letters* **2005,** *5* (4), 709-711.

9. Wang, L.; Zhao, W.; Tan, W., Bioconjugated Silica Nanoparticles: Development and Applications. *Nano Res.* **2008,** *1*, 99-115.

10. Iler, R. K., *The Chemistry of Silica*. Wiley: New York, 1979; p 49-56.

11. Napierska, D.; Thomassen, L. C. J.; Rabolli, V.; Lison, D.; Gonzalez, L.; Kirsch-Volders, M.; Martens, J. A.; Hoet, P. H., Size-Dependent Cytotoxicity of Monodisperse Silica Nanoparticles in Human Endothelial Cells. *Small* **2009,** *5* (7), 846-853.

12. Nishimori, H.; Kondoh, M.; Isoda, K.; Tsunoda, S.-i.; Tsutsumi, Y.; Yagi, K., Silica Nanoparticles as Hepatotoxicants. *Eur. J. Pharm. Biopharm.* **2009,** *72* (3), 496-501.

13. Itoh, H.; Naka, K.; Chujo, Y., Synthesis of Gold Nanoparticles Modified with Ionic Liquid Based on the Imidazolium Cation. *J. Am. Chem. Soc.* **2004,** *126*, 3026-3027.

14. Kim, K.-S.; Demberelnyamba, D.; Lee, H., Size-Selective Synthesis of Gold and Platinum Nanoparticles Using Novel Thiol-Functionalized Ionic Liquids. *Langmuir* **2004,** *20*, 556-560.

15. Jin, Y.; Wang, P.; Yin, D.; Liu, J.; Qin, L.; Yu, N.; Xie, G.; Li, B., Gold Nanoparticles Prepared by Sonochemical Method in Thiol-Functionalized Ionic Liquid. *Colloid Surf., A: Physicochem. and Eng. Aspects* **2007,** *302*, 366-370.

16. Duff, D. G.; Baiker, A.; Edwards, P. P., A New Hydrosol of Gold Clusters. 1. Formation and Particle Size Variation. *Langmuir* **1993,** *9* (9), 2301-2309.

17. Duff, D. G.; Baiker, A.; Gameson, I.; Edwards, P. P., A New Hydrosol of Gold Clusters. 2. A Comparison of Some Different Measurement Techniques. *Langmuir* **1993,** *9* (9), 2310-2317.

18. Kim, J. H.; Bryan, W. W.; Lee, T. R., Preparation, Characterization, and Optical Properties of Gold, Silver, and Gold-Silver Alloy Nanoshells Having Silica Cores. *Langmuir* **2008,** *24* (19), 11147-11152.

19. Tesfai, A.; El-Zahab, B.; Kelley, A. T.; Li, M.; Garno, J. C.; Baker, G. A.; Warner, I. M., Magnetic and Nonmagnetic Nanoparticles from a Group of Uniform Materials Based on Organic Salts. *ACS Nano* **2009,** *3* (10), 3244-3250.

20. Rasch, M. R.; Sokolov, K. V.; Korgel, B. A., Limitations on the Optical Tunability of Small Diameter Gold Nanoshells. *Langmuir* **2009,** *25* (19), 11777-11785.

CHAPTER 4

TEMPLATED SYNTHESIS OF GUMBOS-GOLD CORE-SHELL NANORODS FOR ELECTRONIC APPLICATIONS

4.1 Introduction

Nanomaterials are interesting because of their tunable optical and electronic properties based on size, shape, and functionalization, especially spherical gold nanoparticles as single or composite materials. However, one dimensional (1D) gold nanomaterials such as nanowires, nanorods, and nanotubes have also demonstrated unique properties. Gold nanorods possess optical profiles that differ from spherical nanoparticles which have been advantageous in biomedical applications. For example, El Sayed *et al.* have studied the optical properties of gold nanorods as effective tools for *in vivo* photothermal therapy and cellular imaging of cancer cells.[1] The nanorods are useful for *in vivo* studies because they absorb in the optically transparent, NIR region of the electromagnetic spectrum, overcoming the UV-vis absorption limitation of gold nanoparticles.[2,3] In addition to biological relevance, nanorods have also been attractive for optoelectronic applications. In particular, semiconducting nanorods offer increased band gaps and efficient electron transfer.[4,5,6]

The overall function of composite nanomaterials is the sum of each component; therefore composite nanomaterials can be designed for simultaneous functionality and determination of specific properties. A few scientists have studied the magnetic[7] and surface[8] properties of composite 1D nanomaterials with a gold shell. Bhattacharya *et al.* reported increased electron density and resulting efficiency of an electrochemical biosensor using ZnO-gold nanorods.[9] There has also been much interest in the preparation and optical properties of silica-gold core-

shell 1D nanostructures[10,11] in response to the changes in the optical properties observed in silica-gold nanoparticles.

The present work describes the synthesis of novel 1D nanomaterials composed of [PyrProSH][TPB] GUMBOS with a gold nanoshell. The chemical structure of [PyrProSH][TPB] is displayed in Figure 4.1. GUMBOS are closely related to ILs having the same tunable and physiochemical properties, differing by melting point limitations. The relation to ILs suggests that GUMBOS have conductive properties for which they may be candidates for electrochemical applications. The combination of inherently tunable and conductive core materials with the electronic properties of gold may result in the development of nanomaterials that have properties preferable compared to conventional electronic nanomaterials. The 1D nanoGUMBOS were prepared following a template method using aluminum oxide (AAO) discs previously reported for the synthesis of fluorescent 1D nanoGUMBOS.[12] In addition to the morphological and optical properties of gold-coated 1D nanoGUMBOS, electrochemical studies of GUMBOS in bulk were investigated for subsequent conductivity measurements.

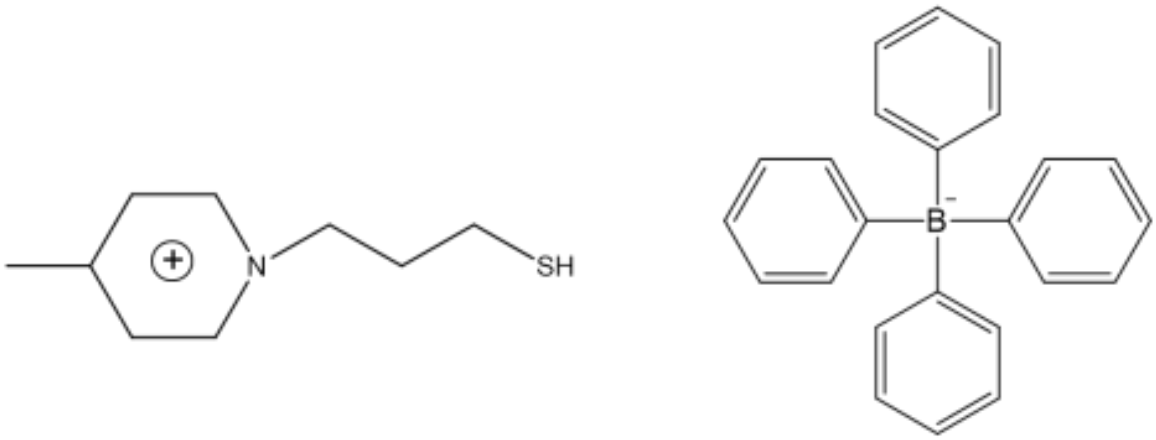

Figure 4.1: Chemical structure of [PyrProSH][TPB].

4.2 Materials and Methods

4.2.1 Materials

Reagents were purchased at the highest quality available and used as received. Sodium tetraphenylborate (NaTPB), potassium carbonate (K_2CO_3), sodium hydroxide (NaOH), 4-picoline, tetrakis(hydroxymethyl)phosphonium chloride (THPC, 80% in water), phosphoric acid, acetone, formaldehyde (37 wt. % solution in water), isopropyl alcohol (IPA), tetrabutylammonium potassium hexafluorophosphate ($TBAPF_6$), ferrocene (bis-cyclopentadienyl iron (II)), acetonitrile, 3-chloro-1-propane thiol, hydrogen tetrachloroaurate trihydrate ($HAuCl_4$), were all obtained from Sigma-Aldrich (St. Louis, MO, USA). Anodic aluminum oxide (AAO) membranes (13 mm disc diameter, 20 μm thickness, and 200 nm pore sizes) manufactured by Whatman were purchased from SPI Supplies and Structure Probe Inc. (West Chester, PA). Ultrapure water (18.2 MΩ · cm) was obtained using an Elga model PURELAB Ultra water filtration system.

4.2.2 Characterization Techniques

Absorbance measurements were performed using a Perkin Elmer LAMBDA 750 UV/Vis/NIR spectrometer with 10 mm reduced volume quartz cells (Starna Cells, Inc, Atascadero, CA). SEM was performed using a SM-6610, JSM-6610LV high and low vacuum scanning electron microscope. Bare nanorods were sputter-coated with platinum under vacuum for 2 min to form a conductive layer necessary for imaging. Micrographs (TEM) were obtained using a JEOL 100CX microscope. Samples were drop cast (2 μL) onto carbon-coated grids and allowed to completely dry.

Cyclic voltammetric measurements were performed using a computer-controlled Autolab Potentiostat equipped with GPES software. The electrochemical cell included a silver/silver

chloride (Ag/Ag^+) reference electrode, platinum working electrode, platinum wire counter electrode, and tetrabutylammonium hexafluorophosphate ($TBAPF_6$) as the supporting electrode.

4.2.3 Preparation of 1D NanoGUMBOS

The synthesis of [PyrProSH][TPB] GUMBOS was performed as previously described in Chapter 2. Prior to 1D nanoGUMBOS preparation, the AAO discs were cleaned using duplicate acetone, methanol, and tetrahydrofuran (THF) rinses for 5 min each. A saturated solution of [PyrProSH][TPB] in acetone was drop cast onto the discs ~20 times allowing each drop to dry before adding another. The discs were then supported in a vial which was added to a container of saturated acetone vapor and completely sealed. The container was then heated in an oil bath at 60 °C for 1 hour. This process ensured complete coverage of GUMBOS within the pores. Excess [PyrProSH][TPB] which accumulated on top of the discs was removed with 180-Grit fine sandpaper. The discs were dissolved in 1mM phosphoric acid solution overnight followed by centrifugation and several deionized water rinses resulting in free nanorods suspended in aqueous solution. Alternatively, an array of nanorods was obtained by adhering the disc with an epoxy adhesive to a surface such as glass (0.5" x 0.5") followed by dissolution in 1 mM phosphoric acid solution overnight. The resulting array was flushed several times with deionized water and freeze-dried overnight.

4.2.4 Preparation of Core-Shell 1D NanoGUMBOS

The procedure for forming gold nanoshells on 1D nanoGUMBOS is similar to that described in Chapter 2. Following the dissolution of the AAO disc, excess gold seeds were added to free 1D nanoGUMBOS solution (5 mL to 1 mL) and stirred for 48 hours. Gold-seeded rods were then centrifuged and resuspended in 5 mL of water. A 1 mL aliquot of seeded rods

was then added to 5 mL of K_2CO_3/$HAuCl_4$ solution. After 5 min of stirring, 0.025 mL of formaldehyde was added inducing a color change to an iridescent hue of blue.

For nanoarray coating, surface supported rods were placed in 5 mL of gold seeds solution for 48 hours allowing the seeds to self-assemble on the nanorod surface. Gold seeds were then flushed with deionized water, followed by the addition of 5 mL gold hydroxide solution and 0.025 mL of formaldehyde. After 1 hour, gold-coated rods were flushed with deionized water and dried under vacuum.

4.2.5 Cyclic Voltammetry

A 0.1 M solution of $TBAPF_6$ was used to prepare dilute solutions of ferrocene and 5 mM [PyrProSH][TPB]. Ferrocene was measured through a potential range of -0.5 to 0.5 V at a scan rate of 0.1 $V \cdot s^{-1}$. The reduction potentials of GUMBOS were scanned from -2 to 0 V, while oxidation potentials ranged from 0 to 1 V. Voltammetric measurements of GUMBOS were recorded at scan rates of 0.05, 0.1, 0.2, 0.3, 0.4, and 0.5 $V \cdot s^{-1}$. All measured solutions were purged with N_2 to eliminate the interference of dissolved oxygen.

4.3 Results and Discussion

4.3.1 Microscopic Characterization of 1D NanoGUMBOS

Figure 4.2 displays SEM micrographs of (a) free and (b) surface-supported 1D nanoGUMBOS using an AAO template. The resulting nanorods had diameters ranging from 240 to 280 nm. These diameters are a little larger than the 200 nm pore size of the AAO disc. Similar reports observed this swelling behavior of nanorods once removed from the template.[12]

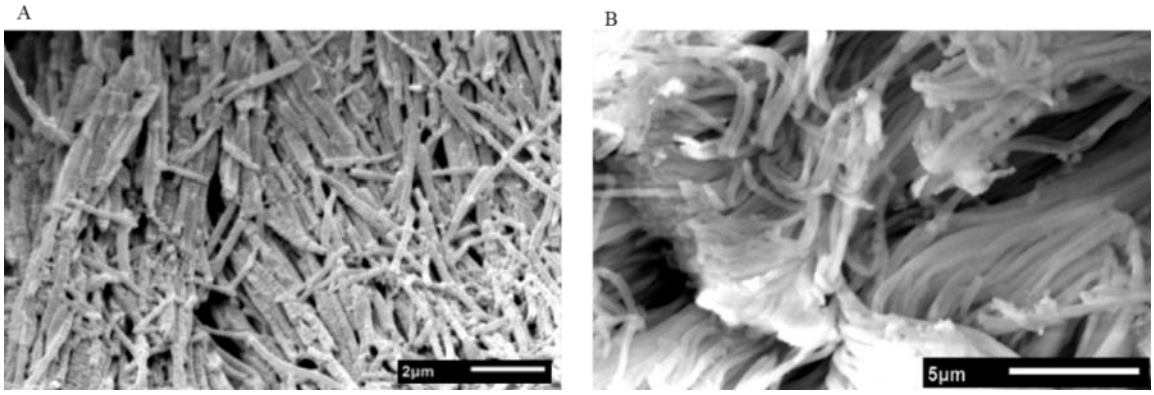

Figure 4.2: SEM micrographs of (A) free and (B) array 1D nanoGUMBOS.

4.3.2 Morphological and Optical Characterizations of Core-Shell 1D NanoGUMBOS

The evolution of core-shell 1D nanoGUMBOS is exhibited in Figure 4.3. Au-seeded nanorods (Figure 4.3B) were obtained after 48 hours of immersion in Au seeds and were not subjected to the gold hydroxide coating process. Figure 4.4 displays the solution of gold-coated nanorods which change from clear to a mixture of purple and blue. Figure 4.5 illustrates the optical responses of bare nanorods and coated nanorods. The common peak at 265 nm represents bare nanorods suspended in aqueous solution. There is a notable increase in absorption of Au-coated nanorods along the entire measured wavelength range. To our knowledge, there are no other reports of such intense absorption for other gold-coated nanorods.

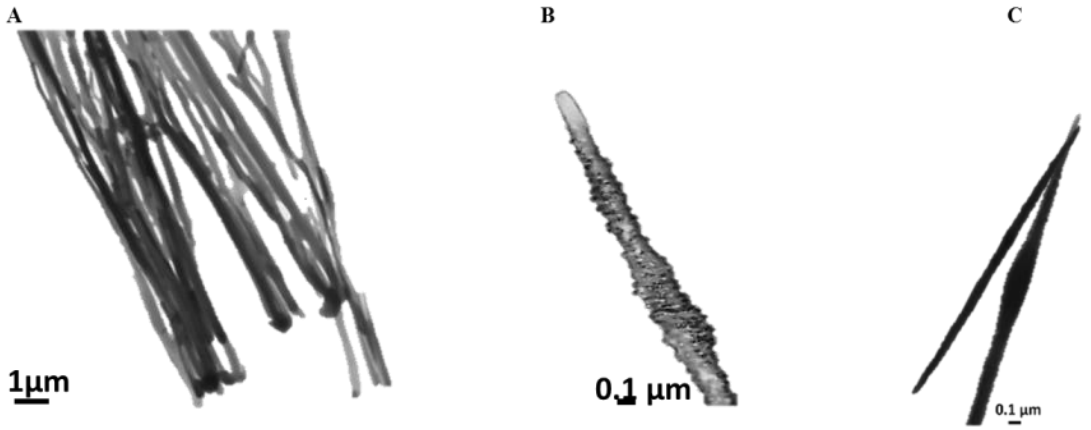

Figure 4.3: TEM micrographs of (A) bare (B) seeded and (C) coated 1D nanoGUMBOS.

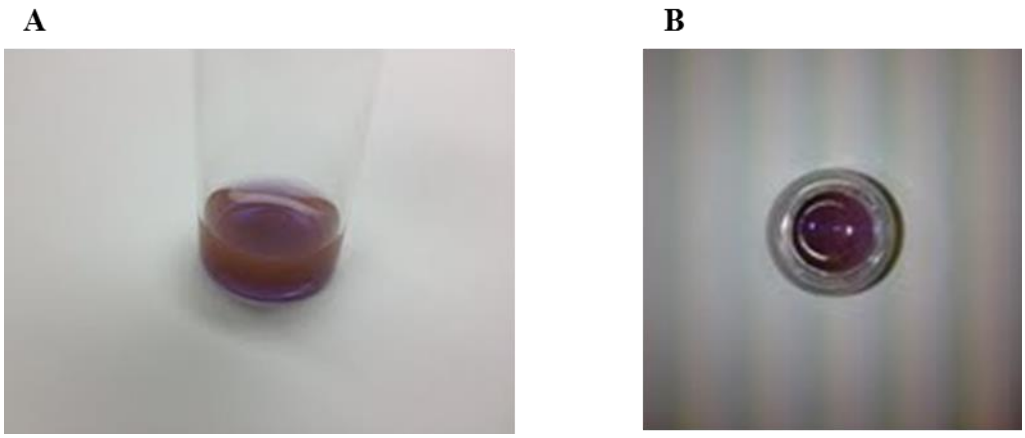

Figure 4.4 (A) Side and (B) top view of gold-coated 1D nanooGUMBOS.

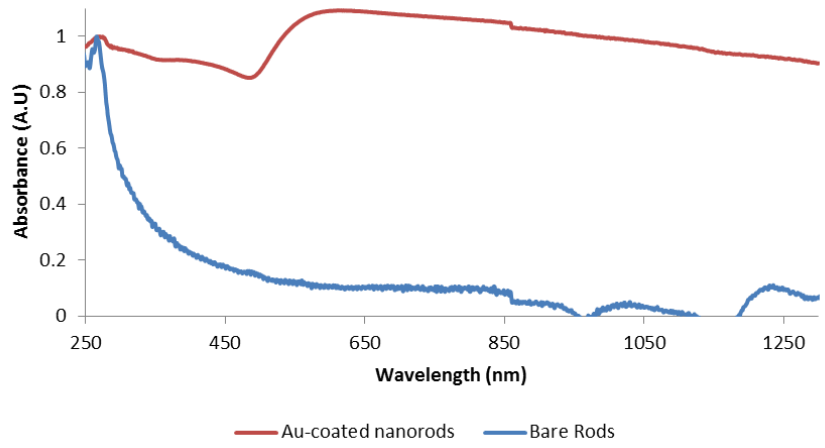

Figure 4.5: Absorption spectrum of bare (blue trace) and gold-coated 1D nanoGUMBOS.

4.3.3 Electrochemical Analysis of [PyrProSH][TPB] GUMBOS

Ferrocene is known to undergo a rapid and reversible single-electron transfer, and it is often used to calibrate reduction and oxidation (redox) potentials of analytes in organic media.[13,14] The cyclic voltammogram of ferrocene is represented by Figure 4.6. The cathodic peak (E_{pc}) and anodic peak potentials (E_{pa}) were measured as 0.071 V and 0.154 V, respectively. The formal potential (E_F^0) of ferrocene corresponds to the average of E_{pc} and E_{pa}. This value,

0.112 V is used to standardize peak potentials generated by measurements for [PyrProSH][TPB] GUMBOS. The cyclic voltammogram of [PyrProSH][TPB] GUMBOS, Figure 4.7, shows an irreversible transfer of electrons. The corresponding representative reduction and oxidation scans are presented in Figure 4.8 and Figure 4.9, respectively. The cathodic and anodic peak potentials of GUMBOS (E_{pc} and $E_{pa)}$ were determined from the average minimum and maximum potentials of the negative and positive scan rates measured, respectively. The E_{pa} was calculated as 0.769 V, and the E_{pc} was determined as -1.77 V. Peak potentials calibrated using ferrocene potentials were determined by subtracting E^0 from E_{pa} and E_{pc}. The E_{pa} and E_{pc} (ferrocene) values were equal to 0.657 V and -1.88 V, respectively.

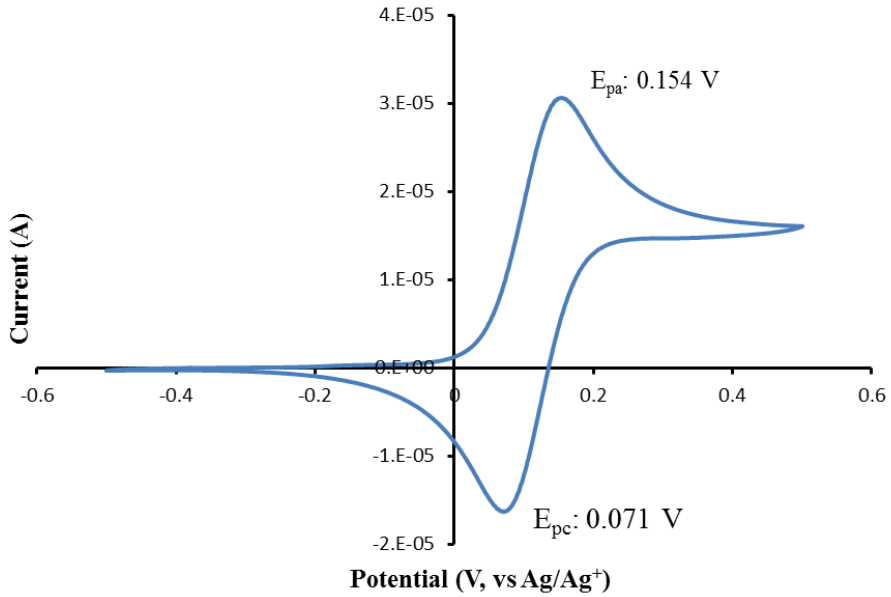

Figure 4.6: Cyclic voltammogram of ferrocene.

Further analysis of cyclic voltammetry data can be useful in the determination of the highest occupied molecular orbital (HOMO) and lowest unoccupied molecular orbital (LUMO) energy states of [PyrProSH][TPB] as well as the corresponding band gap. The HOMO and LUMO energy states were determined following Equations 4.1 and 4.2, respectively.

$$HOMO = -1e\left[\left(E_{pa}(ferrocene) + 4.8\right)\right] V \quad \text{Equation 3.1}$$

$$LUMO = -1e\left[\left(E_{pc}(ferrocene) + 4.8\right)\right] V \quad \text{Equation 3.2}$$

The HOMO and LUMO energies were found to be -5.46 and -2.91 eV, respectively. The difference of the HOMO and LUMO energies provides the band gap. The band gap was valued as 2.54 eV which categorizes [PyrProSH][TPB] a semi-conductive material suitable for use in photovoltaic cells, light-emitting diodes, or as transistors.

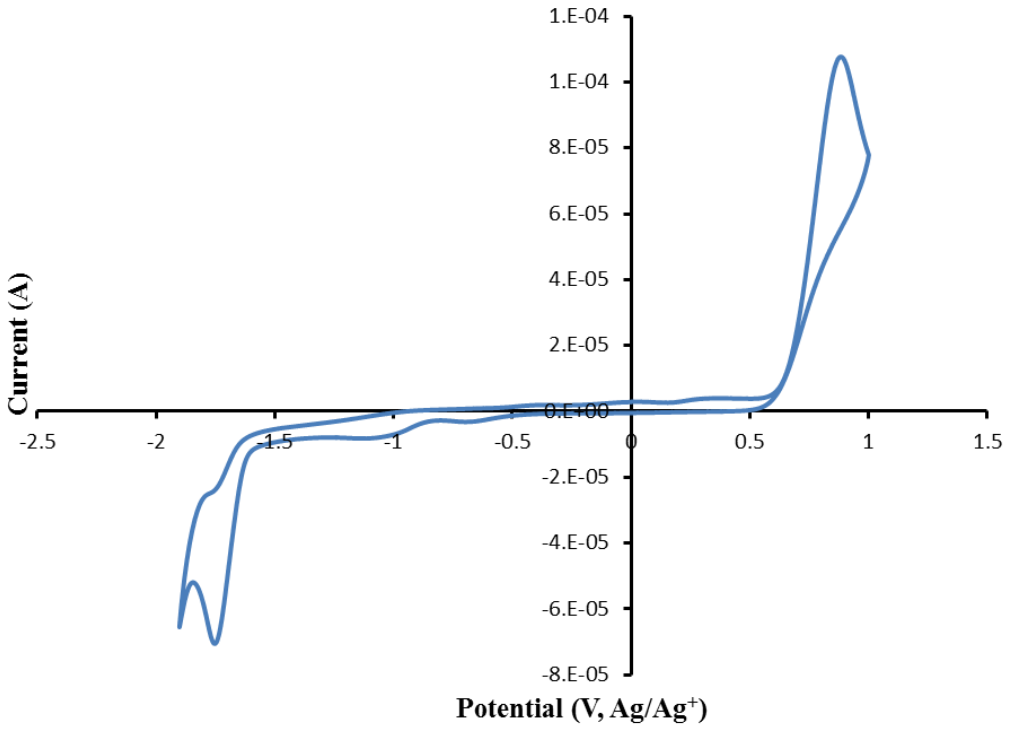

Figure 4.7: Cyclic voltammogram of [PyrProSH][TPB] GUMBOS.

Conductive probe AFM studies were performed (data not shown) on the bare and coated nanorods to determine the conductivity of the nanorods. Based on the cyclic voltammetric data obtained for [PyrProSH][TPB] GUMBOS, the potential boundaries for the CP-AFM

measurements ranged from -0.5 to 0.5 V where no redox activity of the nanoGUMBOS was observed. The corresponding current-voltage plots were generated as well as morphology micrographs.

4.4 Conclusion

This is the first report of the synthesis of gold nanoshells on 1D nanoGUMBOS and their optical properties. NanoGUMBOS with diameters of ~ 240 nm and lengths up to 5 µm, were prepared using a simple AAO templating method, and a seeding procedure was utilized to form gold nanoshells.

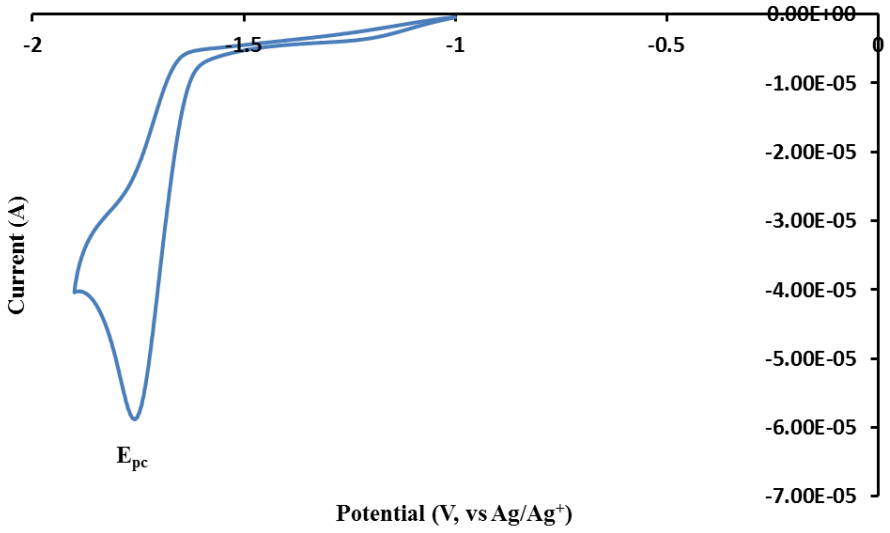

Figure 4.8: Negative cyclic voltammogram for [PyrProSH][TPB].

The addition of the gold coating greatly increased the absorption profile of the nanorods beyond the measured window of NIR wavelengths. The cyclic voltammetry measurements determined that [PyrProSH][TPB] GUMBOS possess semiconductive properties with a band gap of 2.54 eV and can be used in photovoltaic applications.

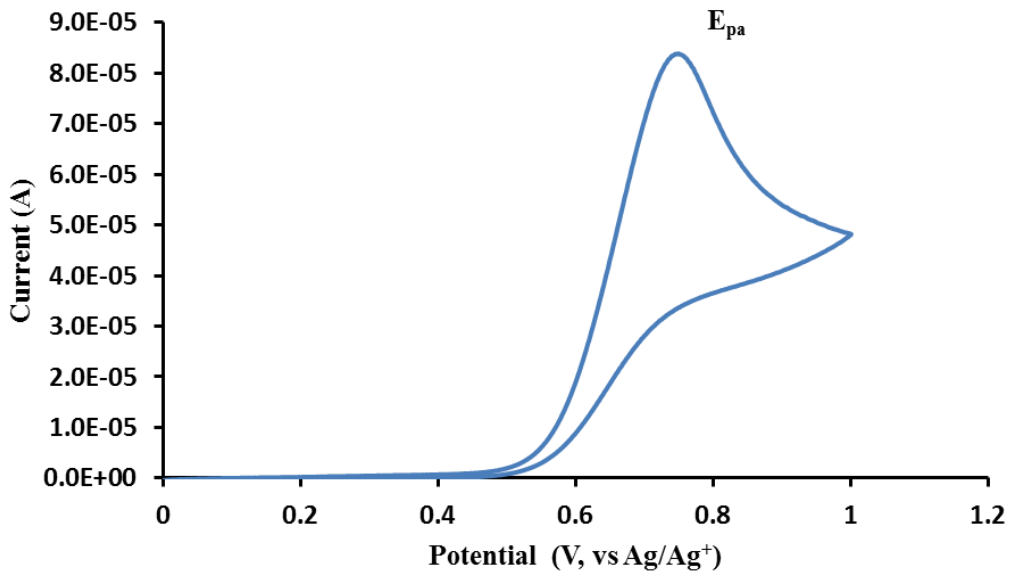

Figure 4.9: Positive cyclic voltammograms for [PyrProSH][TPB].

4.5 References

1. Huang, X.; Neretina, S.; El-Sayed, M. A., Gold Nanorods: From Synthesis and Properties to Biological and Biomedical Applications. *Adv. Mater.* **2009,** *21* (48), 4880-4910.

2. Nikoobakht, B.; El-Sayed, M. A., Preparation and Growth Mechanism of Gold Nanorods (NRs) Using Seed-Mediated Growth Method. *Chem. Mater.* **2003,** *15*, 1957-1962.

3. Gole, A.; Murphy, C. J., Seed-Mediated Synthesis of Gold Nanorods: Role of the Size and Nature of the Seed. *Chem. Mater.* **2004,** *16*, 3633-3640.

4. Terrones, M.; Hsu, W. K.; Kroto, H. W.; Walton, D. R. M., *Nanotubes: A Revolution in Materials Science and Electronics*. Springer Berlin Heidelberg: 1999; p 189-234.

5. Jie, J.; Zhang, W.; Bello, I.; Lee, C.-S.; Lee, S.-T., One-Dimensional II–VI Nanostructures: Synthesis, Properties and Optoelectronic Applications. *Nano Today* **2010,** *5* (4), 313-336.

6. Mieszawska, A. J.; Jalilian, R.; Sumanasekera, G. U.; Zamborini, F. P., The Synthesis and Fabrication of One-Dimensional Nanoscale Heterojunctions. *Small* **2007,** *3* (5), 722-756.

7. Hall, I., J.; Dravid, V. P.; Aslam, M., Templated Fabrication of Co@Au Core-Shell Nanorods. *Nanoscape* **2005,** *2* (1), 67-71.

8. Fan, J.-G.; Zhao, Y.-P., Gold-Coated Nanorod Arrays as Highly Sensitive Substrates for Surface-Enhanced Raman Spectroscopy. *Langmuir* **2008,** *24*, 14172-14175.

9. Bhattacharya, A.; Jain, C.; Rao, V. P.; Banerjee, S., Gold Coated ZnO Nanorod Biosensor for Glucose Detection. *AIP Conf. Proc.* **2012,** *1447*, 295-296.

10. Limmer, S. J.; Chou, T. P.; Cao, G., Formation and Optical Properties of Cylindrical Gold Nanoshells on Silica and Titania Nanorods. *J. Phys. Chem. B* **2003,** *107*, 13313-13318.

11. Qu, Y.; Porter, R.; Shan, F.; Carter, J.; Guo, T., Synthesis of Tubular Gold and Silver Nanoshells Using Silica Nanowire Core Templates. *Langmuir* **2006,** *22* (14), 6367-6374.

12. de Rooy, S. L.; El-Zahab, B.; Li, M.; Das, S.; Broering, E.; Chandler, L.; Warner, I. M., Fluorescent One-Dimensional Nanostructures from a Group of Uniform Materials Based on Organic Salts. *Chem. Comm.* **2011,** *47* (31), 8916-8918.

13. Sharp, M.; Petersson, M.; Edstrom, K., A comparison of the Charge Transfer Kinetics Between Platinum and Ferrocene in Solution and in the Surface Attached State. *J. Electroanal. Chem.* **1980,** *109*, 271-288.

14. Montenegro, M. I.; Pletcher, D., The Determination of the Kinetics of Electron Transfer Using Fast Sweep Cyclic Voltammetry at Microdisc Electrodes. *J. Electroanal. Chem.* **1986,** *200*, 371-374.

CHAPTER 5

SYNTHESIS AND CHARACTERIZATION OF LIPOSOMAL IONOGELS

5.1 Introduction

Gel systems for topical drug delivery are favored over conventional creams because they are better absorbed by the skin, non-greasy, washable with water, stable, and usually have a high lipid solubility which increases drug permeability.[1,2] Hydrogels,[3] liposomal gels,[4] and more recently, ionogels[5] have been utilized as topical drug delivery vehicles. Liposomal gels are formed by embedding drug-encapsulated liposomes within hydrogels. The addition of liposomes allows for the solubilization of hydrophobic and hydrophilic molecules, regulation of release rates of drug molecules as they maneuver through the vesicle layers, and reduction of side effects.[6] Additionally, liposomes are biocompatible since phospholipids are found within the cell membrane. Liposomal gels also show a decreased release rate in comparison to liposome solutions which prolongs the surface retention and decreases the number of applications necessary for treatment. Liposomal gels have been investigated for drug delivery in the treatment of bacterial vaginitis,[4,7,8] acne,[9] and fungal infections.[10]

Ionogels consist of ionic liquids (ILs) as the solvent phase of the gel system. Ionic liquids offer its own advantages such as ionic conductivity, negligible vapor pressure, thermal stability, and biocompatibility.[11,12] The properties of ILs are based on the chosen cation and anion pair which can be tuned for the desired application. Ionogels maintain all the desirable properties of ILs; expect fluidity, while confined within the gel network which considerably expands the range of its applications. Ionogels have been investigated for use in optics, catalysis, biocatalysis, and (bio) sensing, and remain new to drug delivery applications.[5,13] Conventionally, liposomal gels are injected liposomes into cellulose or polymeric-derivative

hydrogel gelators, and ionogels percolate through organic or inorganic polymers. However, to our knowledge, there is no report of the formation of ionogels using liposomes as the gelator. Herein, we describe the development of liposomal ionogels (LIGs) which are composed of an IL liquid phase and liposome gelators.

Liposomal ionogels were prepared using dipalmitoyl-phosphatidylcholesteroline (DPPC) and 1-palmitoyl-2-oleoyl-*sn*-glycero-3-phospho-cholesteroline (POPC) along with an IL which comprises a choline cation and proline anion ([Cho][Pro]). Dipalmitoyl-phosphatidylcholine is a saturated, temperature-sensitive lipid and POPC is an unsaturated, pH-sensitive lipid. The chemical structures of DPPC and POPC are shown in Figure 5.1 and 5.2, respectively. Proline is an essential amino acid responsible for the production of collagen, cartilage, tissue repair, regeneration of skin, and prevention of atherosclerosis. Choline is associated with the vitamin B class.[14] It is important for brain development and memory, especially during the early stages of life. It also lowers cholesterol and homocysteine levels associated with cardiovascular disease, and is helpful in the formation of phosphatidylcholine, which is the backbone of most phospholipids and the primary phospholipid in the cell membrane.

There are several reports on the biodegradable,[15,16,17] non-cytotoxic and biocompatible[18] properties of choline-based ionic liquids. Winther-Jensen *et al.* reported biocompatible self-forming gels that form with choline-based ionic liquids and 2-hydroxyethyl methacylate (HEMA).[14] The characteristics of the ionic pair render [Cho][Pro] a biologically favorable ionic liquid. The liposomes and ILs for the reported hybrid LIGs inherently offer multiple layers of tunability. The LIGs were characterized using rheology, differential scanning calorimetry, thermal gravitational analysis and fluorescence, and have potential use as stimuli-responsive drug delivery tools.

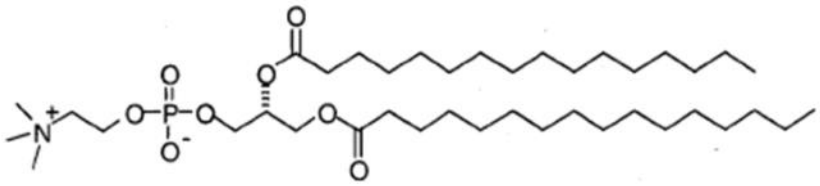

Figure 5.1: Chemical structure of DPPC.

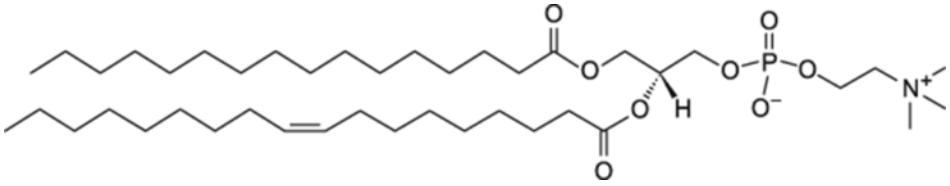

Figure 5.2: Chemical structure of POPC.

5.2 Materials and Methods

5.2.1 Materials

Dipalmitoylphosphatidylcholine (DPPC), 1-palmitoyl-2-oleoyl-*sn*-glycero-3-phospho-cholesteroline (POPC), and cholesterol were purchased from Avanti Polar Lipids, Inc. (Alabaster, AL). Choline hydroxide (46 wt% solution in water), and phosphate buffered saline (PBS) were purchased from Sigma-Aldrich (Milwaukee, WI). Proline (H-Pro-OH) was purchased from Bachem (Torrance, CA). All chemicals were used as purchased.

5.2.2 Characterization Techniques

Proton NMR spectra were obtained using a Bruker DPX-400 instrument. The chemical shifts are provided in parts per million (ppm). Fourier transform infrared spectroscopy measurements were performed on a Bruker Tensor 27 instrument with Opus 6.5 as the data collection program. An advanced thermal analysis (TA) rheometer was used to determine the rheological properties of the LIGs with a cone-and-plate geometry (angle = 2 °C, diameter = 40 mm) at 37 °C. Dynamic oscillatory measurements (frequency sweep tests) were performed to

measure the viscoelastic properties (G'- storage modulus and G"- loss modulus) of the LIGs. Frequencies ranged from 0.1-100 rad/s with an applied strain of 0.1%. In addition, static (steady stress sweep) measurements were performed on a parallel plate geometry to determine the shear viscosity of the gels as a function of shear rates ranging from 0.01-1000 s^{-1}. Thermal stability measurements were performed using a 2950 TGA HR V6 (TA Instruments) by heating samples under nitrogen at a rate of 10 °C · min^{-1} from 25 to 400 °C. Phase transition temperatures were measured using a 2920 Modulated DSC (TA Instruments) by cooling 9-13 mg of sample to -20 °C and subsequently heating up to 300 °C at a rate of 10 °C · min^{-1}.

5.2.3 Synthesis of Choline Proline

The synthesis of [Cho][Pro] was a neutralization between choline hydroxide with the amino acid proline (H-Pro-OH) as displayed in Figure 5.3. Briefly, H-Pro-OH (0.035 mol) was completely dissolved in deionized water by vigorously stirring for 10 min. An equimolar amount of choline hydroxide was added to the solution. The mixture was covered and continued to stir at room temperature for 2 hr. Water was removed under vacuum for 48 h resulting in a light yellow viscous liquid. Due to its hygroscopic nature, [Cho][Pro] was tightly sealed when not in use.

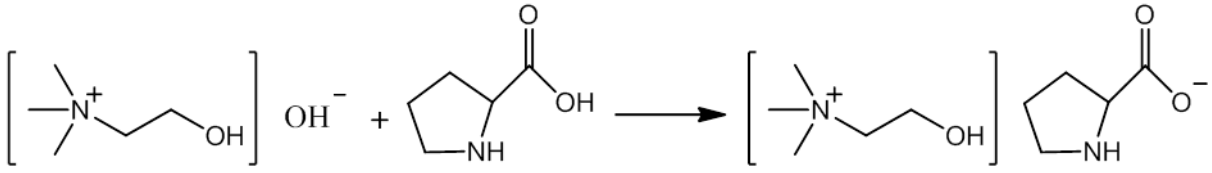

Figure 5.3: Synthesis scheme of [Cho][Pro].

5.2.4 Preparation of Liposomal Ionogels (LIGs)

Liposomal ionogels were prepared using the lipid film rehydration method in the presence of [Cho][Pro]. Initially, lipid (DPPC; 20 mg) or lipid/cholesterol (5% or 10% w/w

cholesterol) mixtures were dissolved in a 2:1 (v/v) ratio of chloroform: methanol. The solvent was removed under a stream of N_2 for 24 h resulting in a film of the lipid or lipid/cholesterol along the base of the vial. A 1 mL aliquot of [Cho][Pro] was added to the lipid film and heated at 55 °C for ~45 min while sealed and with occasional stirring. The lipid film was hydrated using phosphate buffered saline (PBS) buffer (pH 7.4) while simultaneously forming the LIGs. Buffer was added in 200 µL increments for a total of 1 mL. After the addition of 400 µL, the mixture was heated at 60 °C until liquefied, then allowed to cool to room temperature, reforming the gel. POPC LIGs were prepared as described above using 5%, 10%, and 25 % (w/w) cholesterol.

5.3 Results

5.3.1 Synthesis and Characterization of [Cho][Pro]

A one-pot synthesis of equimolar amounts of choline hydroxide and H-Pro-OH yielded [Cho][Pro], yellow viscous liquid, ^{1}H (400 MHz, d_6-DMSO, δ (ppm): 3.78-3.77 (t, 2H); 3.52-3.51 (t, 1H); 3.41-3.40 (t, 1H); 3.1 (s, 3H); 3.01-2.99 (t, 1H); 2.86-2.83 (m, 2H); 2.45-2.45 (m, 2H); 1.78-1.70 (m, 2H); 1.51-1.38 (m, 2H). ^{13}C (100 MHz, d_6-DMSO, δ (ppm): 163.7, 144.4, 136.2, 129.0, 125.9, 122.1, 59.3, 34.9, 22.0, 20.9. FTIR, ν (cm^{-1}): 3274.90, 3030.81, 2960.21, 2870.07, 1580.98, 1377.11, 1087.89, 954.15.

5.3.2 Liposomal Ionogels

Liposomal ionogels were prepared using DPPC, a saturated, temperature-sensitive lipid, and POPC which is an unsaturated, pH-sensitive lipid. The lipid film method of forming liposomes was employed in the presence of [Cho][Pro]. As PBS buffer was added, the lipid film began to dissolve, thus hydrating the liposomes resulting in a final gel with a uniform composition and no visible lipid particulates. Theoretically, multilamellar vesicles (MLVs) were

formed upon hydration and dispersed in the gel. Cholesterol concentrations up to 50% (w/w) were used to investigate the stability of the lipids with increasing cholesterol concentrations. Concentrations were kept below 50% so as not to have the cholesterol dominating the mixture. Photographs of DPPC and POPC LIGs are shown in Figure 5.4 and Figure 5.5, respectively. Cholesterol concentrations greater than 10% with DPPC did not yield stable gels. In the case of POPC, cholesterol concentrations up to 25% formed stable gels.

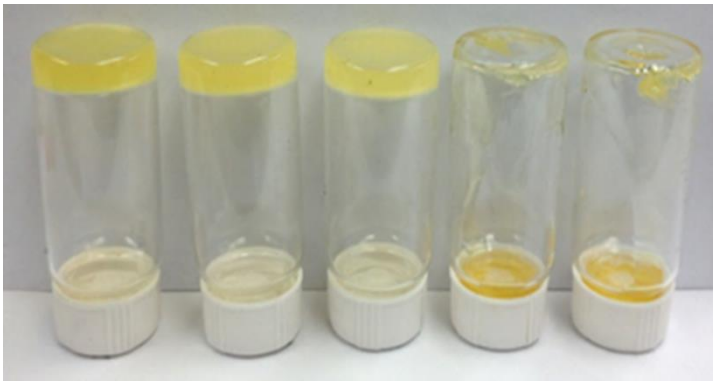

Figure 5.4: DPPC LIGs with 0, 5, 10, 25, and 50% (w/w) cholesterol concentrations.

Figure 5.5: POPC LIGs with 0, 5, 10, 25, and 50% (w/w) cholesterol concentrations.

5.3.3 Rheological Examination of LIGs

Rheological characterizations determine the rigidity, viscosity, deformability, and behavior of the gel network under applied stresses. The main parameters that are obtained are the storage modulus (G'), loss modulus (G"), and the loss tangent (tan δ). The storage modulus

measures the elastic properties of the gel which is related to energy storage, whereas, the loss modulus determines the viscous component of the gel, which is associated with dissipation of energy. The loss tangent refers the damping factor of the gels which is calculated as the ratio between the viscous and elastic portion during gel deformation (tan δ = G"/G'). In the gel state, tan δ < 1; liquid state, tan δ > 1; at gel point, tan δ = 1.

The gels (without cholesterol) were subjected to increasing percentages of applied strain in order to determine their linear viscoelastic (LVE) range. Within the viscoelastic range, the G' values are larger than the G" values and are independent of the strain amplitude. Physically, the gel network does not undergo any rearrangement or deformations. Outside of the LVE region, the gels show strain-dependent behavior and cross over resulting in G" > G'. The LVE plots for DPPC and POPC are displayed in Figures 5.6 and 5.7, respectively. The LVE range for DPPC was 0.01-0.5% and 0.01-1% for POPC LIGs. It was within these respective regions that subsequent rheological measurements were performed. In this study, both gels were subjected to 0.1% strain.

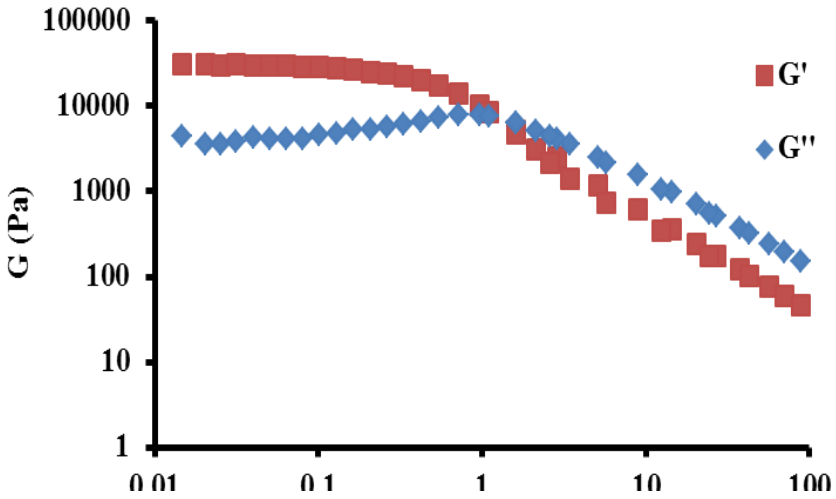

Figure 5.6: Linear viscoelasticity plot for DPPC LIG.

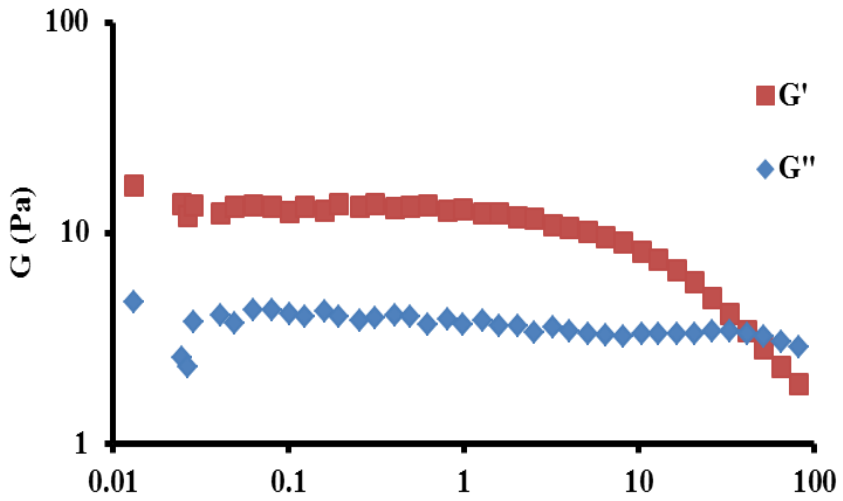

Figure 5.7: Linear viscoelasticity plot for POPC LIG.

5.3.3.1 Viscoelastic Behavior of LIGs and [Cho][Pro]

The storage (elasticity) and loss (viscous) moduli, or mechanical properties, for the LIGs with 0, 5, and 10% cholesterol are shown in Figure 5.8 and Figure 5.9. For each concentration of cholesterol, G' is higher than their respective G" values (tan $\delta < 1$), which supports the moduli behavior for gels. DPPC LIGs (Figure 5.8) exhibit fairly linear plots indicative of relatively stable gels with elastic solid behavior throughout the measured frequencies. This behavior is similar to a rigid gel with high degrees of cross-linking.[19] Therefore, the liposomes generate gels networks comparable to traditional polymers. The G' and G" values for 10% cholesterol are lower than those of 0% and 5% demonstrating the weakest elastic and less viscous material. Gels with 0% cholesterol are more elastic and viscous than the 5% and 10% cholesterol gels.

In the POPC LIGs (Figure 5.9), the viscoelastic stability decreases for cholesterol concentrations from 5, 10, 25, and 0%. The curves are not as linear throughout the studied angular frequency which signifies that the POPC gels are not as stable as the DPPC LIGs. The viscoelastic properties of gels containing 10% and 25% cholesterol overlap over the measured angular frequency range. At frequencies higher than 10 rad/sec, both elastic and viscous

properties of all concentrations of cholesterol weaken, which is indicated by the increase of G' and G" plots. As the frequency approaches 100 rad/s, the G' and G" values begin to equal (tan δ =1). It can be assumed that at frequencies greater than 100 rad/s, POPC gels will exhibit liquid behavior with G" > G' (tan > 1).

Comparatively, DPPC LIGs are 100 fold stable than POPC since the G values of 0% DPPC measure up to 10,000 Pa and the most stable POPC LIG (5%) displays elasticity near 100 Pa. Additionally, the inclusion of cholesterol weakens the viscoelasticity of DPPC LIGs, whereas, POPC LIG without cholesterol has the weakest viscoelastic behavior. These observations can be attributed to the saturated and unsaturated nature of DPPC and POPC, respectively. Cholesterol is known to interact with phospholipids based on their gel-fluid state at room temperature.[20] Phospholipids have phase transition temperatures, (T_p), above which their hydrocarbon chains become more fluid increasing permeability to aqueous solvent. Below the T_p, the phospholipid is in the gel state and the hydrocarbon chains are more rigid. The gel-fluid state is largely dependent upon saturation. Saturated phospholipids are usually in the gel state at room temperature while most saturated phospholipids are in the fluid state. The T_p of DPPC and POPC are 42 °C and -2 °C, respectively. Cholesterol increases fluidity of saturated phospholipid hydrocarbon chains below its T_p. Therefore, as in the case of DPPC which is in its gel state under ambient conditions, the incorporation of cholesterol interferes with its natural rigid conformation and results in destabilization of the bilayers. Conversely, cholesterol reduces fluidity of unsaturated phospholipids above the T_p. Since the hydrocarbon chains of POPC are in the fluid state above -2 °C, the addition of cholesterol stabilizes the bilayers. This behavior is observed in the trends of the viscoelastic properties of DPPC and POPC LIGs with increasing concentrations of cholesterol.

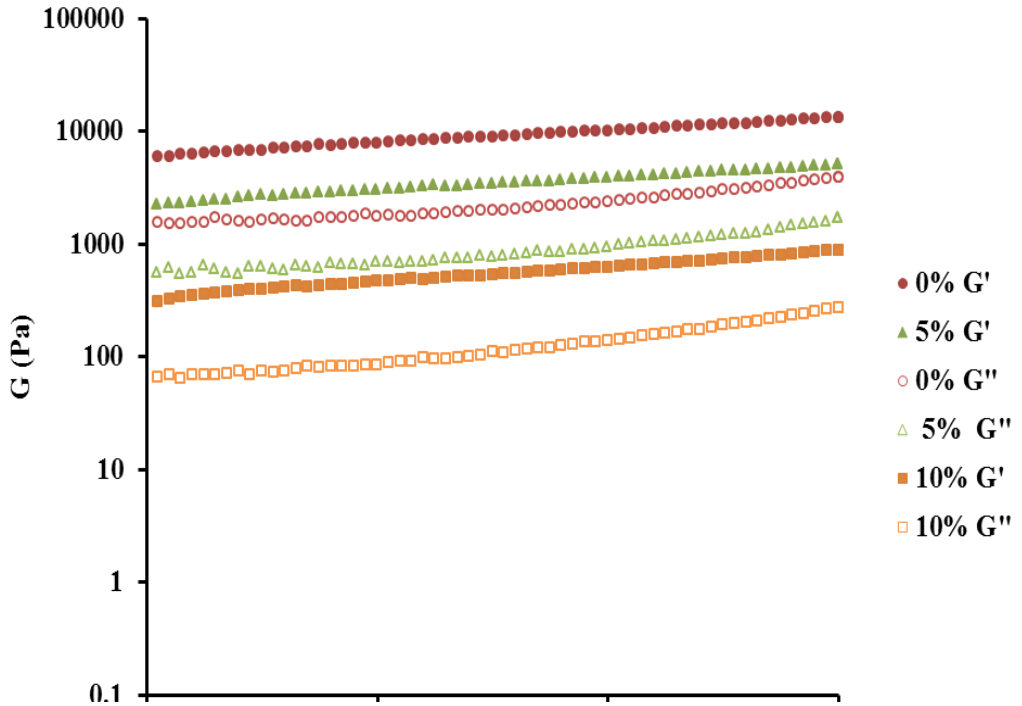

Figure 5.8: Elasticity (G') (closed symbols) and viscosity (G") (open symbols) for DPPC LIGs.

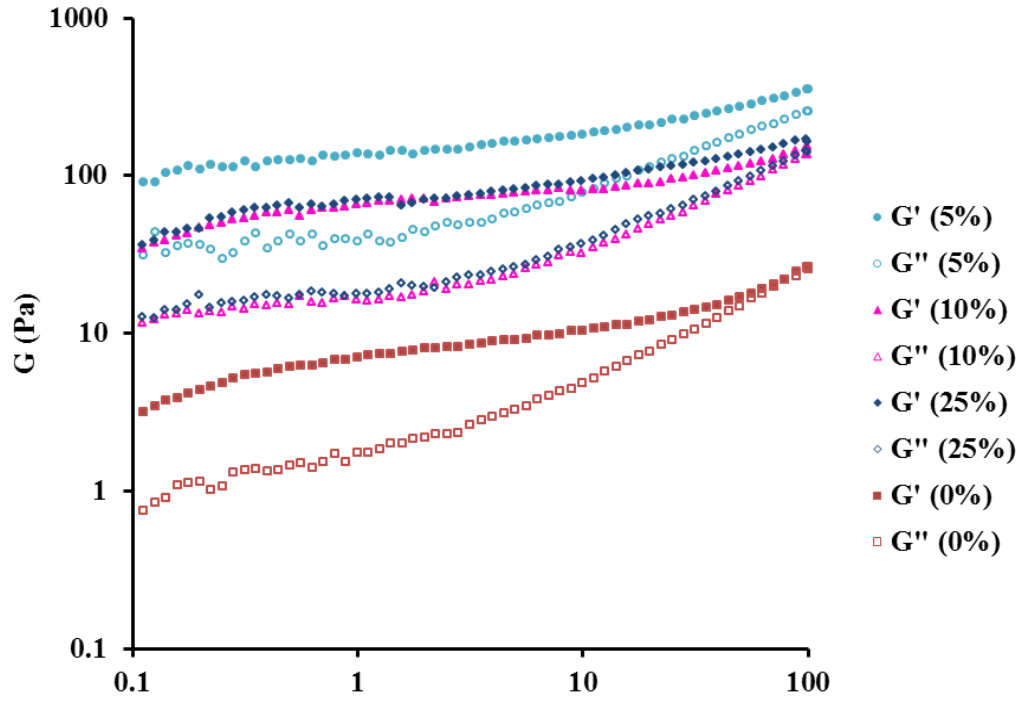

Figure 5.9: Elasticity (G') (closed symbols) and viscosity (G") (open symbols) for POPC LIGs.

Viscoelastic properties were also measured for [Cho][Pro] (Figure 5.10) in order to compare their different behaviors with LIGs. Noticeably for [Cho][Pro], the G" values are increasingly higher than those of G' at all frequencies which is typical for liquids, but opposite from the behaviors of gels. The elasticity component (G') records values below zero. Therefore, the logarithmic scale was not a suitable format to present the data.

The loss tangent plots illustrate the degree of gel crosslinking. Tan δ values < 1 are indicative of stable, rigid, highly elastic gels. As the values increase towards 1, the viscous component of the gels begins to dominate. Liposomal ionogels derived from DPPC (Figure 5.11) show a high degree of crosslinking and elasticity with tan δ values less than 0.4. The tan values of POPC LIGs (Figure 5.12) are increasingly higher than those of DPPC. As the frequency increases, the tan δ values approach 1, which shows a more viscous behavior as observed from the G' and G" relationships.

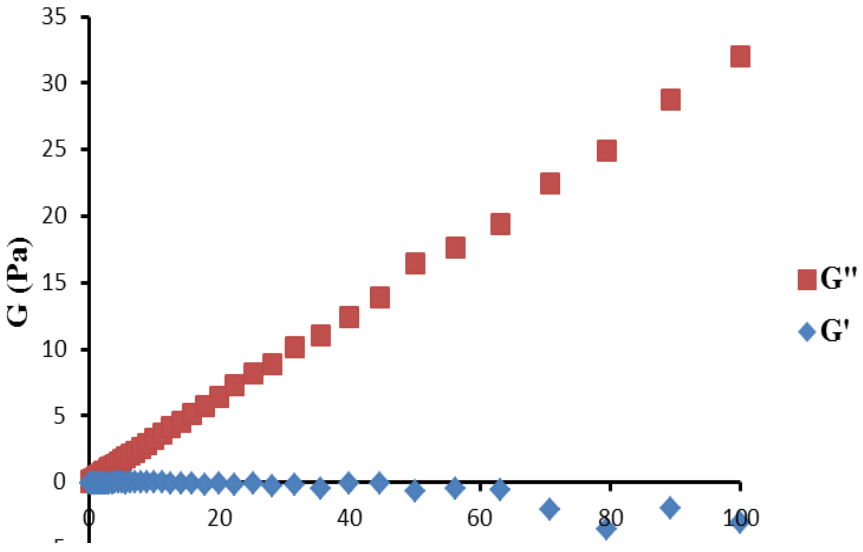

Figure 5.10: Viscoelastic properties of [Cho][Pro].

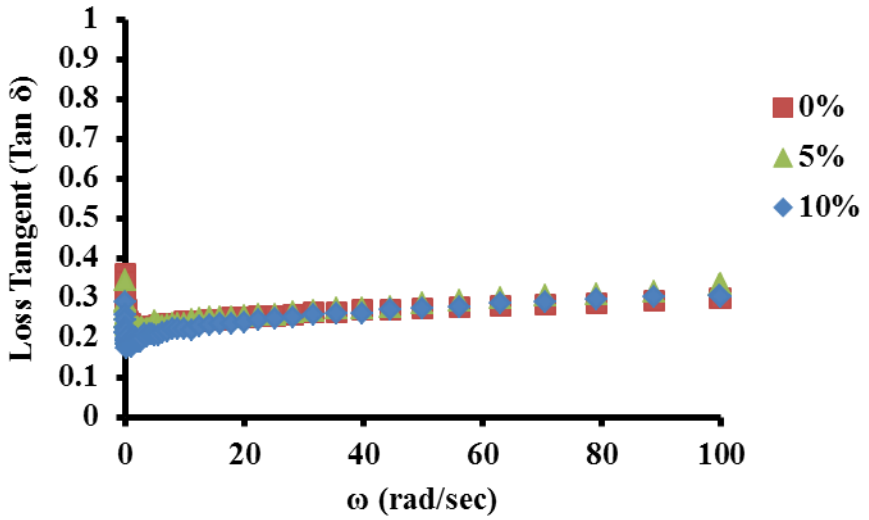

Figure 5.11: Loss tangent plot for DPPC LIGs.

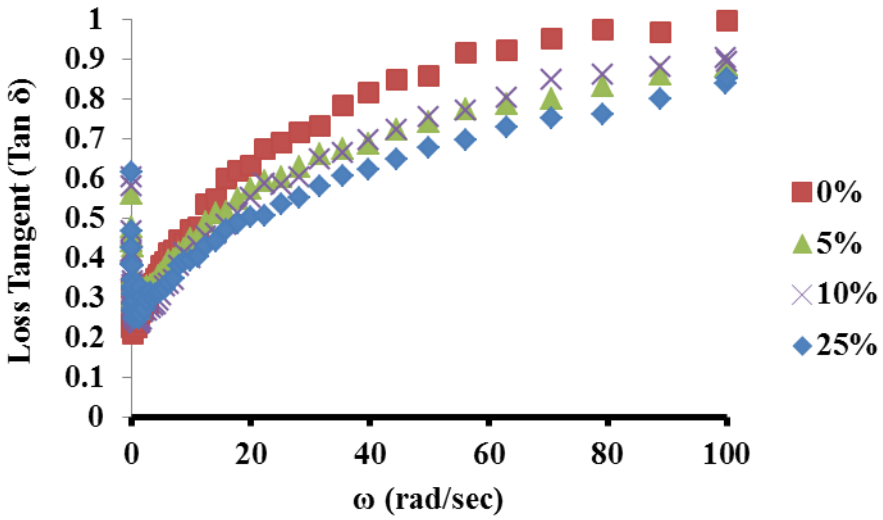

Figure 5.12: Loss tangent plot for POPC LIGs.

5.3.3.2 Viscosity of DPPC and POPC LIGs

The shear viscosity vs. shear rate of LIGs rheogram for [Cho][Pro], DPPC and POPC LIGs is shown below. All gels demonstrate shear thinning behaviors by decreasing in viscosity with increasing shear rates. Figure 5.13 illustrates the shear viscosity properties of DPPC LIGs

and [Cho][Pro]. The shear viscosity of [Cho][Pro] is linear along the shear rate range which is typical of (Newtonian) liquids. In the case of DPPC LIGs, the overall viscosities of the gels decrease with increasing concentrations of cholesterol. Around 90 s^{-1}, the viscosities overlap and demonstrate a reversed behavior where gels with 5 and 10% cholesterol have the same viscosity which is higher than that of 0% cholesterol. This phenomenon can be attributed to the weakening of the lipid membrane by the cholesterol which is seen for saturated lipids such as DPPC. Also, the curves for 5% and 10% begin to plateau demonstrating Newtonian behavior.

Liposomal ionogels with POPC (Figure 5.14) do not display an obvious trend with regard to cholesterol concentrations. Throughout the measured shear rates, the viscosities of all POPC LIGs remained relatively the same with 25% cholesterol showing a slightly lower viscosity.

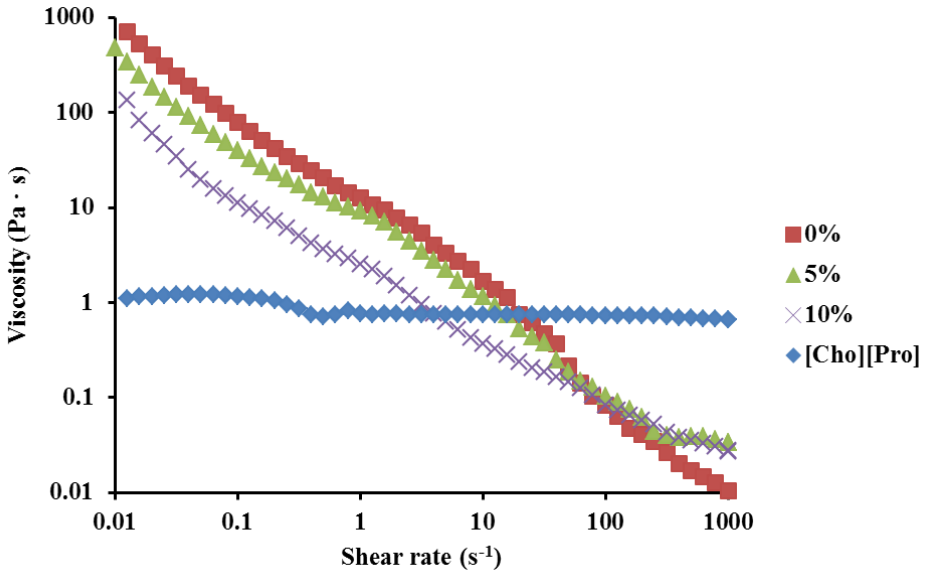

Figure 5.13: Viscosity rheogram for DPPC LIGs.

5.3.4 Thermal Analyses

Thermal gravitational analyses (TGA) were used to measure the thermal stability by way of the decomposition temperatures (T_d) of [Cho][Pro] and the LIGs. Thermal gravitational analysis measures the percentage of sample weight that is lost as the temperature applied to the sample is

increased. The T_d was determined as the temperature extrapolated from the tangent of the onset of decomposition.

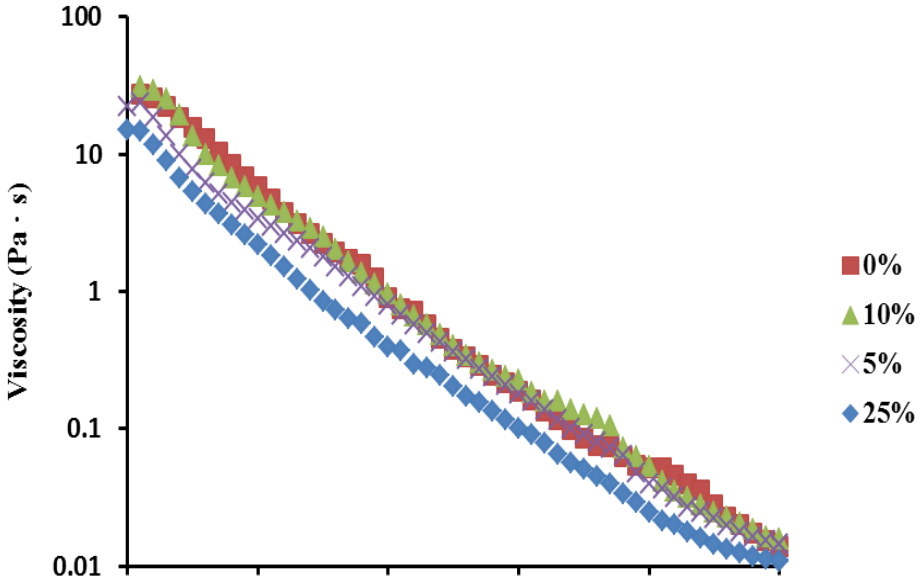

Figure 5.14: Viscosity rheogram for POPC LIGs.

Figure 5.15 and Figure 5.16 represents the decomposition thermograms of DPPC and POPC LIGs, respectively. Table 5.1 summarizes the T_d of [Cho][Pro], DPPC LIGs, and POPC LIGs. Decomposition of [Cho][Pro] occurs at a fast rate of within the first 150 °C. This rapid decrease could be the loss of water which may have been absorbed by the IL. The DPPC LIG with 0% cholesterol displayed a sharp decrease at its T_d of 186 °C. Overall, there was no effect of cholesterol concentrations on the decomposition of DPPC or POPC LIGs. For each gel, the decomposition temperatures were nearly the same.

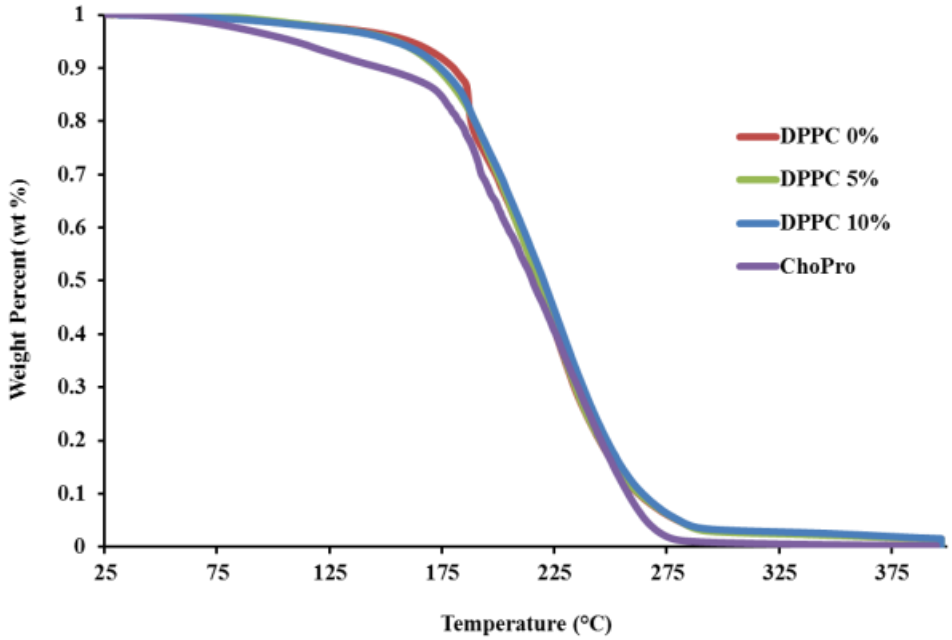

Figure 5.15: Decomposition thermograms for DPPC LIGs.

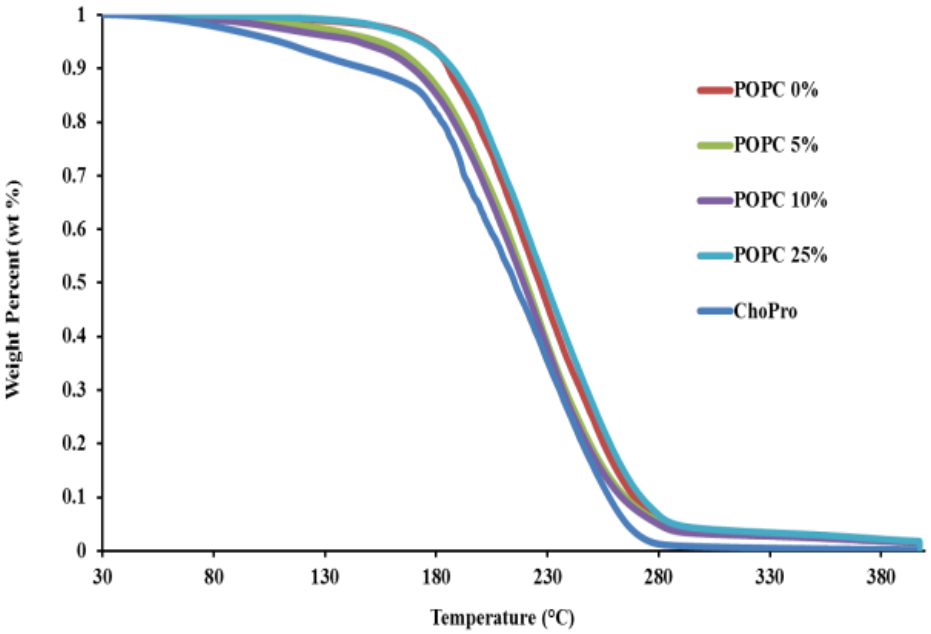

Figure 5.16: Decomposition thermograms for POPC LIGs.

The corresponding phase transition temperatures (T_p) were measured over a range of -20 to 300 °C. These results are summarized in Table 5.2. In general, the T_p of DPPC and POPC gels decreased with increasing cholesterol concentrations. There was a 25 °C difference between

0% cholesterol and 10% or 25% cholesterol for DPPC and POPC LIGs, respectively. These findings suggest that there could be a thermal destabilization of the LIGs with increasing concentrations of cholesterol.

Table 5.1: Thermal decomposition temperatures of [Cho][Pro] and LIGs.

Sample	Cholesterol (%)	T_d (°C)
ChoPro	**-----**	**178.17**
DPPC	**0**	**184.2**
	5	**170.96**
	10	**174.7**
POPC	**0**	**176.95**
	5	**170.53**
	10	**169.52**
	25	**173.14**

5.4 Conclusions

A new type of ionogel with liposomal gelators has been described. Temperature and pH-sensitive liposomes were used to demonstrate the versatility of the composition and potential applications of the LIGs. The mechanical and thermal properties of LIGs were characterized as a function of increasing concentrations of cholesterol. Both gel systems exhibited elastic stability (G' > G") although the DPPC has more characteristics of rigid, elastic solids. The overall viscoelastic properties of DPPC LIGs were 10 fold higher and are completely independent of the applied frequencies. The tangent values were much lower than 1.0 (< 0.4), which demonstrates properties of a stable network. The viscoelastic properties of POPC LIGs show frequency dependent behaviors and begin to favor properties of liquids at higher frequencies.

Table 5.2: Phase transition temperatures of DPPC and POPC LIGs.

Sample	T_p (°C)	Sample	T_p (°C)
DPPC ILLG-0%	**149.4**	**POPC ILLG-0%**	**153.8**
DPPC ILLG- 5%	**141.4**	**POPC ILLG-5%**	**130.3**
DPPC ILLG-10%	**124.0**	**POPC ILLG-10%**	**138.9**
----------	**---------**	**POPC LIG-25%**	**128.0**

A shear thinning behavior was observed for DPPC and POPC gels, which can be translated as a better hold of the gel once applied and easier spreading of the gel in topical drug delivery applications. These LIGs can be tailored for drug delivery based on changes in pH or temperature based on the liposome, and the stability of the gels can be tuned with the concentrations of cholesterol. All of the synthesized gels demonstrated high thermal stability at physiological temperature and the stability is not affected by cholesterol concentrations. In order to investigate their effectiveness as delivery systems, drug release studies can be performed on these gels and under various physiological conditions.

5.5 References

1. Klich, C. M., Gels and Jellies: Encyclopedia of Pharmaceutical Technology. Swarbrick, J.; Boylan, J. C., Eds. Marcel Dekker: New York, 1992.

2. Aly, A. M.; Naddaf, A., Anti-Inflammatory Activities of Colocynth Topical Gel. *J. Med. Sci.* **2006,** *6*, 216-221.

3. Amin, S.; Rajabnezhad, S.; Kohli, K., Hydrogels as Potential Drug Delivery Systems. *Sci. Res. Essays* **2009,** *3* (11), 1175-1183.

4. Pavelic, Z.; Skalko-Basnet, N.; Jalsenjak, I., Characterisation and in vitro evaluation of bioadhesive liposome gels for local therapy of vaginitis. *Int. J. Pharm.* **2005,** *301*, 140-148.

5. Bideau, J. L.; Viau, L.; Vioux, A., Ionogels, Ionic Liquid Based Hybrid Materials. *Chem. Soc. Rev.* **2011,** *40*, 907-925.

6. Maurer, N.; Fenske, D. B.; Cullis, P., Developments in Liposomal Drug Delivery Systems. *Exper Opin. Biol. Ther.* **2001,** *1*, 1-25.

7. Pavelić, Ž.; Škalko-Basnet, N.; Schubert, R., Liposomal Gels for Vaginal Drug Delivery. *Int. J. Pharm.* **2001,** *219* (1–2), 139-149.

8. Pavelić, Ž.; Skalko-Basnet, N.; Jalsenjak, I., Liposomal Gel with Chloramphenicol: Characterisation and *in vitro* Release. *Acta. Pharm.* **2004,** *54*, 319-330.

9. Patel, V.; Misra, A.; Marfatia, Y., Preparation and Comparative Clinical Evaluation of Liposomal Gel of Benzoyl Peroxide for Acne. *Drug Development & Industrial Pharmacy* **2001,** *27* (8), 863.

10. Mitkari, B. V.; Korde, S. A.; Mahadik, K. R.; Kokare, C. R., Formulation and Evaluation of Topical Liposomal Gel for Fluconazole. *Indian J. Pharm. Educ. Res.* **2010,** *44* (4), 324-333.

11. Earle, M. J.; Seddon, K., Ionic Liquids. Green Solvents for the Future. *Pure Appl. Chem.* **2000,** *72* (7), 1391-1398.

12. Hough, W. L.; Smiglak, M.; Rodriguez, H.; Swatloski, R. P.; Spear, S. K.; Daly, D. T.; Pernak, J.; Grisel, J. E.; Carliss, R. D.; Soutullo, M. D.; Davis, J. J. H.; Rogers, R. D., The Third Evolution of Ionic Liquids: Active Pharmaceutical Ingredients. *New J. Chem.* **2007,** *31*, 1429-1436.

13. Viau, L.; Tournae-Peteilh, C.; Devoisselle, J.-M.; Vioux, A., Ionogels as Drug Delivery System: One-Step Sol-Gel Synthesis Using Imidazolium Ibuprofenate Ionic Liquid. *Chem. Commun.* **2010,** *46*, 228-230.

14. Winther-Jensen, O.; Vijayaraghavan, R.; Sun, J.; Winther-Jensen, B.; MacFarlane, D. R., Self Polymerising Ionic Liquid Gel. *Chem. Comm.* **2009,** (21), 3041-3043.

15. Yu, Y.; Lu, X.; Zhou, Q.; Dong, K.; Yao, H.; Zhang, S., Biodegradable Naphthenic Acid Ionic Liquids: Synthesis, Characterization, and Quantitative Structure–Biodegradation Relationship. *Chem. Eur. J.* **2008,** *14* (35), 11174-11182.

16. Abbott, A. P.; Capper, G.; Davies, D. L.; Rasheed, R. K.; Tambyrajah, V., Novel Solvent Properties of Choline Chloride/Urea Mixtures. *Chem. Comm.* **2003,** (1), 70-71.

17. Abbott, A. P.; Boothby, D.; Capper, G.; Davies, D. L.; Rasheed, R. K., Deep Eutectic Solvents Formed between Choline Chloride and Carboxylic Acids: Versatile Alternatives to Ionic Liquids. *J. Am. Chem. Soc.* **2004,** *126* (29), 9142-9147.

18. Weaver, K. D.; Kim, H. J.; Sun, J.; MacFarlane, D. R.; Elliott, G. D., Cyto-toxicity and Biocompatibility of a Family of Choline Phosphate Ionic Liquids Designed for Pharmaceutical Applications. *Green Chem.* **2010,** *12*, 507-513.

19. Gonsior, N.; Hetzer, M.; Kulicke, W.-M.; Ritter, H., First Studies on the Influence of Methylated β-Cyclodextrin on the Rheological Behavior of 1-Ethyl-3-methyl Imidazolium Acetate. *J. Phys. Chem. B* **2010,** *114* (39), 12468-12472.

20. Philippot, J. R.; Schuber, F., *Liposomes as Tools in Basic Research and Industry*. CRC Press, Inc.: Boca Raton, 1994.

CHAPTER 6

CONCLUSIONS AND FUTURE STUDIES

6.1 Conclusions

In summary, a new class of nanomaterials dubbed a group of uniform materials based on organic salts, has been utilized as core components of core-gold shell nanomaterials and a novel gel system, liposomal ionogels (LIGs) was characterized. The GUMBOS are an extension of ILs. Therefore, the have the same properties as ILs; however, GUMBOS have a higher melting temperature limit (250 °C) than ILs (100 °C). A brief history of ILs, GUMBOS, and nanoGUMBOS describe the foundation of this work. The use of gold nanomaterials has been in existence for some time, yet the possibilities of their applications continue to grow with emerging materials. The addition of gold nanoshells on nanoGUMBOS has assisted in the development of a new class of composite materials. The abundance of ionic combinations for ILs has led to the design of a gel system that can possess multiple tunable properties based on the functionality of its IL and liposomal components.

Chapter 3 focused on zero-dimensional nanostructures. There were two methods that were used to prepare nanoparticles. The reprecipitation method resulted in particles with diameters around 98 nm. The reverse micellar method was able to produce particles of differing sizes based on concentration of the reactants. Smaller concentrations yielded smaller particle diameters, while larger concentrations produced larger particles. Gold nanoshells were then added to the different-sized particles and their corresponding optical properties were investigated. The completion of gold nanoshells was based on the ratio of gold-plating solution and precursor nanoparticles. The coverage of gold adsorbed onto the surface of the nanoGUMBOS increased with increasing ratios. The coverage could also be monitored by the

absorption profiles. The absorption maximum consistently red-shifted with increasing ratios until uniform coverage was achieved. Any further addition of gold resulted in a blue shift of the absorption maximum. There are several applications of the gold-coated nanoGUMBOS. In this report, we investigated their sensitivity to a range of organic solvents. Once exposed to acetonitrile, methanol, and chloroform, the nanoGUMBOS, the absorption maximum red-shifted in relation to the boiling points and densities of the solvents. The magnitude of the absorption shifts were relative the gold coverage on the nanoGUMBOS surface.

Chapter 4 discussed 1D nanoGUMBOS as composite nanostructures. Nanorods were prepared using a template method. Gold-coated nanorods were prepared using similar procedures as nanoparticles. However, the optical properties of nanorods were different than nanoparticles. The absorption of gold-coated 1D nanoGUMBOS was noticeably higher than bare nanorods and extended well into the NIR region of the electromagnetic spectrum. Cyclic voltammetry was used to investigate the electrochemical characteristics of GUMBOS. The formal, anodic, and cathodic potentials were measured against ferrocene. The potentials were then used to calculate the HOMO and LUMO energy levels of the GUMBOS which characterized [PyrProSH][TPB] GUMBOS as semi-conductive materials.

Chapter 5 described a novel LIG system composed of a biocompatible IL and liposome gelators. Gels were prepared with a temperature-sensitive liposome, DPPC, and a pH-sensitive liposome, POPC. The mechanical and thermal properties of DPPC and POPC LIGs were investigated with varying concentrations of cholesterol. The “designer” gels can be prepared with multi-functionalities in relation to the type and concentration of its constituents. In general, saturated, DPPC LIGs have 100 times the viscoelasticity properties of POPC LIGs. They also showed decreasing stability, demonstrated by the G’ and G”, trends with increasing

concentrations of cholesterol which can be attributed to the weakening of the DPPC bilayers. Meanwhile, POPC LIGs with 0% cholesterol were reported to be the least viscoelastic of the four cholesterol concentrations. Liposomal ionogels have the possibility of being tailored for drug delivery applications dependent on the chosen phospholipid or IL.

6.2 Future Studies

The tunability of GUMBOS broadens the scope of their potential applications. Although GUMBOS based on conventional pyridinium and imidazolium cations and traditional anions were used as a proof-of-concept study in this dissertation, there are several other alternative salts that may be suitable for this work. In order to effectively utilize gold-coated GUMBOS as photothermal therapy or drug delivery tools, a more biologically friendly approach should be taken. Biocompatible thiol or amine-functionalized salts can be used as alternative ions. For example, cysteine is a thiol-functionalized amino acid. Therefore, it can serve as a cationic or anionic species. Cellular studies would verify the biocompatibility of the GUMBOS and subsequent nanoGUMBOS. We have shown nanoparticle preparation techniques for solid and liquid salts, which can be used regardless of the physical state of the final GUMBOS. Our laboratory has also demonstrated the encapsulation capabilities of nanoGUMBOS, which is useful for the encapsulation of drugs in drug delivery applications.

One dimensional nanoGUMBOS can also be studied for effectiveness as therapy agents. The absorption profile of 1D nanoGUMBOS is more intense and extends to longer wavelengths in the NIR region of the electromagnetic spectrum in comparison to the spherical nanoGUMBOS. The electrochemical studies of 1D nanoGUMBOS can be further investigated in semiconductive applications such as photovoltaics, catalysis, and as energy storage devices.

The current application of LIGs is drug delivery as topical agents. Drug release studies will be necessary to monitor the rates at which the various gels release potential drugs. The studies should also be performed under different physiological conditions to highlight stimuli tunability. For example, for bacterial vaginosis applications, pHs above 4.5 and at 37 °C would be relevant, or an acidic range between pH 4.5 and 5.5 is applicable for cancer sites. Other possible characteristics that can be incorporated into LIGs include: moisturizing and antibacterial.

VITA

Ashleigh R. Wright was born in Charleston, SC and raised in Saint Stephen, SC to Richard and Julia Wright. She attended Timberland High School where she graduated number three in her class of 306 students (June 2000). Ashleigh then graduated from Wofford College with a B.S. in Chemistry in 2004. She was awarded a Wofford College Scholarship throughout her matriculation. In 2007, she received her M.S. in Chemistry from North Carolina Agricultural and Technical State University. Her thesis entitled *Spectrofluorometric Characterization of Trace Amounts of Tryptophan and Epinephrine Antidepressants* was completed under the guidance of Dr. William K. Adeniyi. In 2007, Ashleigh was acknowledged as a Merit Graduate Student for the College or Arts and Sciences. In the fall of 2007, Ashleigh began her doctoral studies at Louisiana State University. She began research under the tutelage of Dr. Isiah M. Warner. Ashleigh will receive her doctor of philosophy in Chemistry during the May 2013 commencement services. A collection of her publications, presentations, awards and activities are listed below.

PUBLICATIONS

Wright, A.R., Li, M., El-Zahab, B., Das, S., Warner, I.M. "NanoGUMBOS-Gold Core-Shell: Synthesis and Characterization," *in preparation for ACS Nano.*

Wright, A.R., Das, S., Warner, I.M. "Characterizations of a New Drug Delivery System Using Liposomal Ionogels," *in preparation.*

Hoppens, M.A., Wheeler, Z.E.W., Qureshi, A.T., **Wright, A.R.,** Stanley, G., Young, D., Savage, P., Hayes, D. Synthesis and Characterization of Cergenin Functionalized Iron Core, Silver Shell Nanomaterials. *submitted J. Phys. Chem. C.*

Adeniyi, W.K., **Wright, A.R**. Novel Fluorimetric Assay of Trace Analysis of Epinephrine in Human Serum. *Spectrochimica Acta Part A.* **2009**, *74*, 1001-1004.

PROFESSIONAL PRESENTATIONS AND ACTIVITIES

2012 **Judge**, Triple Ex (Excite, Explore, Experiment) Raising Researchers Workshop for Undergraduate Research, Integration of Education and Mentoring, Baton Rouge, LA.

2011 **Moderator**, Triple Ex (Excite, Explore, Experiment) Raising Researchers Workshop for Undergraduate Research, Integration of Education and Mentoring, Baton Rouge, LA.

2011 **Wright, A.R.** Li, M., El-Zahab, B., Warner, I.M. "Gold-Coated NanoGUMBOS Incorporating a Group of Uniform Materials Based on Organic Salts," National Organization for the Professional Advancement of Black Chemists and Chemical Engineers (NOBCChE) Annual Meeting, Houston, TX.

2011 Cadigan, M., **Wright, A.R.**, de Rooy, S., Jordan, A., Jagadish, N.N., Das, S., Daniels-Race, T., Warner, I.M. "Conductive and Optical Properties of Nanorods Composed of a Group of Nanomaterials Based on Organic Salts," Summer Undergraduate Research Forum, Baton Rouge, LA.

2010 Warner, I. M.; El-Zahab, B.; Li, M.; Bwambok, D. K.; De Rooy, S. L.; Das, S.; Challa, S.; Tesfai, A.; **Wright, A. R.** "Production of Tunable Nanoparticles Using a Group of Uniform Materials Based on Organic Salts (GUMBOS)," Pittcon Orlando, Florida, February 28-March 5, 2010.

2010 Turner, D., **Wright, A.R.,** El-Zahab, B., Warner, I.M., "Encapsulation of Ionic Liquids in Liposomes," Summer for Undergraduate Research Forum, Baton Rouge, LA.

2010 Hernández, N., **Wright, A.R.**, Li, M., El-Zahab, B., Warner, I.M. "Investigations of Metal Extraction Using Thiol-Functionalized Ionic Liquids and Amino Acid Derivatives," Summer for Undergraduate Research Forum, Baton Rouge, LA.

2010 Wright**, A.R**., Li, M., El-Zahab, B., Warner, I.M. "Development of Optically Active Gold-Functionalized NanoGUMBOS," Southeastern/Southwestern Regional Meeting of the American Chemical Society, New Orleans, LA.

2009 **Judge,** Iberville Parish District Science Fair, Plaquemine, LA.

2009 Hernández, N., **Wright, A.R.**, Li, M., El-Zahab, B., Warner, I.M. "Metal Extraction Using Thiol-Functionalized Ionic Liquids and Amino Acids," Summer for Undergraduate Research Forum, Baton Rouge, LA.

HONORS/AFFILIATIONS

2009-2011 Louisiana State University Graduate School Enhancement Award
2010 Graduate Education Alliance in Louisiana Award (GAELA)
2007-2009 National Science Foundation Bridge to Doctoral Fellowship